Lehigh University
Lehigh Preserve

Theses and Dissertations

2013

Light Element Impurities in Multi-crystalline Si

Haoxiang Zhang
Lehigh University

Follow this and additional works at: http://preserve.lehigh.edu/etd

Part of the Physics Commons

Recommended Citation
Zhang, Haoxiang, "Light Element Impurities in Multi-crystalline Si" (2013). *Theses and Dissertations.* Paper 1687.

This Dissertation is brought to you for free and open access by Lehigh Preserve. It has been accepted for inclusion in Theses and Dissertations by an authorized administrator of Lehigh Preserve. For more information, please contact preserve@lehigh.edu.

Light Element Impurities in Multi-crystalline Si

by

Haoxiang Zhang

A Dissertation

Presented to the Graduate and Research Committee

of Lehigh University

in Candidacy for the Degree of

Doctor of Philosophy

in

Physics

Lehigh University

May 2013

© 2013 Copyright
Haoxiang Zhang

Approved and recommended for acceptance as a dissertation in partial fulfillment of the requirements for the degree of Doctor of Philosophy

Haoxiang Zhang
Light Element Impurities in Multi-crystalline Si

01/21/2013
____
Defense Date

____
Dissertation Director

01/21/2013
____
Approved Date

Committee Members:

____
Dr. Michael J. Stavola

____
Dr. Gary DeLeo

____
Dr. Volkmar Dierolf

____
Dr. W. Beall Fowler

____
Dr. Svetlana Tatic-Lucic

Acknowledgements

I want to express my first and deepest thanks to my dissertation advisor, Professor Michael J. Stavola, for his helpful guidance in this work, his patience in teaching me through my PhD education. I also thank the other members of my dissertation committee: Professor Gary Deleo, Professor Volkmar Dierolf, Professor W. Beall Fowler, Professor Svetlana Tatic-Lucic, for their helpful comments and corrections, and for their interest in this work.

I want to express my gratitude to Joseph Zelinski for his expert technical assistance. I also thank the secretarial assistance of Lois Groff and Pamela Gescek. In addition, my gratitude goes to my lab mates, Chao Peng, Lanlin Wen, Figen Bekisli.

I wish to express my most heartfelt gratitude to my parents, Chi Zhang and Mei Rong. I am also grateful to Fang Rong, Hong Rong, and Lang Rong for their help and care during my stay in US.

Finally, I thank the Physics Department of Lehigh University, the Sherman Fairchild Foundation, and the National Science Foundation for their financial support.

Contents

Title page i

Copyright ii

Certificate of Approval iii

Acknowledgements iv

List of Figures viii

List of Tables xviii

Abstract 1

Chapter 1 Introduction 2

References for Chapter 1 4

Chapter 2 Fundamentals 5

2.1 FTIR 5

2.1.1 Theory - how FTIR works 5

2.1.2 Instrument – FTIR spectrometer in our lab 9

2.2 Instrumentation 11

2.2.1 Infrared detectors 11

2.2.2 Shallow levels in compensated samples .13

2.3 Experimental methods 19

2.3.1 Vibrational spectroscopy of light element impurities 19

2.3.2 Isotopic substitutions 20

2.4 Silicon 21

2.5 Defect structures in silicon 29

References for Chapter 2 33

Chapter 3 VH_4 center trapped by C in Si 35

3.1 Introduction 35

3.2 Experimental methods 37

3.3 Annealing behavior of IR spectra 38

3.4 A VH_4 center trapped by substitutional carbon in Si 41

3.4.1 Vibrational spectroscopy of light element impurities 41

3.4.2 Theory 46

3.5 Conclusion 50

3.6 Acknowledgement 51

References for Chapter 3 52

Chapter 4 Nitrogen in Si by FTIR 56

4.1 Introduction 56

4.2 Survey of nitrogen centers 57

4.3 Multi-crystalline silicon nitrogen centers in mid IR 65

4.4 Far IR studies of nitrogen centers in multi-crystalline silicon 81

4.5 Conclusion: N-centers in mc-Si 94

References for Chapter 4 96

Vita 99

List of Figures

Figure 2.1 The layout of the Michelson interferometer[2.1] 7

Figure 2.2 The function sin σ / σ 8

Figure 2.3 The optical configuration of the Bomem DA 3.16 Fourier Transform Infrared Spectrometer[2.2] 10

Figure 2.4 A 4.2 K bolometer detector[2.3] 13

Figure 2.5 The n-type doping of silicon by the addition of a substitutional P impurity[2.4]. The delocalized electron is shown by the shaded region 14

Figure 2.6(a) Electronic transitions of acceptor impurities in compensated p-type Si without any supplementary light illumination. A hole is promoted from the ground state to its excited states. Empty electron states are not seen 15

Figure 2.6(b) Electronic transitions of donor and acceptor impurities in p-type Si seen with supplementary illumination with visible light. Electron-hole pairs are generated. These electrons and holes then fill the donor and acceptor ground state levels. Infrared transitions from the donor and acceptor ground states to the shallow excited states can then be seen under supplementary white-light illumination 15

Figure 2.7(a) Absorption spectrum of phosphorus donors in neutron transmutation doped silicon.[2.5] 16

Figure 2.7(b) Absorption spectrum of boron acceptors in silicon. There is also a small concentration of phosphorus in this sample. The IR beam contains above band gap light which populates the P impurities with electrons, even in p-type material.[2.5] 17

Figure 2.8 The far IR experimental setup used to observe the spectra of shallow impurities in compensated samples 18

Figure 2.9 Silicon lattice 21

Figure 2.10 Silicon metal[2.6] 22

Figure 2.11 Polycrystalline silicon 23

Figure 2.12(a) The Czochralski process for growing single crystal ingots of silicon[2.7] 24

Figure 2.12(b) The Czochralski process for silicon crystal growth[2.8] 24

Figure 2.13 The float zone process[2.9] 25

Figure 2.14(a) A multi-crystalline silicon wafer. Grains are a few mm to 1 cm in size.[2.10] 27

Figure 2.14(b) A multi-crystalline ingot of silicon[2.10] .27

Figure 2.15 From top to bottom: illustrations show a vacancy, a substitutional defect, and an interstitial defect.[2.11] 30

Figure 2.16 A dislocation[2.11] 31

Figure 2.17 Grain boundaries[2.11] 31

Figure 2.18 Model for the interstitial configuration of oxygen in silicon [2.12] . . 32

Figure 2.19 Model for the split interstitial configuration [2.13] 32

Figure 3.1 IR absorption spectrum (4.2 K) of a Si sample that had been hydrogenated by annealing in an H_2 ambient at 1250 ℃ followed by a rapid quench to room temperature. The sample was made from cast, mc-Si with a carbon concentration of [C] = 8.8×10^{17} cm^{-3}. The inset shows the structures of H_2^* defects trapped by substitutional carbon in Si. The 2210 and 2688 cm^{-1} lines have been assigned to the $SiH_{bc}CH_{ab}$ structure shown on the left[3.6, 3.11, 3.12]. The 1922 and 2752 cm^{-1} lines have been assigned to the $CH_{bc}SiH_{ab}$ structure on the right[3.10-3.12] 36

Figure 3.2 IR spectra (4.2 K) of a mc-Si sample into which H had been introduced by an anneal at 1250 ℃ in an H_2 ambient followed by a rapid quench to room temperature. This sample was annealed sequentially for 30 minutes at the

temperatures: (a) as grown, (b) 100 ℃, (c) 200 ℃, (d) 250 ℃, (e) 300 ℃, (f) 350 ℃, (g) 400 ℃, (h) 450 ℃, (i) 500 ℃, (j) 550 ℃, (k) 600 ℃, (l) 650 ℃, (m) 700 ℃, (n) 750 ℃ and (o) 800 ℃ 40

Figure 3.3 IR spectra (4.2K, 0.3 cm^{-1} resolution) of mc-Si samples into which H (or H+D) had been introduced by an anneal at 1250 ℃ in an H_2 (or $H_2 + D_2$) ambient followed by a rapid quench to room temperature. These samples were subsequently annealed at 500 ℃ for 30 minutes to produce the hydrogen centers of interest. Spectrum (a) is for a sample that contained H alone. Spectrum (b) is for a sample that contained H+D with H>D. Spectrum (c) is for a sample that contained H+D with H=D. Spectrum (d) is for a sample that contained H+D with H<D . . .42

Figure 3.4 IR spectra (4.2 K, 0.3 cm^{-1} resolution) of mc-Si samples into which H (or H+D) had been introduced by an anneal at 1250 ℃ in an H_2 (or $H_2 + D_2$) ambient followed by a rapid quench to room temperature. The H and D content of these samples were determined in Figure 3.3. These samples were subsequently annealed at 550 ℃ for 30 minutes to produce the hydrogen centers of interest. Spectrum (i) is for a sample that contained H alone. Spectrum (ii) is for a sample that contained H+D with H>D. Spectrum (iii) is for a sample that contained H+D with H<D. (a) shows the Si-H stretching region. The Si-H lines are labeled by their $VH_{3-n}D_n$-HC assignments. Each of the Si-H lines is split into a closely spaced doublet. The component of the doublet at lower frequency is for the center

containing C-H. The component at higher frequency is for the center containing C-D. (b) shows the C-H stretching region. The C-H components are labeled by the number, n, of Si-D bonds in the $VH_{3-n}D_n$-HC center 43

Figure 3.5 An expansion of the spectra shown in Figure 3.4 that reveals the splittings of the Si-H stretching modes in the frequency range 2182 to 2188 cm^{-1} for samples with H>D and H<D 44

Figure 3.6 The isochronal (30 minutes) annealing dependence of the integrated intensities of the IR lines at 2223 and 2183.4 cm^{-1}. These hydrogen centers were produced by a thermal treatment (1250 ℃, 1 hour) in an H_2 ambient. (a) is for a Si sample grown by the floating-zone method and with a carbon concentration of $[C] = 0.2\times10^{17}$ cm^{-3}. (b) is for a cast, mc-Si sample with a carbon concentration of $[C] = 8.8\times10^{17}$ cm^{-3} 46

Figure 3.7 The structure (Ref. 26) of the VH_3-CH center predicted by CRYSTAL06 (Ref. 24). The C relaxes away from the vacancy by 0.29 Å, and each Si relaxes away by 0.18 Å. An H attached to Si is 1.83 Å from another H attached to Si, and it is 2.25 Å from the H attached to C 48

Figure 4.1 The structure of the N-N pair in the silicon lattice[4.5] 58

Figure 4.2(a) The 770 cm^{-1} (77K) N-N asymmetric stretching mode along the [001] direction[4.6] 58

Figure 4.2(b) The 967 cm^{-1} (77K) N-N asymmetric stretching mode along the [110] direction[4.6] 58

Figure 4.3 A comparison between FZ and CZ samples of correlation plots, IR absorption coefficient at 963 cm^{-1} for the N-N pair center vs. the nitrogen concentration determined independently.[4.7] 59

Figure 4.4 N-N pair with an additional O atom bonded nearby[4.9] 60

Figure 4.5 Difference spectra for nitrogen and oxygen containing defects in silicon, measured in a boron-doped CZ silicon sample with a N concentration between ~10^{14} and 1.4×10^{15} cm^{-3} and an O concentrations of about 7×10^{17} cm^{-3}.[4.11] 61

Figure 4.6 Absorption spectra showing electronic transitions of N-O_n complexes in Si[4.12] 63

Figure 4.7 Nitrogen-oxygen shallow donor centers seen in far IR absorption spectra of CZ silicon that contains N impurities[4.11]. The spectrum shown in black is for a sample annealed at 650 ℃. The spectrum shown in red is for a sample annealed at 1000 ℃ 64

Figure 4.8(a) Room temperature IR spectra from sample LDK T2 with thicknesses of 2 mm and 5 mm. Spectra of the N-N pair lines are shown in the insert 68

Figure 4.8(b) Room temperature IR spectra from sample LDK B2 with thicknesses of 2 mm and 5 mm. Spectra of the N-N pair lines are shown in the insert 68

Figure 4.8(c) Room temperature IR spectra from sample A8 T3 with thicknesses of 2 mm and 5 mm. Spectra of the N-N pair lines are shown in the insert 69

Figure 4.8(d) Room temperature IR spectra from sample A8 B3 with thicknesses of 2 mm and 5 mm. Spectra of the N-N pair lines are shown in the insert 69

Figure 4.8(e) Room temperature IR spectra from sample E8 T3 with thicknesses of 2 mm and 5 mm. Spectra of the N-N pair lines are shown in the insert 70

Figure 4.8(f) Room temperature IR spectra from sample E8 B3 with thicknesses of 2 mm and 5 mm. Spectra of the N-N pair lines are shown in the insert 70

Figure 4.9 Absorbance spectra for sample LDK B2, annealed at 1000 ℃, measured at both room temperature and 77 K 71

Figure 4.10 IR spectra (77K) for the line at 967 cm^{-1} due to N-N centers in Si. These results are for mc-Si samples provided by MEMC. Spectra are shown for

samples in their as-solidified state, after an anneal at 1000 ℃, and for the difference of these results 73

Figure 4.11 Calibration line for FZ silicon (solid line), data for CZ silicon taken from Itoh *et al.* (circles, right scale), and data for multi-crystalline silicon that combine absorption coefficients for the 967 cm^{-1} line measured at Lehigh (77K, left scale) with SIMS data for the N concentration provided by MEMC (squares). The absorption coefficient for the 967 cm^{-1} line is increased by an anneal at 1000 ℃ (triangles, left scale). Points for different samples are labeled with letters according to the labels in Figure 4.10 76

Figure 4.12 IR spectra (77K) due to NN-O_n centers in Si. These results are for mc-Si samples provided by MEMC. Spectra are shown for samples in their as-solidified state, after an anneal at 1000 ℃, and for the difference of these results 78

Figure 4.13 A difference spectrum for the multi-crystalline silicon sample LDK B2. Upward going lines are due to NN defects. Downward going lines are due to nitrogen-oxygen complexes removed by the anneal at 1000 ℃. Assignments of lines are given in Table 4.1 79

Figure 4.14 Difference spectra for mc-Si samples annealed at 1000 ℃ and for samples from the same test slab in its as-solidified condition 81

Figure 4.15 Absorption spectra (4.2K, resolution 0.5 cm^{-1}), measured with an empty sample holder for reference, for p-type CZ silicon annealed at 450 ℃ for 6 hours. Label numbers on the left panel are boron lines.[4.18] Labels on the right panel are for thermal donor lines assigned previously.[4.19] 84

Figure 4.16 Absorbance spectra (4.2K, resolution 0.5 cm^{-1}) measured with an empty sample holder for reference, for p-type CZ silicon annealed at 600 ℃ for 15 hours. Label numbers on the left panel are boron lines[4.18] 85

Figure 4.17 A spectrum for the same CZ Si sample as shown in Figure 4.17, in the N-O shallow donor FIR region. The labels are for N-O related lines.[4.13] Two boron lines are also labeled with number 1 and 2[4.18] 86

Figure 4.18 Absorbance spectra (4.2K, resolution 0.5 cm^{-1}) measured with an empty sample holder for reference, for p-type CZ silicon annealed at 800 ℃. Label numbers on the left panel are boron lines[4.18]. A phosphorus line is also labeled[4.20] 88

Figure 4.19 Far IR spectra measured for sample LDK B2 at 4.2K with a resolution of 0.5 cm^{-1}. Thin lines are for spectra taken without light illumination. Thicker lines (red in PDF) are taken with 120W light bulb illumination. (a), (b) and (c) are samples under as-grown, 800 ℃ annealed, and 600 ℃ annealed

conditions respectively. (d), (e) and (f) are the same spectra in an expanded scale (5 X) 90

Figure 4.20 Far IR spectra measured for sample A8 B3 at 4.2K with a resolution of 0.5 cm^{-1}, thin lines are for spectra taken without light illumination. Thicker lines (red in PDF) are taken with 120W light bulb illumination. (a) and (b) are samples under as-grown and 600 ℃ annealed conditions respectively. (c) and (d) are the same spectra in an expanded scale (5 X) 92

List of Tables

Table 2.1 The three IR subregions 11

Table 3.1 Measured and predicted vibrational frequencies of Si-H and C-H stretching modes of the VH_3-HC center in Si and related centers that result from the partial substitution of D for H 45

Table 4.1 Assignments of nitrogen and oxygen containing defects shown in Figure 4.5[4.11] 62

Table 4.2 The frequencies of the $1s \rightarrow 2p_{\pm}$ transitions of the family of N-O shallow thermal donors (STDs) in Si.[4.13] 65

Table 4.3 Concentrations of C, O and N from FTIR measurements at Lehigh and from the MEMC Company 67

Table 4.4 Absorption coefficients and N concentrations for mc-Si samples obtained from MEMC determined from the IR data shown in Figure 4.10 74

Table 4.5 Data for the absorption coefficient of the B acceptor and the concentration of neutral B, determined from the data in Figure 4.15 84

Table 4.6 Data for the absorption coefficient of the B acceptor line at 278 cm^{-1} and N-O donor lines determined from Figures 4.16 and 4.17. The concentrations of neutral B and N-O donors estimated from these data are also shown 87

Table 4.7 Data for the absorption coefficient of the B acceptor line at 278 cm^{-1} shown in Figure 4.18 along with the concentration of neutral B determined from this data 88

Table 4.8 Data for the peak absorption coefficient and shallow donor concentration for the donors NO(3) and NO(5) whose spectra are shown in Figure 4.19. These data are for sample LDK B2 in its as-solidified state, annealed at 800 ℃ and annealed at 600 ℃ 91

Table 4.9 Data for the peak absorption coefficient and shallow donor concentration for the donors NO(3) and NO(5) whose spectra are shown in Figure 4.20. These data are for sample A8 B3 in its as-solidified state and annealed at 600 ℃ 93

Abstract

Light element impurities in multi-crystalline Si have been investigated with Fourier transform infrared spectroscopy. These experiments include defect studies in silicon with a high concentration of carbon and also with various concentrations of both nitrogen and oxygen.

A thermally stable VH_4 center trapped by carbon was discovered. The vibrational properties of this defect have been studied for the case of mixed H and D isotopes to establish its structure. The new lines we have found are assigned to the Si-H(D) and C-H(D) stretching modes of the defect center.

We have studied N- and O-related defects in multi-crystalline Si used by industry to fabricate solar cells. The N-N center is the dominant N-related defect. However, N is also found to be bonded with O in multi-crystalline Si. NN-O_n centers are most likely seen when the oxygen concentration in the sample is high. We have also studied the properties of electrically active N-O centers that contain a single N atom. These N-O shallow donors are found to be present in multi-crystalline Si samples containing oxygen and nitrogen but with a lower concentration than is present in oxygen-rich Czochralski-grown Si that contains nitrogen.

Chapter 1: Introduction

The study of defects in semiconductors has a long history. A large variety of impurity atoms are used to control the electrical properties of semiconductors. Impurities are also unintentionally introduced at all production stages. Many materials have been used for semiconductor devices, among which silicon has remained by far the most widely used semiconductor. In this dissertation, I use Fourier transform infrared spectroscopy (FTIR) to probe and understand the local vibrational modes of light element impurities, such as carbon and nitrogen, in multi-crystalline silicon substrates. The investigation of impurity structures and impurity concentrations leads to a deeper understanding of the structural, chemical, and electronic properties of cast silicon[1.1], thus providing fundamental insight into defect engineering for photovoltaic applications.

In chapter 2 the fundamentals of FTIR are introduced. The FTIR spectrometer used throughout my research is discussed. In addition to the FTIR spectrometer, the other instruments used in this research are described. This includes the description of InSb and HgCdTe detectors, as well as a silicon bolometer. The far-infrared measurement setup is also explained. Next, the experimental methods for detecting vibrational spectra, isotope substitution, and annealing methods used in this research are described. And last, solar grade silicon and impurity structures in silicon are surveyed[1.2].

The Si materials typically used to fabricate solar cells often contain high concentrations of carbon and hydrogen impurities. One of the more thermally stable defects in Si that contains both C and H gives rise to a Si-H vibrational line

at 2183.4 cm^{-1}. In chapter 3, we show that this center also gives rise to additional weak Si-H and C-H lines at 2214.4 and 2826.9 cm^{-1} (4.2K). When D is partially substituted for H, rich isotopic splittings of these IR lines are produced. An analysis of these data reveals that the 2183.4, 2214.4, and 2826.9 cm^{-1} lines are due to a VH_4 defect bound to a substitutional C impurity, i.e., a VH_3-HC center.

In chapter 4, nitrogen-related defects in multi-crystalline silicon are investigated. Two types are considered: N-N pair centers in the mid IR and N-O centers in the far IR. The goal of these experiments is to determine what N-containing defect complexes are present in multi-crystalline Si and how these defects depend on the impurity content of the sample. Electrically inactive centers are probed via their vibrational transitions in the mid-infrared. Electrically active centers are probed via their electronic transitions in the far-infrared.

References

1.1 Ian Thomas Witting, *Defect and impurity distributions in traditionally cast multicrystalline and cast monocrystalline silicon for solar substrates*, Master's Thesis, North Carolina State, Raleigh, NC, 2008.

1.2 A. Luque and S. Hegedus, *Handbook of Photovoltaic Science and Engineering*, 2nd ed., John Wiley and Sons, Chichester, 2011.

Chapter 2: Fundamentals

2.1 FTIR

The primary instrument that has been used throughout my research is a Bomem DA 3.16 Fourier Transform Infrared (FTIR) spectrometer. FTIR is used to obtain the infrared absorption spectrum of a solid sample. In this section, both the principles of FTIR and the experimental setup of the FTIR spectrometer in our lab are introduced.

2.1.1 Theory – how FTIR works

In order to measure how a sample absorbs light of different frequencies, absorption spectroscopy is used. The most straightforward way of doing this is to use a dispersive spectrometer which measures how much light is absorbed after passing a monochromatic light beam through a sample. The spectral information is obtained by varying the frequency so that the entire spectrum is determined by making a measurement of one frequency element at a time, multiplied by the number of frequency elements in the spectrum. This can require a long time if the frequency range is broad and the resolution is narrow. In addition, the monochromator's slits only allow a small amount of the beam to pass through which discards a large portion of the total energy in the beam.

While the conventional dispersive spectrometer works with several disadvantages as described above, there is an alternative solution which finds increasing application: by converting the information from the frequency domain to the time

domain, where detectors are able to track both frequency and intensity information, an improved spectrometer can be constructed. This is the basis of FTIR spectroscopy.

An FTIR spectrometer measures a spectrum by illuminating a Michelson interferometer with a broad band light source. The output light passes through a sample, is attenuated, and is then received by a detector. This process gives an interferogram signal that can be Fourier transformed to give a spectrum. The characteristics of a sample we are interested in can be determined by taking the ratio of two spectra measured with and without the sample.

The Michelson interferometer consists of four arms (illustrated in Figure 2.1). They include (1) the light source, (2) a stationary mirror, (3) a moving mirror and (4) the sample and detector. At the intersection of these four arms is a beamsplitter which transmits half of the radiation and reflects half of it. A beam of light is generated by the light source and is split into two beams. One of the light beams travels a fixed distance while the other travels a variable distance determined by the distance from the moving mirror to the beamsplitter. When the light leaves the interferometer, it passes through the sample and is focused upon the detector. The detector produces an electrical signal proportional to the intensity of light it receives. The optical path difference is also recorded at the same time. Thus, a plot of detector response versus optical path difference is generated when the moving mirror is translated back and forth. One scan is defined by the moving mirror translating back and forth once. And the plot of light intensity vs. path length is a complete interferogram.

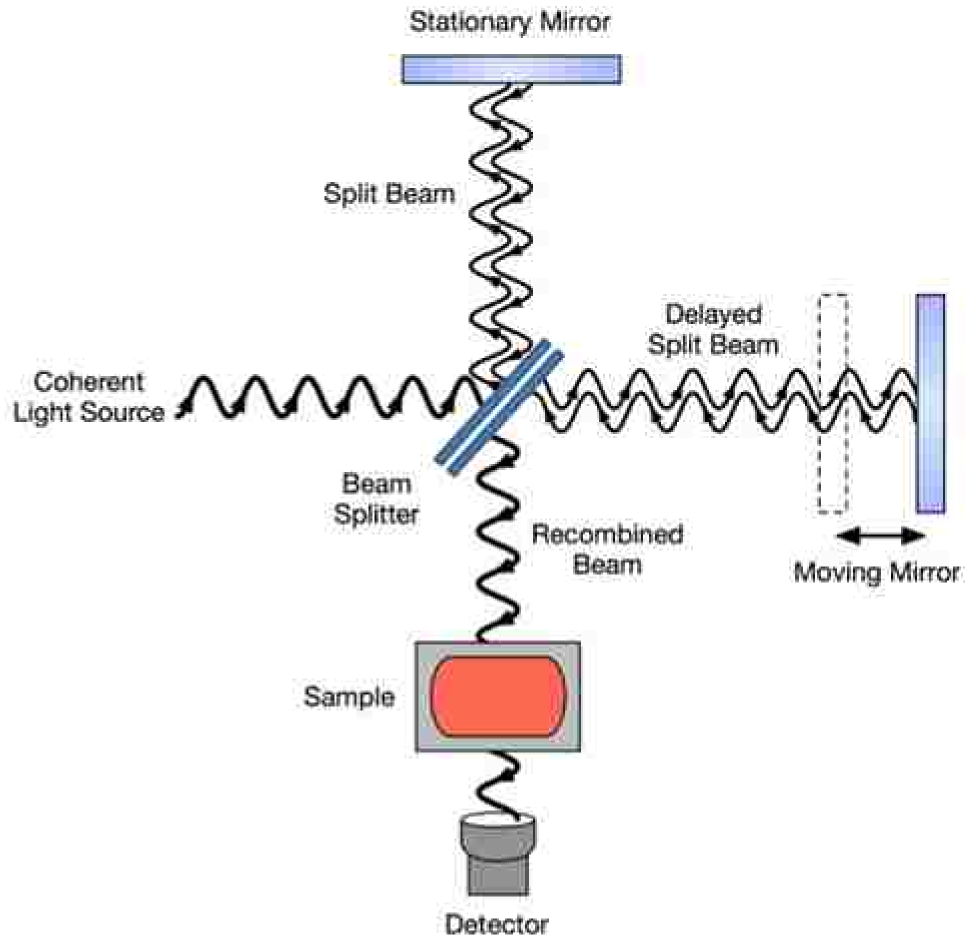

Figure 2.1 The layout of the Michelson interferometer[2.1]

The Fourier theorem relates the interferogram with the spectrum. Since any waveform can be expressed as the sum of many sine wave components of different frequencies and amplitudes, the interferogram can be decoded to sort out the intensities and frequencies presented. The mathematical form of the Fourier transform is shown in the equations below:

$$I(x) = \int B(\sigma) e^{i2\pi\sigma x} d\sigma$$

$$B(\sigma) = \int I(x) e^{-i2\pi\sigma x} dx$$

Here I(x) is the interferogram and B(σ) is the spectrum as a function of frequency in wavenumber units. In practice, the scan distance must be finite and only a portion of the interferogram is collected. All elements of the interferogram outside the region enclosed by the finite scan are discarded. The multiplication of the infinite interferogram by a box function has an effect of convoluting the Fourier transform of the infinite interferogram with the Fourier transform of a box function which is a sinc function.

Any features narrower than the instrument resolution will have the pattern of the transform of the box function, as shown in Figure 2.2. The sidebands could interfere with an adjacent peak. A technique called apodization is used to minimize sidebands. It multiplies the interferogram by a function designed to reduce the truncation effects.

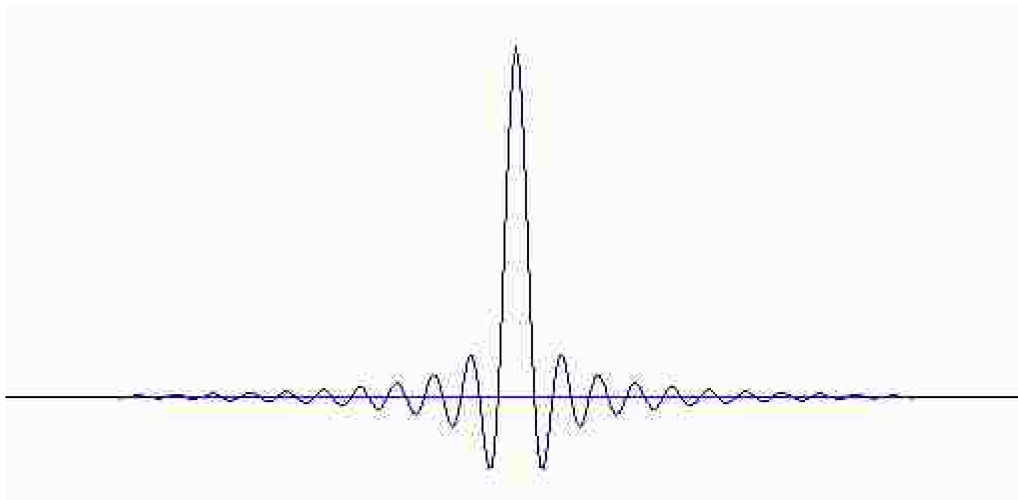

Figure 2.2 The function sin σ / σ

2.1.2 Instrument – FTIR spectrometer in our lab

In our lab, we have a Bomem DA 3.16 FTIR spectrometer, the optical components of which are shown in Figure 2.3. It has two choices of light sources: a silicon carbide globar or a quartz halogen lamp. A six-position rotary filter wheel is equipped with a metal screen at position 6 that can be used to reduce the intensity of light to 50%. An iris is used to control the size of the aperture from 0.5 to 10 mm. The beamsplitter is mounted at the center of the spectrometer. There are three types of beamsplitters: a 10 cm quartz beamsplitter for the visible/UV range, a 10 cm diameter KBr beamplitter coated with Ge/ZnSe for the 450 ~ 5000 cm^{-1} range, and a mylar beamsplitter for the far IR $\leq$ 450 cm^{-1}.

The spectrometer is controlled by Bomem PCDA software installed on a personal computer. The interferogram is saved on the personal computer and the same Bomem PCDA software is used to send a command to an interface computer, whose task is to perform the Fourier transform. Afterward, a spectrum that has been Fourier transformed from the interferogram is generated on the personal computer. Bomem GRAMs/32 software and OriginLab software are used for the purpose of display and manipulation of spectra.

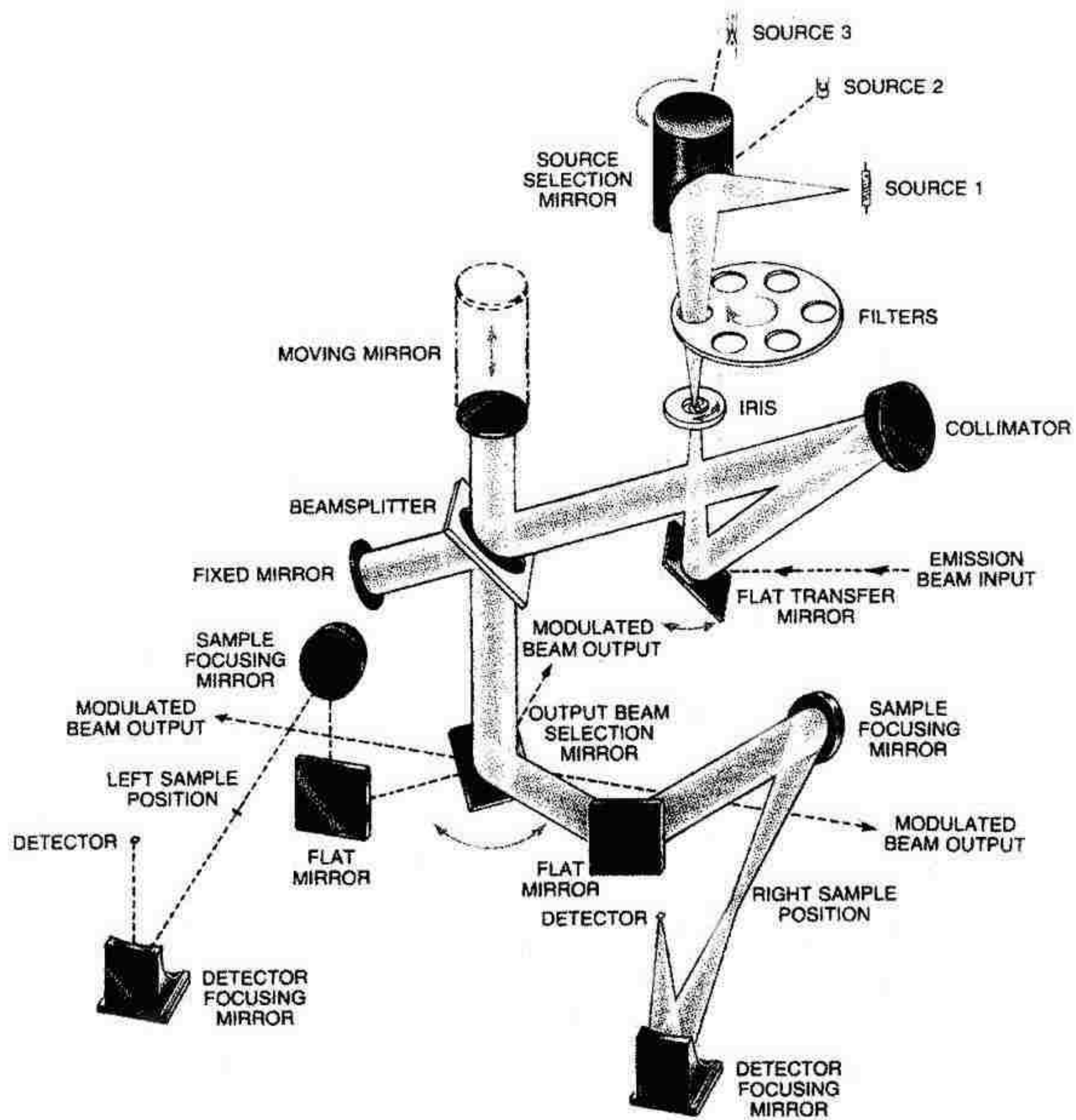

Figure 2.3 The optical configuration of the Bomem DA 3.16 Fourier Transform Infrared Spectrometer[2.2]

2.2 Instrumentation

2.2.1 Infrared detectors

The infrared is a segment of the electromagnetic spectrum ranging from the microwave to the red end of the visible range. IR absorption is typically measured as a function of either wavenumber or wavelength. Wavenumber is defined as the number of waves per unit length and is the unit used in this research. The unit of wavenumber is cm^{-1}, and is called the reciprocal centimeter. The wavenumber unit is convenient because wavenumbers are proportional to frequency, as well as the energy of the IR light. IR absorption data are shown in the form of a spectrum with either the percent transmittance or absorbance as the y-axis and wavenumber as the x-axis.

The IR region is composed of the three subregions shown in Table 2.1.

	Near IR	Mid IR	Far IR
Wavenumber	13,000 – 4,000 cm^{-1}	4,000 – 400 cm^{-1}	400 – 10 cm^{-1}

Table 2.1 The three IR subregions

Three types of infrared detectors have been used in our experiments to cover the mid IR and far IR regions we are interested in. The first is an InSb detector for the range 1800 to 8500 cm^{-1}. The second is a HgCdTe (MCT) detector for the range 800 to 8000 cm^{-1}. The third is a bolometer for the range from 200 to 2000 cm^{-1}. Both the InSb and MCT detectors work at liquid nitrogen temperature. The Si bolometer works at liquid helium temperature.

The InSb detector and MCT detector are PN junction detectors. They are diodes with a band gap less than the energy of the infrared photons to be detected. When the PN junction is illuminated by photons, electron-hole pairs are generated in the depletion region. Therefore, a photocurrent is produced in the external circuit. If the device is operated in an open circuit configuration, an external potential will be measurable. This is called the photovoltaic mode of operation and the InSb detector works in this way. If the device is operated in a short circuit configuration, an external photo-current flows and is measurable. This is the photoconductive mode of operation. The MCT detector works in this mode.

The bolometer is a type of thermal detector. By the absorption of radiation, the temperature changes; this causes a change in the electrical resistance of the sensing element used in the bolometer. The change in the bolometer resistance causes a change of the output voltage that can be measured. Our bolometer element consists of a diamond absorber that is bonded to a heavily boron-doped silicon resistor. The layout of the bolometer is shown in Figure 2.4.

The bolometer is cooled to 4.2 K to reduce noise. The detector sits behind a filter wheel that is also cooled to 4.2 K. There are 4 long pass filters mounted on the wheel that can be selected from outside the He cooled unit. These filters are used to select the appropriate frequency region to be studied. Narrowing the IR frequency band pass with a cold filter improves the signal to noise ratio of the measurement.

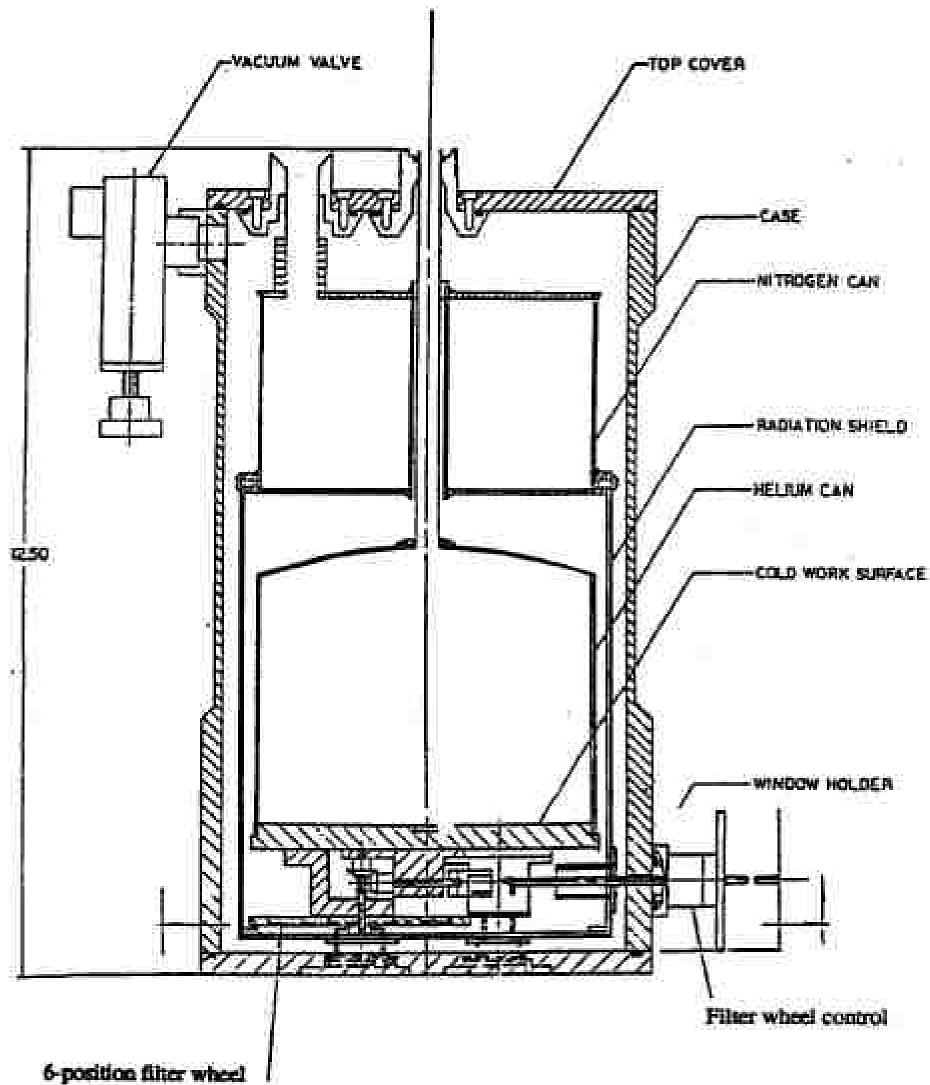

Figure 2.4 A 4.2 K bolometer detector[2.3]

2.2.2 Shallow levels in compensated samples

In the far IR range, absorbance spectra due to the electronic transitions of shallow donors and acceptors can be measured. The n-type doping of a semiconductor (shown in Figure 2.5) introduces a series of energy levels below the conduction band edge. These states are called donor levels. They are illustrated in Figure 2.6.

When the ground states of the donors are occupied, it is possible to absorb photons, and to promote these electrons to the excited states of the donors. The same effect can occur for holes in p-type materials, using IR light to promote holes from the ground state of the acceptor to its excited states.

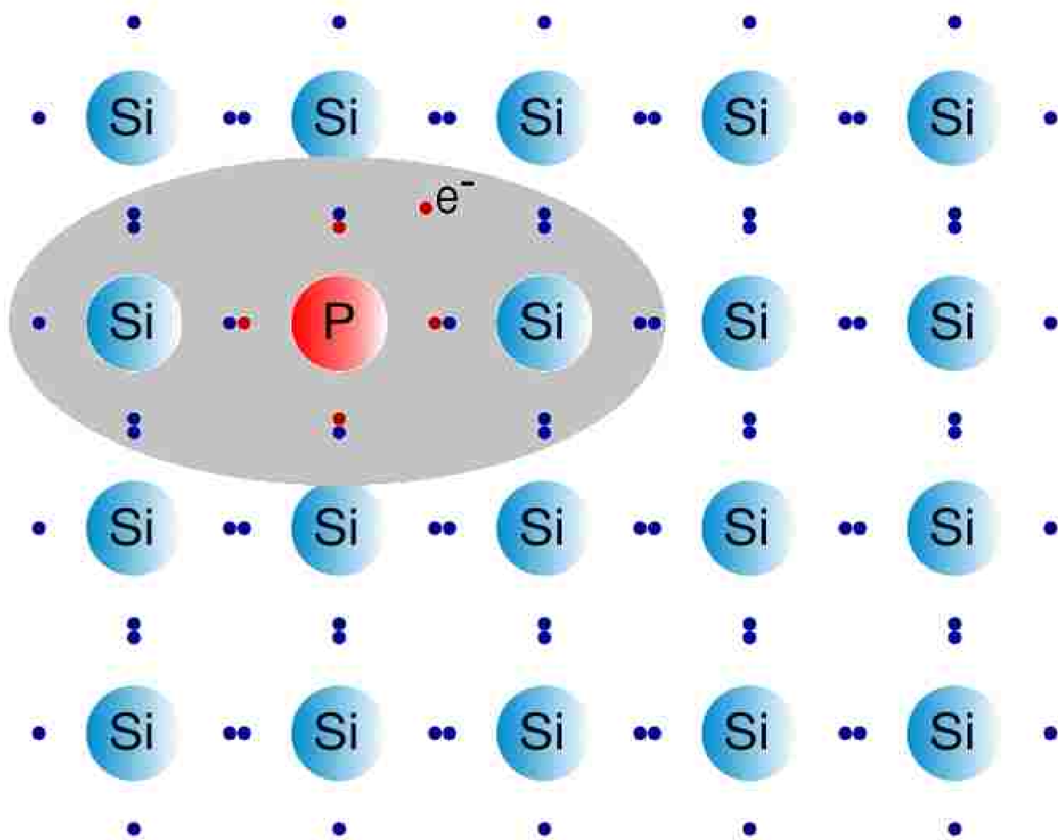

Figure 2.5 The n-type doping of silicon by the addition of a substitutional P impurity[2.4]. The delocalized electron is shown by the shaded region.

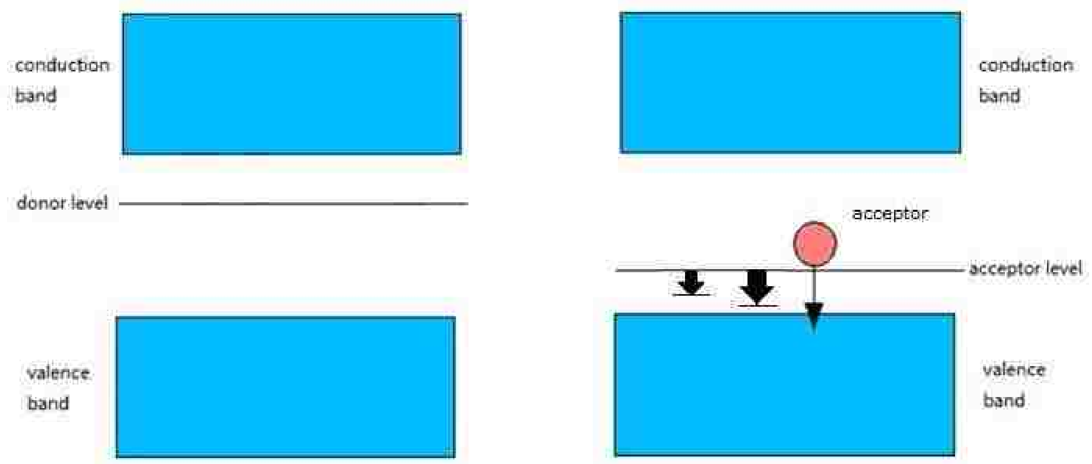

Figure 2.6(a) Electronic transitions of acceptor impurities in compensated p-type Si without any supplementary light illumination. A hole is promoted from the ground state to its excited states. Empty electron states are not seen.

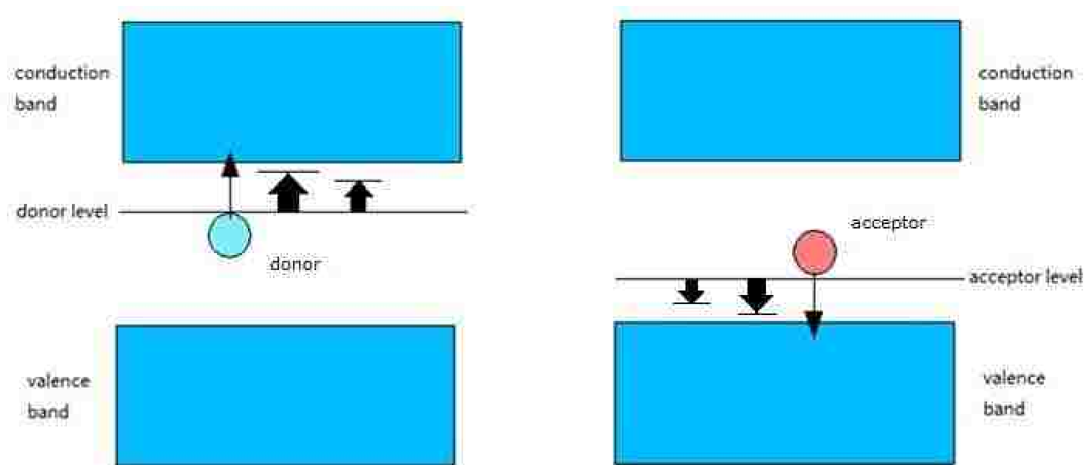

Figure 2.6(b) Electronic transitions of donor and acceptor impurities in p-type Si seen with supplementary illumination with visible light. Electron-hole pairs are generated. These electrons and holes then fill the donor and acceptor ground state levels. Infrared transitions from the donor and acceptor ground states to the shallow excited states can then be seen under supplementary white-light illumination.

The absorption spectra of phosphorus and boron in silicon are shown in Figures 2.7(a) and (b) respectively.[2.5] In Figure 2.7(b) the weak Si(P) lines are labeled “P” in parentheses. The boron lines are labeled with numbers.

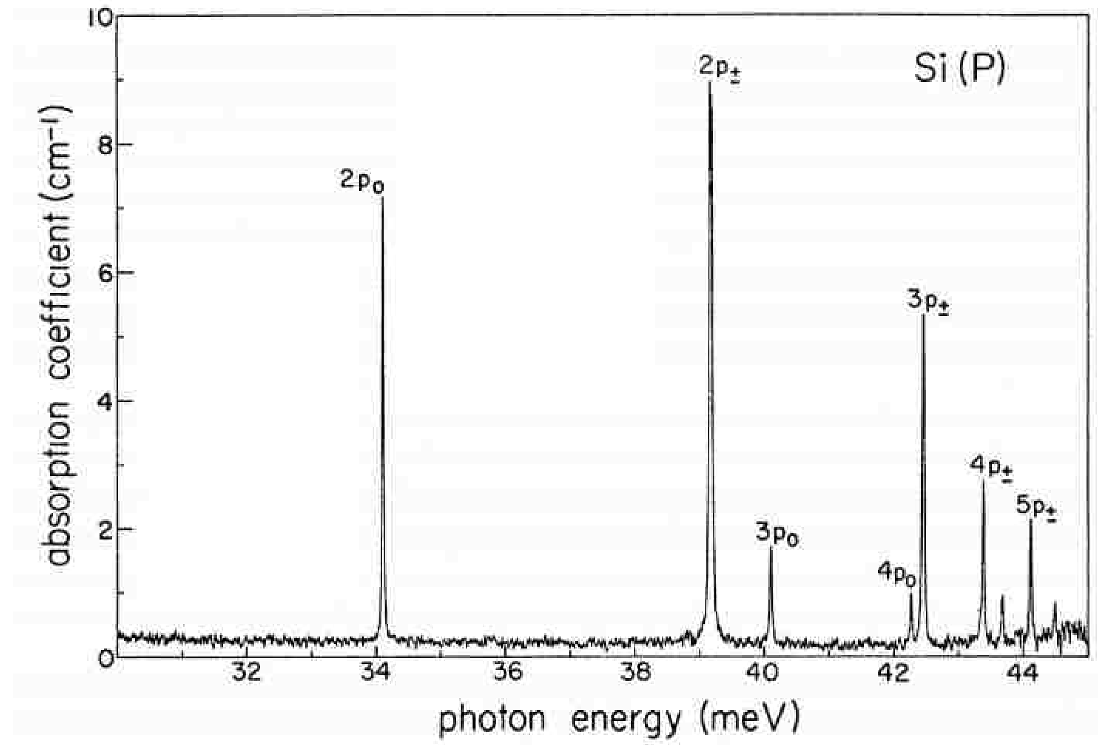

Figure 2.7(a) Absorption spectrum of phosphorus donors in neutron transmutation doped silicon.[2.5]

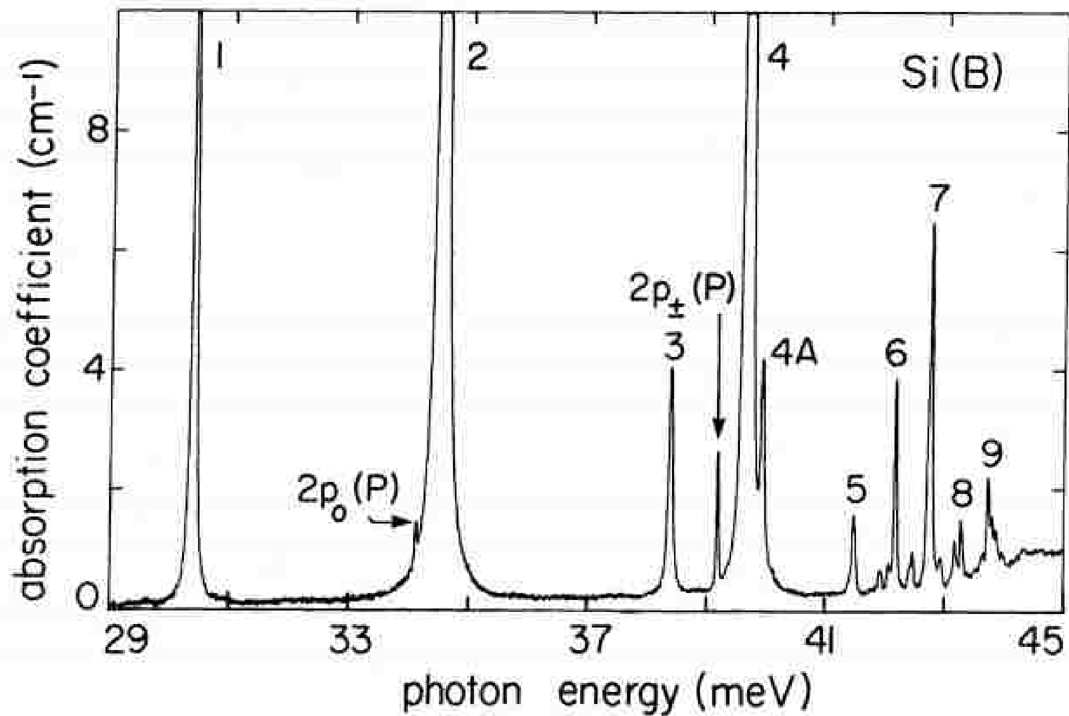

Figure 2.7(b) Absorption spectrum of boron acceptors in silicon. There is also a small concentration of phosphorus in this sample. The IR beam contains above band gap light which populates the P impurities with electrons, even in p-type material.[2.5]

Compensated samples that contain both shallow donors and acceptors present a special problem. Only the dominant impurity type is occupied by electrons or holes in darkness. To see both n- and p-type impurities one can excite the sample by light so electron-hole pairs are generated. These electrons and holes then refill donor and acceptor levels as is illustrated in Figure 2.6.

Our far IR experimental setup is shown in Figure 2.8. The IR beam from the globar first passes through a Si filter at room temperature to remove light with energy above the band gap of the Si sample held at 4.2 K. A spectrum is first measured without additional illumination. A second spectrum is then measured

while the sample is illuminated from the side with visible light to create electrons and holes that can be trapped by impurities in the sample. The difference of these spectra shows the transitions made possible by the further addition of electrons and holes. For example, this technique makes possible the observation of donor impurities in p-type samples. The intensity of the visible light used for side illumination is increased until no further change in the absorption due to shallow impurities is seen.

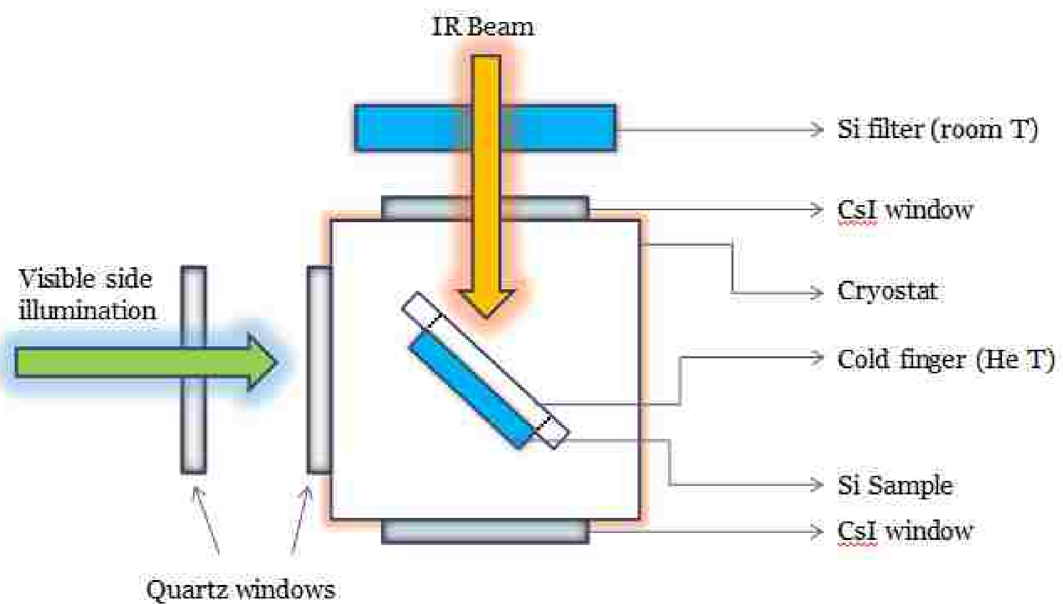

Figure 2.8 The far IR experimental setup used to observe the spectra of shallow impurities in compensated samples.

2.3 Experimental methods

2.3.1 Vibrational spectroscopy of light element impurities

The atoms in molecules and solids have characteristic vibrational properties. Similar to a classical mechanical mass-spring system, the masses of the moving atoms and the strengths of the bonds connecting them determine a characteristic vibrational energy. A vibrational spectrum shows this vibrational energy in a spectral region, usually the infrared. This spectrum can be used to help determine the structure of a defect molecule or to probe its concentration.

Vibrational spectra are obtained by measuring infrared absorption or Raman scattering spectra. Different modes of vibration are active for the different experimental methods. A change in dipole moment is necessary for a vibrational mode to appear in an infrared spectrum, and a change in the molecular polarizability is necessary for a vibrational mode to appear in a Raman spectrum.

When an atom in a crystal is replaced by an impurity atom, one or more new vibrational modes may appear. A special case occurs when the impurity is lighter than the host atoms. In this case, the vibrational frequency will usually be above the phonon frequency range, and this vibrational mode of the impurity is referred to as a local vibrational mode (LVM) because only the light impurity and its first neighbors participate appreciably.

2.3.2 Isotopic substitutions

To identify defect atoms and their neighbors, isotopic substitutions of the atoms in the defect are helpful. The vibrational frequency shifts if the mass of the light impurity atom is changed.

The diatomic molecule is a useful model for understanding the vibrational properties of a light-element impurity in a solid. Assume a light atom of mass m is bound to a heavier atom of mass M. The vibrational frequency is then

$$\omega = k^{1/2}\left(\frac{1}{m} + \frac{1}{M}\right)^{1/2}$$

One sees that ω is sensitive to both the mass of the light impurity and also the mass of its neighbor. In a solid, this equation is modified to be

$$\omega = k^{1/2}\left(\frac{1}{m} + \chi\frac{1}{M}\right)^{1/2}$$

The factor χ accounts for the fact that the neighbor atom is bonded to the solid.

In the case the defect complex might contain hydrogen, when hydrogen is replaced by the heavier isotope deuterium, the vibrational frequency will be lowered by a factor near 1/√2. In this case, it becomes unambiguous to assert that the complex is indeed hydrogen-related. If that H atom is attached to a Si neighbor, then frequency shifts due to the three naturally abundant isotopes of Si are also seen [^{28}Si(92%), ^{29}Si(5%), ^{30}Si(3%)].

2.4 Silicon

Silicon is the second most abundant element in weight of the earth's crust. It is also the most widely used semiconductor. The silicon crystal has a diamond cubic structure which is shown in Figure 2.9. The lattice is composed of two interpenetrating face-centered-cubic lattices displaced by ¼ <111>, with each atom surrounded by four nearest neighbors. Different crystal growth methods will influence the properties of the silicon crystal by introducing different types of impurities and defects. In this section, the main manufacturing processes for silicon of different purity levels are surveyed.

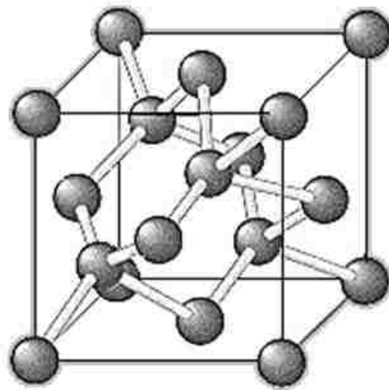

Figure 2.9 Silicon lattice

Metallurgical grade silicon usually has a silicon content > 95%. It is also called silicon metal (shown in Figure 2.10). An electric arc furnace filled with quartz and carbon materials is heated to over 1,900 ℃. The carbon and silica undergo the chemical reaction:

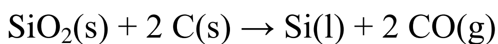

$$SiO_2(s) + 2\ C(s) \rightarrow Si(l) + 2\ CO(g)$$

The resulting liquid silicon is trapped in the bottom of the furnace, which is then cooled. The main impurities are iron, aluminium, calcium, titanium, carbon and oxygen. Dopant impurities like phosphorus and boron are uncontrolled.

Figure 2.10 Silicon metal[2.6]

Another type of silicon with greater purity is polycrystalline silicon (shown in Figure 2.11) with impurities in the ppb(a)—ppt(a) range. The most popular process for manufacturing polycrystalline silicon is the Siemens process. In the Siemens process, metallurgical grade silicon is reacted with hydrochloric acid. The product obtained is trichlorosilane, which is purified through fractional distillation. High-purity silicon rods are then exposed to trichlorosilane. The thermal decomposition of trichlorosilane at 1100 ℃ deposits additional silicon onto the rods:

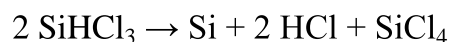

$$2\ SiHCl_3 \rightarrow Si + 2\ HCl + SiCl_4$$

Figure 2.11 Polycrystalline silicon

Mono-crystalline silicon is a form of silicon in which the crystal lattice of the entire solid is continuous. The two main processes used to grow mono-crystalline silicon are the Czochralski method and the floating zone method. In the Czochralski process (shown in Figures 2.12(a) and (b)), the polysilicon is melted in a quartz crucible with impurities doped intentionally into the melt. A seed crystal is dipped into the molten silicon. The seed crystal is slowly pulled upwards and a cylindrical ingot is extracted from the melt.

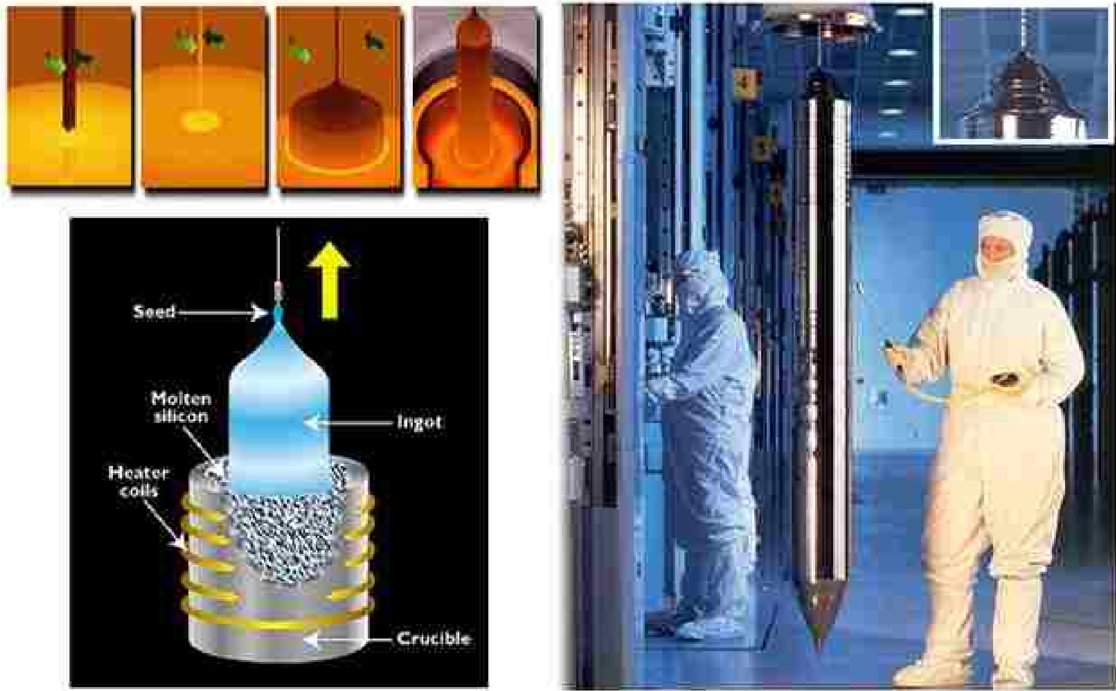

Figure 2.12(a) The Czochralski process for growing single crystal ingots of silicon[2.7]

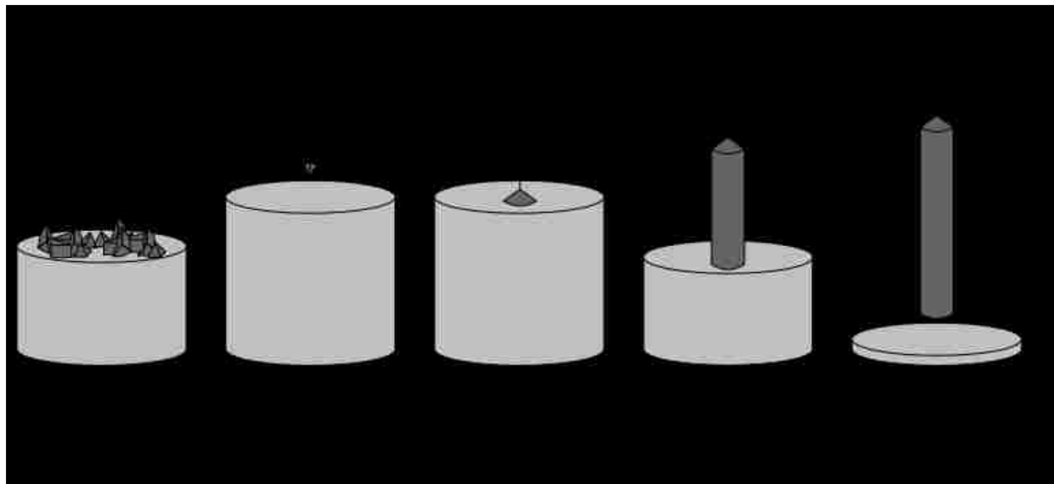

Figure 2.12(b) The Czochralski process for silicon crystal growth[2.8]

In the floating zone process (shown in Figure 2.13), a seed crystal is used to start the growth of a crystal ingot from one end of a polycrystalline silicon rod. When the rod is passed through an RF heating coil, a localized molten zone is created. The crystal ingot starts to grow from the molten zone and the impurities remain preferentially in the molten zone.

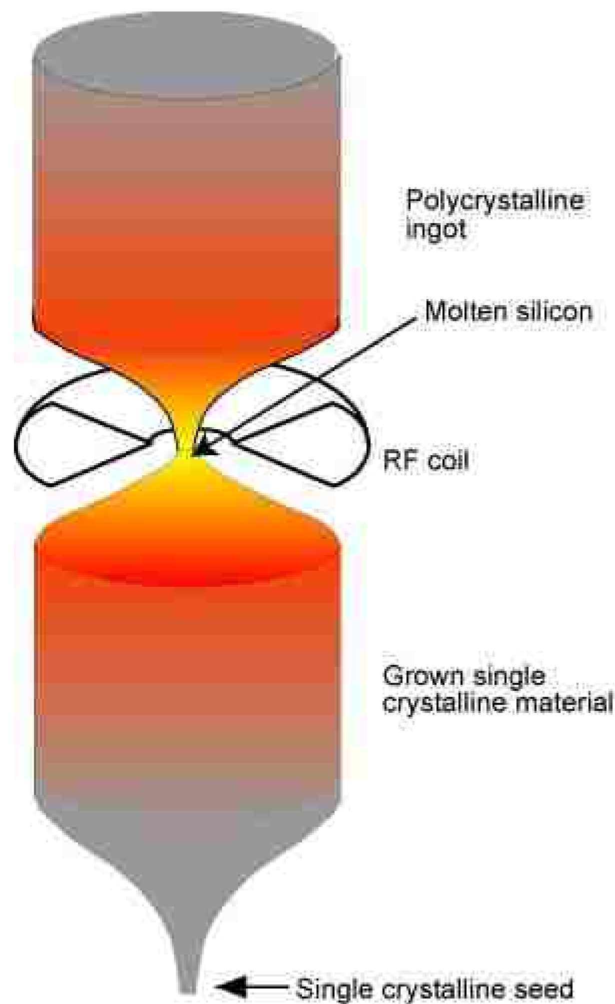

Figure 2.13 The float zone process[2.9]

Multi-crystalline silicon is an alternative to mono-crystalline silicon. It is widely used in the photovoltaic industry. A silicon nitride (Si_3N_4)-coated quartz crucible is used to melt the silicon raw material and to subsequently solidify the multi-crystalline ingot. The purpose of the Si_3N_4 coating is to prevent the adhesion of the silicon ingot to the crucible. By reducing the temperature below the melting temperature of silicon, crystallization starts at the bottom of the crucible. The crystallization front moves in a vertical direction upwards through the crucible. This is called directional solidification. The multi-crystalline silicon grown by the directional solidification method shows similar defect structures. The material quality of multi-crystalline silicon is lower than that of mono-crystalline silicon due to the presence of grain boundries and dislocations (see Figures 2.14(a) and (b)). The advantage of multi-crystalline silicon over mono-crystalline silicon is an approximately 4 times greater solidification rate and therefore a cheaper manufacturing cost. The inherent rectangular or square wafer shape, compared with round mono-crystalline wafers, also provides a better utilization of the wafer area.

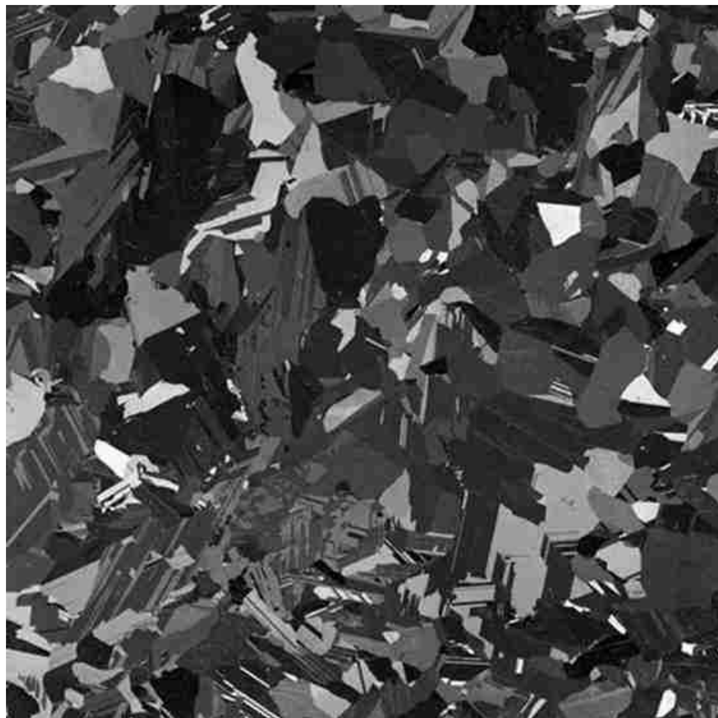

Figure 2.14(a) A multi-crystalline silicon wafer. Grains are a few mm to 1 cm in size.[2.10]

Figure 2.14(b) A multi-crystalline ingot of silicon[2.10]

Several companies are experimenting with cast silicon that is nearly single crystal, called "mono-cast". For mono-cast Si, the melt is seeded from the bottom to produce an ingot that is mostly crystalline. Mono-cast Si still contains more defects than Si grown by the Czochralski or floating-zone methods, primarily as dislocations. It is not yet clear that the advantages of mono-cast Si will outweigh the increased difficulty in growing nearly single-crystal ingots or its increased cost.

Most silicon for photovoltaics applications is grown from electronics grade polycrystalline starting material. There is some interest in using cheaper, lower quality starting materials. Si crystals and ingots can be produced from up-graded metallurgical (UMG) Si. In this case, the concentrations of dopants and harmful metal impurities are not as well controlled. It remains to be seen if processes can be developed for the fabrication of solar-cells with competitive efficiencies from UMG Si.

Other growth methods are possible, for example, the growth of Si ribbons that do not have to be sawn into wafers. At this point in time, ribbon-growth is not competitive with bulk growth in the solar-cell industry.

2.5 Defect structures in silicon

Defects break the periodic arrangement of the atoms in silicon crystals. The electrical and mechanical properties of silicon can be changed by defects. Thus it is important to understand defects and to implement defect engineering strategies to improve the performance of silicon.

Defects can be generally classified into groups by the dimension of their existence. There are point defects, dislocations, grain boundaries and precipitates.

Point defects consist of a few incorrect, missing, or additional atoms in the crystal (see Figure 2.15). When an atom on a lattice site is absent, a vacancy defect is formed. A substitutional impurity occurs when an atom in the lattice is replaced by an impurity atom. Substitutional impurities are very important in semiconductors because they can be used to control the electrical conductivity. Group V elements (such as P) when doped into silicon give rise to an excess of electrons while group III elements (such as B) give rise to an excess of holes. An additional host atom or an impurity atom can sit between the host atoms and is called an interstitial defect.

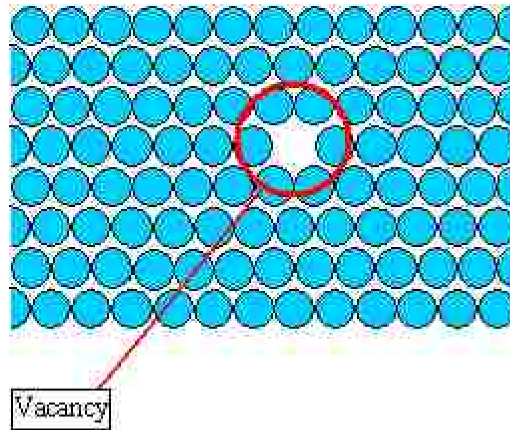

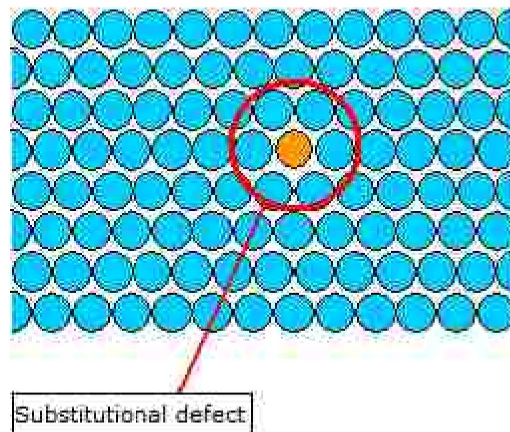

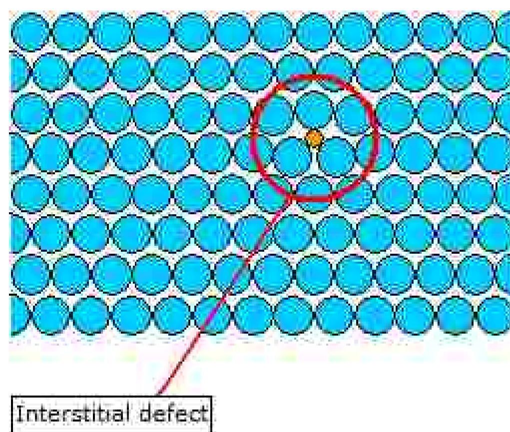

Figure 2.15 From top to bottom: illustrations show a vacancy, a substitutional defect, and an interstitial defect.[2.11]

Dislocations are line defects in the crystal (see Figure 2.16). A dislocation can be illustrated by inserting a half piece of paper in a stack of paper. The edge of the half sheet of paper is the dislocation.

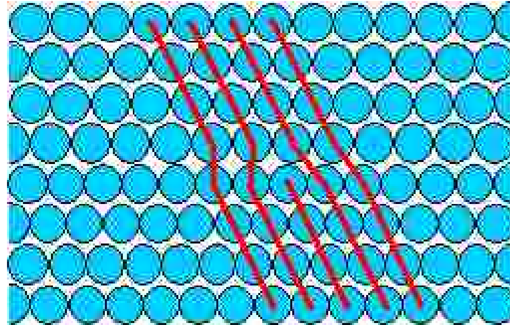

Figure 2.16 A dislocation[2.11]

There are also three dimensional volumetric defects. Grain boundaries extend over an area in the bulk (see Figure 2.17). They originate from the mismatch between neighbor areas of different crystal orientation. Precipitates start to grow with nuclei of defects in a silicon crystal when impurity concentrations are larger than their solubility.

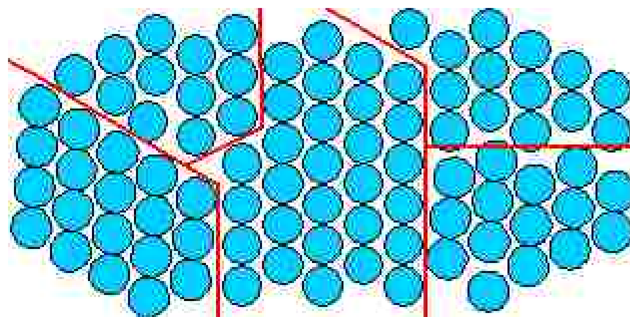

Figure 2.17 Grain boundaries[2.11]

The defects containing light elements that are of interest in this dissertation are H, B, C, N and O. B and C are substitutional impurities. H, N and O are interstitial impurities. H can take a variety of configurations, sometimes with H at a bond-center, sometimes at a tetrahedral interstitial site, and sometimes as an H_2 molecule at a tetrahedral interstitial site. Interstitial O interrupts a Si-Si bond and sits at a bond center (see Figure 2.18). N defects involve a split interstitial configuration where N shares a lattice site with a Si host atom (see Figure 2.19).

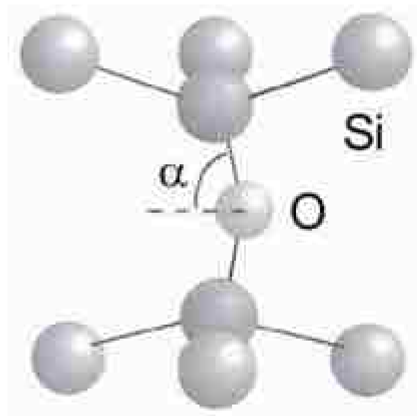

Figure 2.18 Model for the interstitial configuration of oxygen in silicon [2.12]

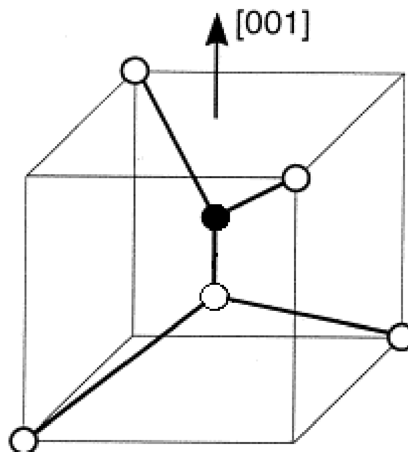

Figure 2.19 Model for the split interstitial configuration [2.13]

References

2.1 http://en.wikipedia.org/wiki/Fourier_transform_infrared_spectroscopy (January 22, 2013).

2.2 Marcie G. Weinstein, *Identification of Hydrogen-containing defects in the III-V nitrides and in Si from advanced applications of vibrational spectroscopy*, PhD Thesis, Lehigh University 2000.

2.3 The Si:B bolometer IPH6200L instruction manual.

2.4 http://org.ntnu.no/solarcells/pages/pn-junction.php (January 22, 2013).

2.5 C. Jagannath, Z. W. Grabowski, and A. K. Ramdas, Phys. Rev. B. 23, 2082 (1981).

2.6 http://www.siliconmetal.net (January 22, 2013).

2.7 http://cnfolio.com/ELMnotes15 (January 22, 2013).

2.8 http://en.wikipedia.org/wiki/Czochralski_process (January 22, 2013).

2.9 http://pveducation.org/pvcdrom/manufacturing/float-zone-silicon (January 22, 2013).

2.10 http://pveducation.org/pvcdrom/manufacturing/multi-crystalline-silicon (January 22, 2013).

2.11 http://www.doitpoms.ac.uk/tlplib/dislocations/printall.php (January 22, 2013).

2.12 http://www.itst.ucsb.edu/~vinhnguyen/dynamics_of_LVM.htm (January 22, 2013).

2.13 R. Newman, Mater. Sci. Eng. B 66, 39 (1999).

Chapter 3: VH_4 center trapped by C in Si

3.1 Introduction

Hydrogen is commonly introduced into Si solar cells to passivate defects in the Si bulk and improve solar-cell performance.[3.1-3.5] When H is introduced into multi-crystalline Si (mc-Si) with a high carbon content that is often used to fabricate solar cells, the dominant defects seen by IR spectroscopy have hydrogen in configurations in which H is trapped by C.[3.6] These C-H centers provide a reservoir of H and play a role similar to that of H_2 molecules in high-purity Si.

One of the more thermally stable defects found in Si that contains both C and H is a center with a vibrational line at 2183.4 cm^{-1}. While this vibrational line has been observed previously,[3.6-3.8] it has not been assigned to a specific defect structure. In the present chapter, vibrational spectroscopy and theory show unambiguously that the 2183.4 cm^{-1} line is due to a VH_4 center trapped by a carbon impurity in Si.

Previous results for the defects that are formed by C and H in single-crystal Si provide a foundation for our studies.[3.9-3.13] A defect structure known as H_2^* that contains one H atom at a bond-centered site (H_{bc}) and a second H atom at an antibonding site (H_{ab}), along the same trigonal axis, can be trapped by a substitutional C impurity to form H_2^*(C) defects.[3.9-3.12] The vibrational properties of the two possible H_2^*(C) configurations have been studied, and defect structures have been proposed (see Figure 3.1). A Si-H vibrational mode at 2210 cm^{-1} and a C-H mode at 2688 cm^{-1} have been assigned to the SiH_{bc}-CH_{ab} structure.[3.6, 3.11, 3.12]

A Si-H vibrational mode at 1922 cm^{-1} and a C-H mode at 2752 cm^{-1} have been assigned to the CH_{bc}-SiH_{ab} structure.[3.10-3.12]

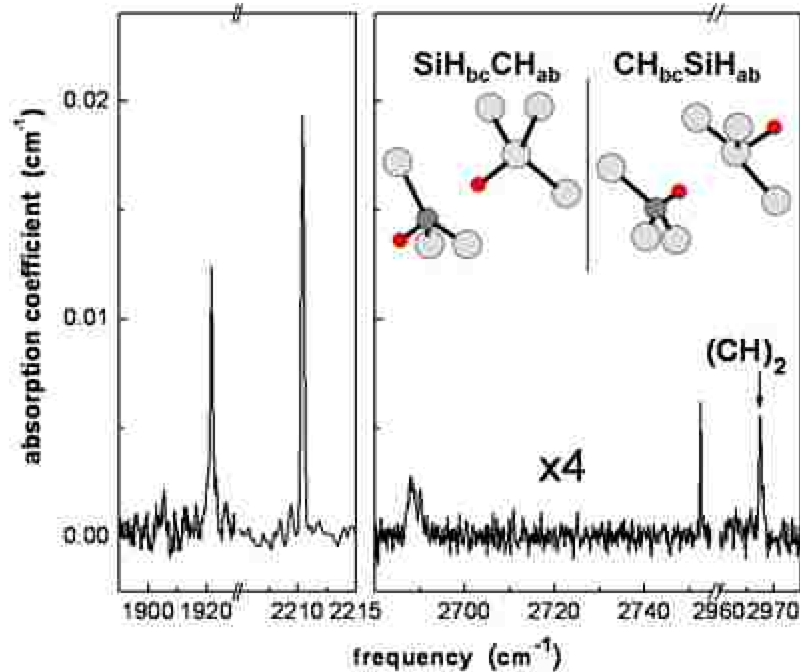

Figure 3.1 IR absorption spectrum (4.2 K) of a Si sample that had been hydrogenated by annealing in an H_2 ambient at 1250°C followed by a rapid quench to room temperature. The sample was made from cast, mc-Si with a carbon concentration of [C] = 8.8×10^{17} cm^{-3}. The inset shows the structures of H_2^* defects trapped by substitutional carbon in Si. The 2210 and 2688 cm^{-1} lines have been assigned to the $SiH_{bc}CH_{ab}$ structure shown on the left[3.6, 3.11, 3.12]. The 1922 and 2752 cm^{-1} lines have been assigned to the $CH_{bc}SiH_{ab}$ structure on the right[3.10-3.12].

In other experiments, electron irradiation damage was used to produce pairs of nearest-neighbor substitutional C atoms. When H interacts with these C_s-C_s pairs, a $(CH)_2$ defect is formed with a CH-HC structure.[3.13] The $(CH)_2$ center has a C-H mode at 2967 cm^{-1} that is also shown in Figure 3.1. It has been found that for Si with a C concentration [C] > 5 x 10^{17} cm^{-3}, a substantial concentration of

substitutional C pairs is formed in the absence of radiation damage and that these C pairs provide a thermally stable trap for H.[3.6]

The implantation of protons into Si produces a number of different centers in which H decorates the dangling bonds of vacancy centers that were introduced by the bombarding protons.[3.14] Similar defects are produced by the electron irradiation of Si that contains H.[3.15, 3.16] Of particular interest here is a VH_4 center in which H atoms terminate the four dangling bonds of a Si vacancy. The VH_4 defect has a well-known vibrational line[3.14] at 2223 cm^{-1} (4.2 K) that can also be produced in hydrogenated Si by thermal annealing without any radiation damage.[3.6, 3.7, 3.17] The partial substitution of D for H produces an isotopic structure in the vibrational spectrum of VH_4 that reveals its composition and symmetry.[3.14, 3.17] Similarly, in this chapter the partial substitution of D for H in Si containing a high concentration of C is shown to give a rich isotopic structure that helps us to determine the microscopic structure of the defect giving rise to the 2183.4 cm^{-1} line.

Finally, a few of the IR lines to be studied here were observed in a previous study by Pajot *et al.*[3.8] of Si crystals grown in H_2 or D_2. While these lines were not attributed to specific defects, the existence of these weak IR lines, tabulated by *Pajot et al.*, proves useful here.

3.2 Experimental methods

Si samples containing an especially high concentration of carbon impurities were chosen for our experiments. These samples were cut from bulk, cast-Si material to

have dimensions of approximately $8\times6\times10$ mm^3 and were multi-crystalline with grain sizes from a few millimeters to one centimeter.

In order to investigate the interaction of hydrogen with C in mc-Si, samples were annealed at 1250 ℃ in sealed ampoules containing H_2 gas or mixtures of H_2 and D_2 (2/3 atm at room temperature) followed by a rapid quench in water to room temperature.[3.6, 3.18] Any subsequent anneals were performed in a conventional tube furnace under flowing He. These anneals were also terminated by a rapid quench.

IR spectra were measured with a Bomem DA3 Fourier transform IR spectrometer. An InSb detector (77K) was used for measurements of H-stretching modes. A Si bolometer (4.2K) was used to characterize the concentration of carbon. For IR measurements of H stretching modes, samples were cooled to near 4.2K with a Helitran, continuous-flow cryostat.

To characterize the concentration of carbon, the IR line at 607 cm^{-1} assigned to substitutional C was measured at room temperature.[3.19] The mc-Si samples used in the experiments reported here had a carbon concentration of [C] = 8.8×10^{17} cm^{-3}. Reference samples for our infrared spectra were cut from Si grown by the floating zone method and had a carbon concentration of [C] = 0.2×10^{17} cm^{-3}.

3.3 Annealing behavior of IR spectra

Figure 3.2 shows the evolution upon annealing of the defects in a mc-Si:C sample into which H had been introduced. [The vibrational line at 2967 cm^{-1} due to the

$(CH)_2$ center, shown in Figure 3.1, is thermally stable throughout the annealing sequence[3.6].] The vibrational lines due to $H_2^*(C)$ centers (1922, 2210, and 2752 cm^{-1}) begin to disappear at 350 ℃ while the 2223 cm^{-1} IR line due to VH_4 grows in. At 550 ℃, the 2223 cm^{-1} line due to VH_4 disappears while a Si-H mode at 2183.4 cm^{-1} grows in along with an additional line at 2826.9 cm^{-1} in the C-H stretching range. We have found that the 2826.9 cm^{-1} line shifts to 2819.3 cm^{-1} in a Si sample containing the ^{13}C isotope, confirming its assignment to a C-related vibrational mode.[3.20]

The 2826.9 cm^{-1} line has the same annealing behavior as the Si-H mode at 2183.4 cm^{-1}, suggesting that both of these IR lines are due to an unknown defect structure in Si that contains both C and H.

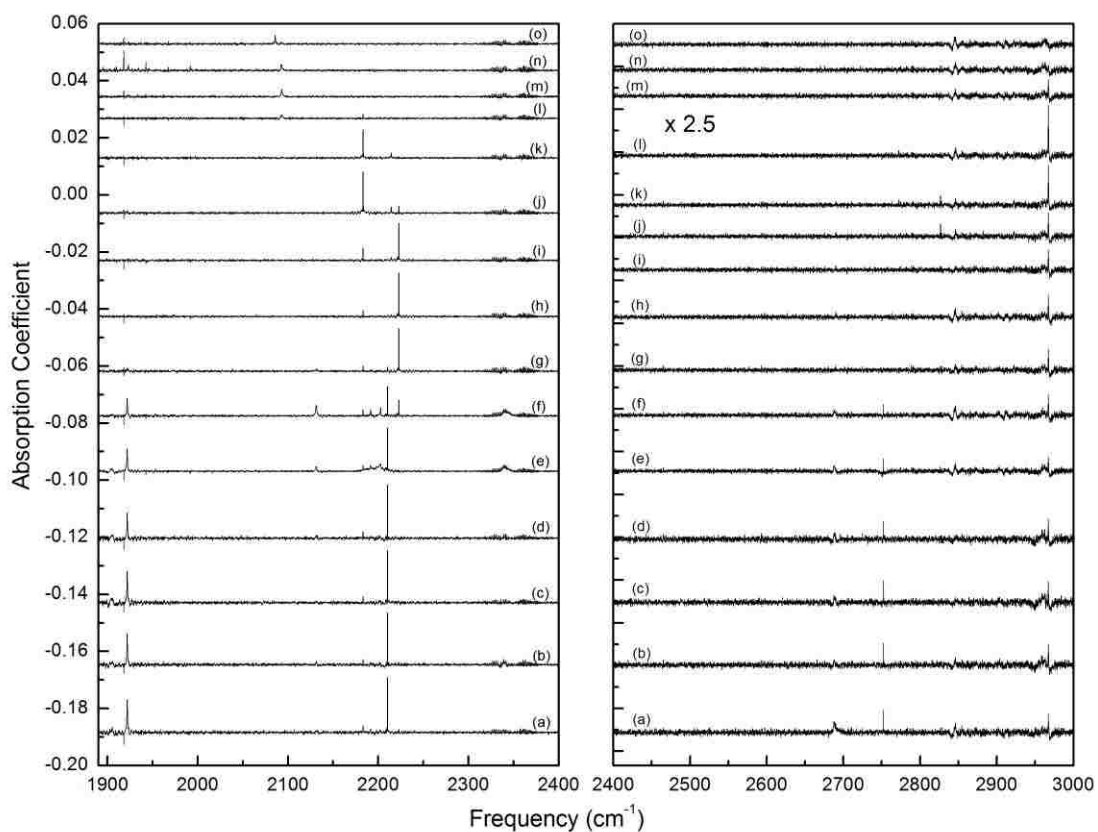

Figure 3.2 IR spectra (4.2 K) of a mc-Si sample into which H had been introduced by an anneal at 1250 °C in an H_2 ambient followed by a rapid quench to room temperature. This sample was annealed sequentially for 30 min at the temperatures: (a) as grown, (b) 100 °C, (c) 200 °C, (d) 250 °C, (e) 300 °C, (f) 350 °C, (g) 400 °C, (h) 450 °C, (i) 500 °C, (j) 550 °C, (k) 600 °C, (l) 650 °C, (m) 700 °C, (n) 750 °C and (o) 800 °C.

3.4 A VH_4 center trapped by substitutional carbon in Si

3.4.1 IR absorption spectra

Samples of multi-crystalline Si were prepared that contained different relative concentrations of H and D for our experiments. The relative concentrations of H and D in a sample could be estimated independently by examining the relative intensities of the IR lines due to the VH_4 complex and its isotopic siblings $VH_{4-n}D_n$. Figure 3.3 shows that the VH_4 complex with its IR line at 2223 cm^{-1} is dominant following an anneal at 500 ℃. Figure 3.3 shows spectra in the frequency range where $VH_{4-n}D_n$ lines appear for our H- and D-containing samples following an annealing at 500 ℃. The assignments of the IR lines, made originally by Bech Nielsen et al.[3.14], show that these samples contain (a) only H, (b) H > D, (c) H ≈ D, and (d) D > H.

Spectra for mc-Si:C samples that contain H [spectrum (i)] or mixtures of H and D [spectra (ii) and (iii)] are shown in Figure 3.4. These samples had been annealed at 550 ℃ to produce the 2183.4 and 2826.9 cm^{-1} lines and their isotopic siblings. The relative concentrations of H and D in these samples were determined independently by examining the relative intensities of the isotopically shifted lines of the $HD^*(C)$ centers that were studied prior to any post-hydrogenation annealing treatments and also from the relative intensities of the $VH_{4-n}D_n$ center shown in Figure 3.3.[3.21]

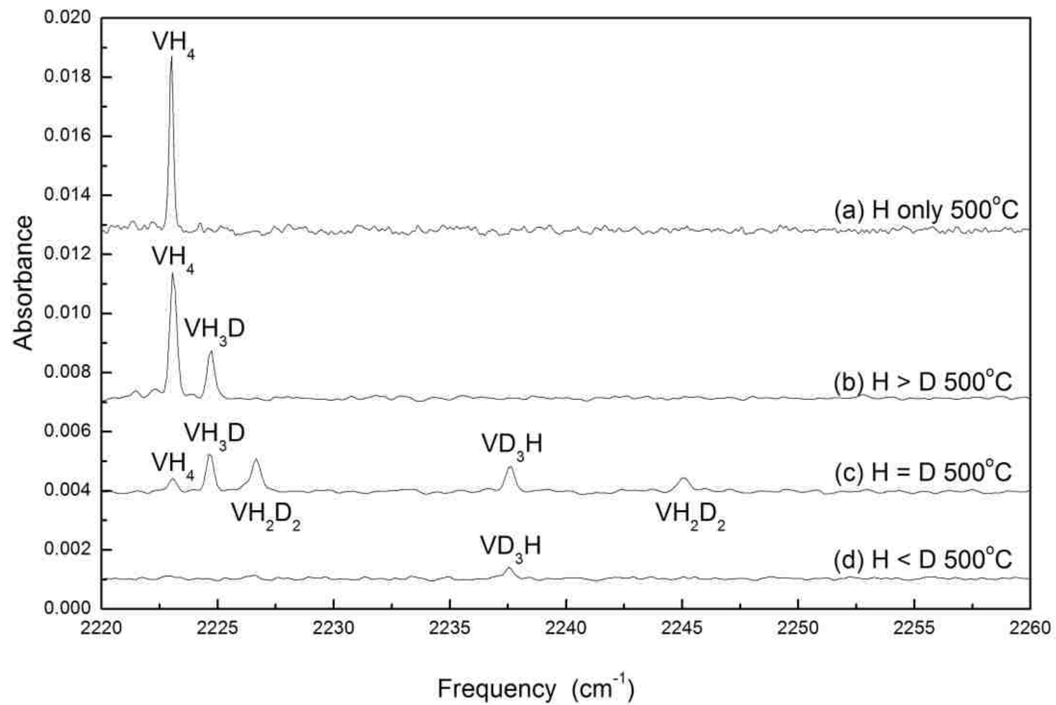

Figure 3.3 IR spectra (4.2 K, 0.3 cm^{-1} resolution) of mc-Si samples into which H (or H+D) had been introduced by an anneal at 1250 °C in an H_2 (or $H_2 + D_2$) ambient followed by a rapid quench to room temperature. These samples were subsequently annealed at 500 °C for 30 min to produce the hydrogen centers of interest. Spectrum (a) is for a sample that contained H alone. Spectrum (b) is for a sample that contained H+D with H>D. Spectrum (c) is for a sample that contained H+D with H=D. Spectrum (d) is for a sample that contained H+D with H<D.

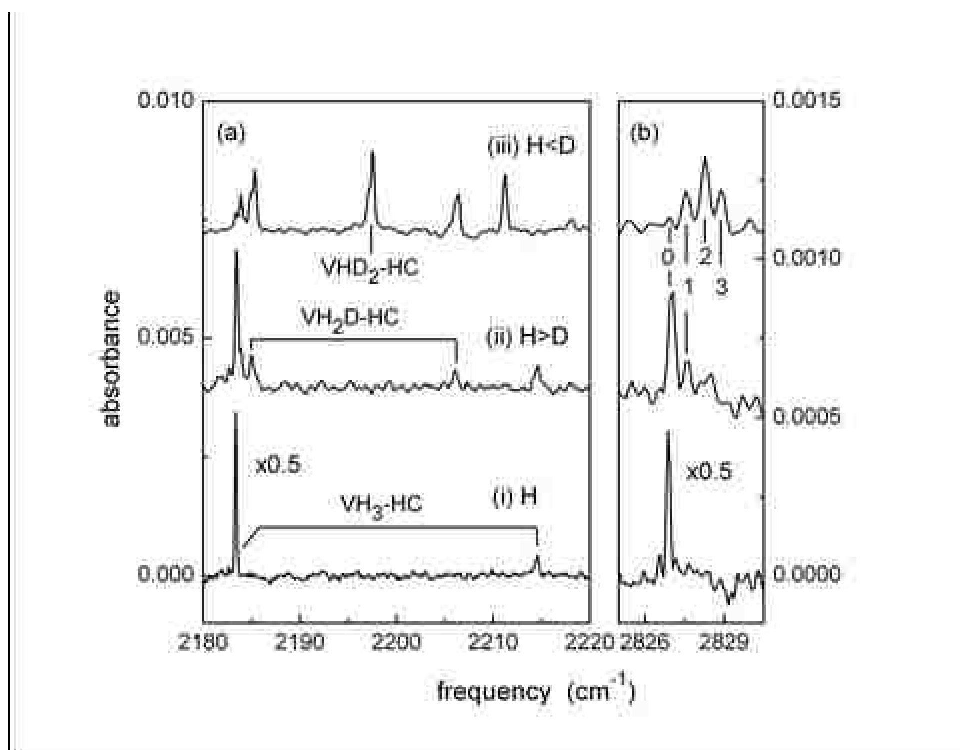

Figure 3.4 IR spectra (4.2 K, 0.3 cm^{-1} resolution) of mc-Si samples into which H (or H+D) had been introduced by an anneal at 1250 °C in an H_2 (or H_2 + D_2) ambient followed by a rapid quench to room temperature. The H and D content of these samples were determined in Figure 3.3. These samples were subsequently annealed at 550 °C for 30 min to produce the hydrogen centers of interest. Spectrum (i) is for a sample that contained H alone. Spectrum (ii) is for a sample that contained H+D with H>D. Spectrum (iii) is for a sample that contained H+D with H<D. (a) shows the Si-H stretching region. The Si-H lines are labeled by their $VH_{3-n}D_n$-HC assignments. Each of the Si-H lines is split into a closely spaced doublet. The component of the doublet at lower frequency is for the center containing C-H. The component at higher frequency is for the center containing C-D. (b) shows the C-H stretching region. The C-H components are labeled by the number, n, of Si-D bonds in the $VH_{3-n}D_n$-HC center.

Spectra (ii) and (iii) in Figure 3.4(a) and (b) for samples containing both H and D show a rich isotopic structure. The Si-H line at 2183.4 cm^{-1} is split into several components, each of which has a doublet structure (Figure 3.5) that is spaced by approximately 0.4 cm^{-1}. The C-H line at 2826.9 cm^{-1} is split into four components. Furthermore, a closer examination of spectrum (i) in Figure 3.4(a) for the sample containing H alone shows a weak line at 2214.6 cm^{-1} seen also by Pajot et al.[3.22] All but one of the IR lines in Figure 3.4 show the same behavior upon annealing, suggesting that they are isotopic siblings of a common defect structure. The one line that does not show the same behavior as the others lies at 2211 cm^{-1}. The 2211 cm^{-1} line has been assigned previously to the $(CD)_2$ center[3.13] which is the isotopic partner of the $(CH)_2$ defect that gives rise to the 2967 cm^{-1} line shown in Figure 3.1. The frequencies of the IR lines seen in Figure 3.4 are listed in Table 3.1.

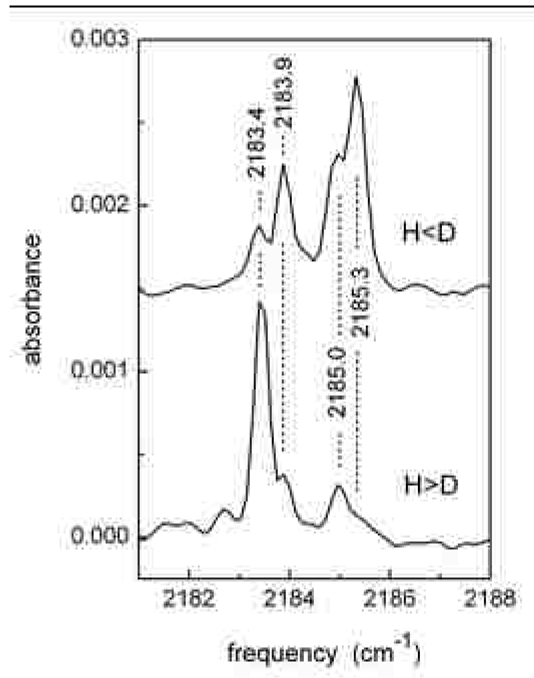

Figure 3.5 An expansion of the spectra shown in Figure 3.4 that reveals the splittings of the Si-H stretching modes in the frequency range 2182 to 2188 cm^{-1} for samples with H>D and H<D.

Configuration	Measured (cm^{-1})	Predicted (cm^{-1})
VH_3-HC	2183.4	2184.7
	2214.6	2216.5
	2826.9	2827.1
VH_3-DC	2183.9	2184.7
	2215.4	2217.2
VH_2D-HC	2185.0	2184.7
	2206.1	2206.2
	2827.6	2827.0
VH_2D-DC	2185.3	2184.7
	2206.4	2206.7
VHD_2-HC	2197.1	2195.6
	2828.3	2827.0
VHD_2-DC	2197.5	2195.9
VD_3-HC	2828.9	2827.0

Table 3.1 Measured and predicted vibrational frequencies of Si-H and C-H stretching modes of the VH_3-HC center in Si and related centers that result from the partial substitution of D for H.

The complicated vibrational structure seen for the spectra of the 2183.4, 2214.6, and 2826.9 cm^{-1} lines and their isotopic siblings that is produced by the partial substitution of D for H is not consistent with a defect structure that contains just two H atoms. The annealing behavior of the 2183.4 cm^{-1} line suggests another possible assignment. Figure 3.6(a) shows isochronal annealing data for the 2223 cm^{-1} line assigned to VH_4 for a Si sample grown by the floating zone method. Figure 3.6(b) shows isochronal annealing data for the 2223 and 2183.4 cm^{-1} lines for a mc-Si sample with a carbon concentration of $[C] = 8.8\times10^{17}$ cm^{-3}. These data show that the 2223 cm^{-1} line disappears at a lower annealing temperature in mc-Si with higher carbon content than in FZ Si with much lower carbon content. These annealing results suggest an interaction between VH_4 and C impurities in Si.

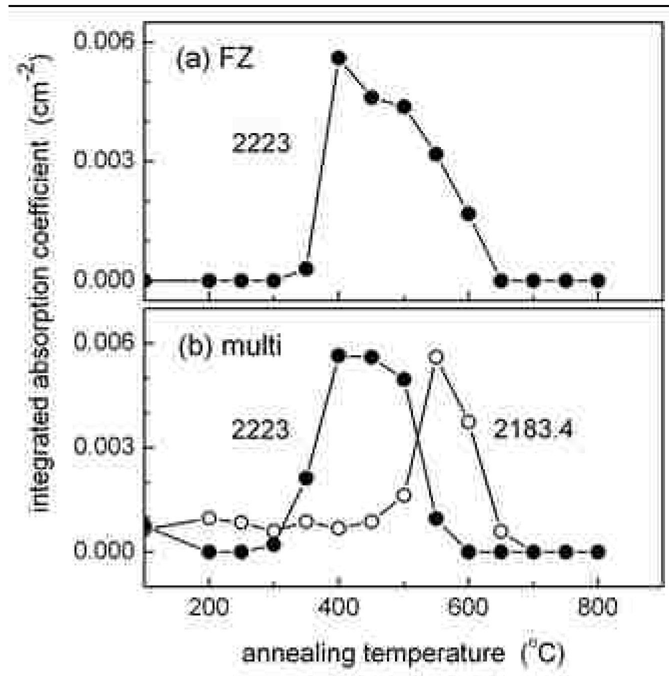

Figure 3.6 The isochronal (30 min) annealing dependence of the integrated intensities of the IR lines at 2223 and 2183.4 cm^{-1}. These hydrogen centers were produced by a thermal treatment (1250 °C, 1 hour) in an H_2 ambient. (a) is for a Si sample grown by the floating-zone method and with a carbon concentration of [C] = 0.2×10^{17} cm^{-3}. (b) is for a cast, mc-Si sample with a carbon concentration of [C] = 8.8×10^{17} cm^{-3}.

3.4.2 Theory

Our experiments suggest a VH_4 center trapped by C (i.e., a VH_3-HC center) as a candidate for the 2183.4, 2214.6, and 2826.9 cm^{-1} lines. Our collaborator, Prof. W. B. Fowler, has performed a theoretical analysis within this model, focusing on the shift of the 2214.6 cm^{-1} line to 2206.1 cm^{-1}, and to 2197.1 cm^{-1} observed as Si-H bonds are replaced by Si-D. A model was constructed that includes bond-bond coupling and the anharmonicity of the modes.[3.20]

Several theoretical approaches were used to study these defects. First-principles calculations using SIESTA[3.23] and CRYSTAL06[3.24] have been carried out on this defect and its isotopes to predict equilibrium configurations and vibrational frequencies. The vibrational frequencies determined from first-principles calculations agree only qualitatively with experiment because of anharmonic corrections. Peng *at al.* used these first-principles results to determine the magnitude of the Si-H, bond-bond, coupling constants. A model was then constructed to explain the vibrational properties of the VH_3-HC center that included two stretch force constants, two coupling force constants, and anhamonicity. The predictions resulting from a fit of this model to our data are shown in Table 3.1.

As can be seen from the results in Table 3.1, the positions of the Si-H stretching modes and their shifts for centers with Si-H bonds partially substituted by Si-D are reproduced by Fowler's model with near cm^{-1} accuracy.[3.25] The relaxed structure for the VH_3-HC center is shown in Figure 3.7[3.26].

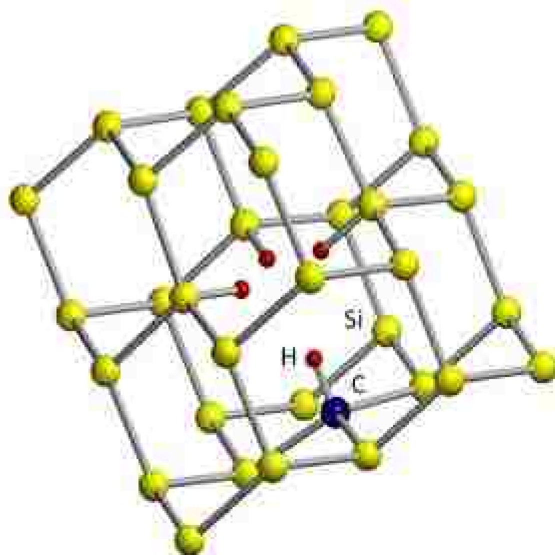

Figure 3.7 The structure (Ref. 26) of the VH_3-CH center predicted by CRYSTAL06 (Ref. 24). The C relaxes away from the vacancy by 0.29 Å, and each Si relaxes away by 0.18 Å. An H attached to Si is 1.83 Å from another H attached to Si, and it is 2.25 Å from the H attached to C.

The doublet structure of the Si-H modes is explained by the small shift in frequency that occurs when a C-H bond is substituted by C-D for a particular isotopic variant of the VH_3-HC center. Our results show the greater effect of substituting Si-D for Si-H than occurs for substituting C-D for C-H. This occurs primarily because the Si-H modes lie closer in frequency and interact more strongly than the Si-H and C-H modes. Furthermore, the relaxation of the C atom away from the vacancy that is found by theory (Figure 3.7) reduces the Si-H and C-H coupling because of the greater spatial separation of the H atoms.

Small upward shifts are seen in our spectra [Figure 3.4(b)] for the C-H line of the $VH_{3-n}D_n$-HC centers as n increases from 0 to 3 to give rise to 4 closely spaced C-H lines. This C-H line structure provides further strong support for our VH_3-HC assignment. However, these small shifts (~0.7 cm^{-1}) are not predicted by Fowler's model calculations and may arise from anharmonic coupling effects that are not included in the theory.

In addition to the Si-H and C-H lines that have been observed in our experiments for the VH_3-HC center and its isotopic siblings, the existence of corresponding Si-D and C-D stretching modes is anticipated. However, we have searched for these vibrational lines in our spectra without success. Fortunately, two of these lines were observed by Pajot et al.[3.8] in their study of silicon crystals grown in H_2 or D_2. A search of their table of H and D lines not attributed to specific defect structures reveals the Si-D and C-D modes of the VD_3-DC structure that correspond to the 2183.4, 2214.6 and 2826.9 cm^{-1} lines of VH_3-HC. The positions of the D-shifted lines for the 2183.4 and 2826.9 cm^{-1} lines are at 1587.8 and 2105.1 cm^{-1}.

3.5 Conclusion

We have studied the interaction of H with C in mc-Si. In addition to the IR lines assigned previously to $H_2^*(C)$ and $(CH)_2$ centers,[9-11] vibrational lines at 2183.4 and 2826.9 cm^{-1} are produced when a hydrogenated sample is annealed near 550 ℃.

Our spectroscopic results reveal that the 2183.4 and 2826.9 cm^{-1} lines give rise to a complicated line structure when D is partially substituted for H. Furthermore, a weak line at 2214.6 cm^{-1} was found. The vibrational line structures we have observed are too complicated to be consistent with a defect containing only two H atoms.

Theory shows that a VH_3-HC center explains the rich vibrational spectra that are seen when D is partially substituted for H. The splitting of the defect's Si-H modes is explained well by a model that accounts for the coupling of the Si-H bonds. The Si-H lines are also split into closely spaced doublets. Theory shows that these small splittings occur when a C-D bond is substituted for C-H in a particular isotopic variant of the VH_3-HC center.

The C-H line of the VH_3-HC center shifts by a few tenths of a cm^{-1} to higher frequency when Si-D bonds are substituted for Si-H. There are four components, a finding that provides further strong support for our assignment of the 2183.4, 2214.6, and 2826.9 cm^{-1} lines to the Si-H and C-H stretching modes of a VH_3-HC center.

Our experimental results and their analysis by Fowler and coworkers establish that one of the more thermally stable hydrogen-related centers in silicon containing a high concentration of carbon is a VH_4 center trapped by a carbon impurity.

3.6 Acknowledgement

The work performed at Lehigh University has been supported by NSF Grant No. DMR 0802278, an NSF REU site grant, and the Silicon Solar Research Center SiSoC Members through NCSU Subaward No. 2008-0519-02.

I also would like to thank Michael Stavola, Chao Peng, W. Beall Fowler, Stefan K. Estreicher, Andris Docaj, Lode Carnel and Mike Seacrist for their contributions to this work.

References

3.1 J. Hanoka, C. H. Seager, D. J. Sharp, J. K. G. Panitz, Appl. Phys. Lett. 42, 618 (1983).

3.2 A. G. Aberle, Sol. Energy Mater. Sol. Cells 65, 239 (2001) reviews the SiNx passivation of c-Si solar cells and includes a historical overview.

3.3 F. Duerinckx and J. Szlufcik, Sol. Energy Mater. Sol. Cells 72, 231 (2002).

3.4 A. Cuevas, M. J. Kerr, and J. Schmidt, Proceedings of the 3rd World Conference on Photovoltaic Energy Conversion, IEEE Cat. No. 03CH37497, Part 1 (Arisumi Printing Inc., Japan, 2003), p. 913.

3.5 S. Kleekajai, F. Jiang, M. Stavola, V. Yelundur, K. Nakayashiki, A. Rohatgi, G. Hahn, S. Seren, and J. Kalejs, J. Appl. Phys. 100, 093517 (2006).

3.6 C. Peng, H. Zhang, M. Stavola, V. Yelundur, A. Rohatgi, L. Carnel, M. Seacrist, and J. Kalejs, J. Appl. Phys. 109, 053517 (2011).

3.7 N. Fukata and M. Suezawa, J. Appl. Phys. 87, 8361 (2000).

3.8 B. Pajot, B. Clerjaud and Z.-J. Xu, Phys. Rev. B. 59, 7500 (1999).

3.9 P. Leary, R. Jones, S. Öberg, Phys. Rev. B 57, 3887 (1998).

3.10 V. P. Markevich, L. I. Murin, J. Hermansson, M. Kleverman, J. L. Lindström, N. Fukata, M. Suezawa, Physica B 302-303, 220 (2001).

3.11 B. Hourahine, R. Jones, S. Öberg, P. R. Briddon, V. P. Markevich, R. C. Newman, J. Hermansson, M. Kleverman, J. L. Lindström, L. I. Murin, N. Fukata, and M. Suezawa, Physica B 308-310, 197 (2001).

3.12 J. L. McAfee and S. K. Estreicher, Physica B 340-342, 637 (2003).

3.13 E. V. Lavrov, L. Hoffmann, B. Bech Nielsen, B. Hourahine, R. Jones, S. Öberg, and P. R. Briddon, Phys. Rev. B 62, 12859 (2000).

3.14 B. Bech Nielsen, L. Hoffman, and M. Budde, Mater. Sci. Engr. B 36, 259 (1996).

3.15 T. S. Shi, G. R. Bai, M. W. Qi, and J. K. Zhou, Mater. Sci. Forum 10-12, 597 (1986).

3.16 M. Suezawa, Phys. Rev. B 63, 035201 (2000).

3.17 G. R. Bai, M. W. Qi, L. M. Xie, and T. S. Shi, Solid State Commun. 56, 277 (1985).

3.18 I. A. Veloarisoa, M. Stavola, D. M. Kozuch, R. E. Peale, and G. D. Watkins, Appl. Phys. Lett. 59, 2121 (1991).

3.19 G. Davies and R. C. Newman, in *Handbook on Semiconductors*, Vol. 3B, Materials, Properties, and Preparation, edited by S. Mahajan and T. S. Moss (North-Holland, Amsterdam, 1994), p. 1557. The carbon concentration is related to the peak absorption coefficient at 607 cm^{-1}, A_{607} (in units cm^{-1}), by the relationship, $[C] = (1.0\times10^{17}\ cm^{-2})\ A_{607}$.

3.20 C. Peng, H. Zhang, M. Stavola, W. Beall Fowler, B. Esham, S. K. Estreicher, A. Docaj, L. Carnel, and M. Seacrist, Phys. Rev. B 84, 195205 (2011).

3.21 We also annealed the samples whose spectra are shown in Fig. 3 at 500 ℃ prior to the 550 ℃ treatment that was used to produce the 2183.4 cm^{-1} center. The 500 ℃ anneal produced the VH_4 center (without C) and its $VH_{4-n}D_n$ isotopic siblings. The relative intensities of the various $VH_{4-n}D_n$ lines in our samples were also examined to determine the relative concentrations of H and D.

3.22 In fact, the theoretical model for the vibrational properties of the VH_3-HC center predicted the existence of the 2214.6 cm^{-1} line which was subsequently found in our IR spectra.

3.23 P. Ordejón, E. Artacho, and J.M. Soler, Phys. Rev. B 53, 10 441 (1996);D. Sánchez-Portal, P. Ordejón, E. Artacho, and J.M. Soler, Int. J. Quantum Chem. 65, 453 (1997).

3.24 R. Dovesi, V. R. Saunders, C. Roetti, R. Orlando, C. M. Zicovich-Wilson, F. Pascale, B. Civalleri, K. Doll, N. M. Harrison, I. J. Bush, Ph. D'Arco, M. Llunell, Crystal06 User's Manual, University of Torino, Torino, 2006.

3.25 We also note the qualitative similarity of the Si-H modes predicted for the VH_3-HC center to the vibrational properties of the isolated VH_3 center that has the same symmetry and its isotopic siblings (Ref. 12). The Si-H lines of isolated VH_3, however, are not split into closely spaced doublets.

3.26 P. Ugliengo et al., Z. Kristallogr. 207, 9 (1993); P. Ugliengo, "MOLDRAW: A program to display and manipulate molecular and crystal structures," Torino, 2006, available on the web at http.//www.moldraw.unito.it.

Chapter 4: FTIR Studies of N in Si

4.1 Introduction

When silicon wafers for microelectronics applications are manufactured, nitrogen is sometimes intentionally added to control oxygen precipitation in Czochralski (CZ) silicon, to harden the silicon, and to affect the concentrations of native vacancies and interstitials[4.1]. Nitrogen is also present in multi-crystalline silicon. Nitrogen dissolves into multi-crystalline silicon from the quartz crucible, which is lined with silicon nitride to prevent the adhesion of silicon to the crucible wall.

Several N-related complexes have been reported in CZ silicon doped with nitrogen. The defects seen in the mid infrared range are N-N pairs and N-N pairs decorated by additional oxygen atoms. Another family of defects is the set of electrically active N-O-related shallow donors with a single nitrogen atom. These N-O centers can also be decorated by additional O atoms.

Multi-crystalline silicon has been found by SIMS measurements made by our collaborators at MEMC Electronic Materials to have a concentration of nitrogen up to 8×10^{15} cm^{-3}. This N concentration is approximately 4 times larger than is present in CZ Si where N has been deliberately introduced. Furthermore, SiN inclusions are also seen in mc-Si.

It is not known what N-containing point defects are present in mc-Si that contains an unusually large concentration of N or if this N interacts with other impurities also present in mc-Si. Addressing these questions are the goal of our work. What

N-centers are present in mc-Si and with what concentration? How does N interact with O and C that are also present in the mc-Si sample? Are any of these defect electrically active, and if so, with what concentration? This basic knowledge is intended to help our collaborators in the solar cell industry understand the defect properties of mc-Si materials that are widely used to fabricate solar cells.

4.2 Survey of nitrogen centers

Nitrogen in silicon was first studied in the 1950's. Kaiser and Thurmond reported that liquid silicon exposed to gaseous N_2 during crystal growth by the floating zone method may grow Si_3N_4 under certain conditions.[4.2]

Stein measured the infrared absorption of local vibrational modes due to N for Si samples that had been implanted with the nitrogen isotopes (^{14}N, ^{15}N) and also combinations of these isotopes. These results revealed that pairs of nitrogen atoms exist in silicon.[4.3] Two LVM absorption lines with IR frequencies (room temperature) of 963 cm^{-1} and 766 cm^{-1} were identified.

The structure of this nitrogen pair defect was subsequently determined by channeling, infrared local vibrational mode spectroscopy, and ab initio local density functional theory.[4.4] The structure of the nitrogen pair in the silicon lattice is shown in Figure 4.1. This structure consists of two N split-interstitial defects aligned in opposite directions. For the two IR active modes at 766 and 963 cm^{-1}, the two nitrogen atoms are dynamically coupled and move in the same direction, along the [001] or the [110] direction, respectively. The motions of the atoms that give these lines are shown in Figure 4.2(a) and Figure 4.2(b).

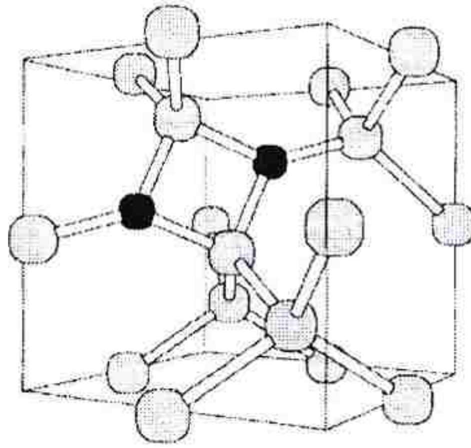

Figure 4.1 The structure of the N-N pair in the silicon lattice[4.5]

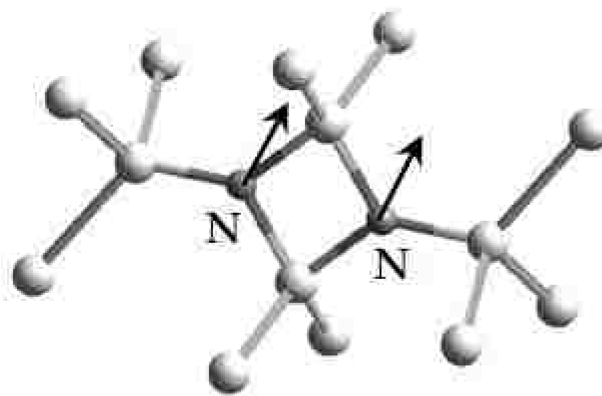

Figure 4.2(a) The 770 cm^{-1} (77K) N-N asymmetric stretching mode along the[001] direction[4.6]

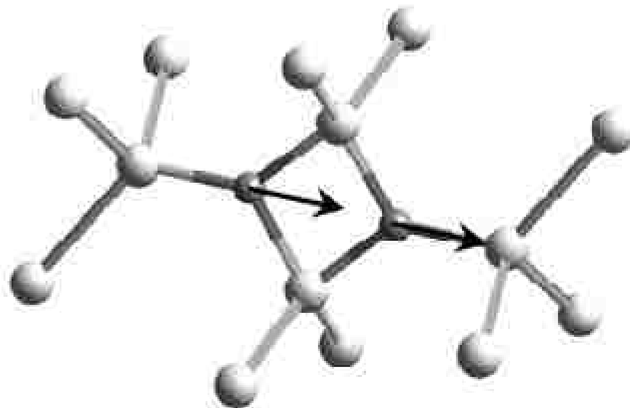

Figure 4.2(b) The 967 cm^{-1} (77K) N-N asymmetric stretching mode along the [110] direction[4.6]

In oxygen-free silicon grown by the floating-zone (FZ) method, the nitrogen di-interstitial pair is the dominant nitrogen center that exists. Itoh et al. used the absorption coefficient of the N-pair line at 963 cm^{-1} to measure the nitrogen concentration in silicon.[4.7] They compared the correlation plot, absorption coefficient vs. nitrogen concentration, for FZ and CZ silicon samples with different N concentrations. A comparison of FZ and CZ samples is shown in Figure 4.3. For these plots, the N concentration was determined independently by neutron activation analysis.

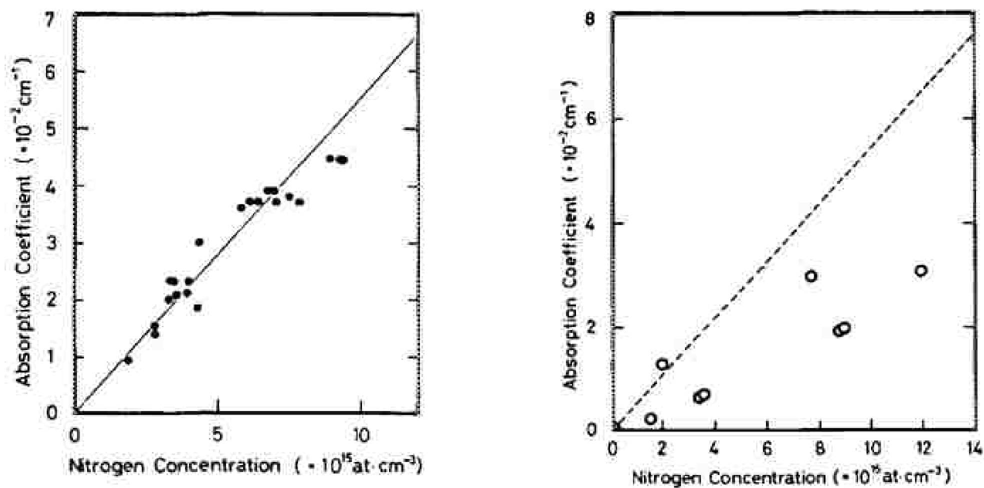

Figure 4.3 A comparison between FZ and CZ samples of correlation plots, IR absorption coefficient at 963 cm^{-1} for the N-N pair center vs. the nitrogen concentration determined independently.[4.7]

For the FZ samples with different N concentrations, a calibration curve can be drawn that relates the absorption coefficient at 963 cm^{-1} to the N concentration. However, the corresponding absorption coefficient data from the CZ sample lie

below the calibration curve. A comparison of the IR results for FZ and CZ samples shows that CZ silicon contains nitrogen defects other than the N-pairs that give rise to the 963 cm^{-1} line.

In oxygen-rich CZ silicon, a series of additional LVM absorption lines was found in the mid IR.[4.8] These IR lines have been assigned to the nitrogen pair with additional interstitial oxygen atoms bonded nearby to form NNO_x (x=1, 2) centers. A representative structure is shown in Figure 4.4.

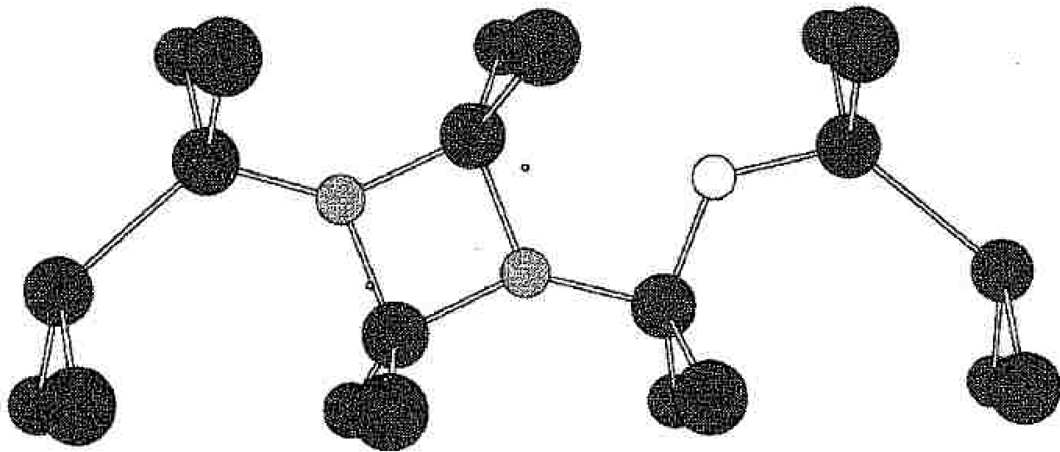

Figure 4.4 N-N pair with an additional O atom bonded nearby[4.9]

The complexes of nitrogen with oxygen have been found to be formed in CZ silicon during long anneals (several hours) at temperatures near 600 ℃ to 650 ℃.[4.10] These complexes are dissociated by anneals at temperatures between 800 ℃ and 1000 ℃.

Many of the N-O defects have been assigned by Alt and coworkers.[4.11] The difference of spectra measured for a sample annealed near 1000 ℃ and a sample annealed near 650 ℃ reveals the IR peaks that are changed by these annealing treatments. This is a convenient strategy for identifying weak IR features due to nitrogen and oxygen and for separating these features from silicon background absorption that is not affected by annealing. Such difference spectra are shown in Figure 4.5. Upward going peaks are due to N-N centers whose concentration is increased by annealing at 1000 ℃. Downward going peaks are due to N-O centers formed by annealing near 600 ℃ and then removed by the subsequent anneal at higher temperature. Table 4.1 shows the assignments of the N-O defects with their peak positions.

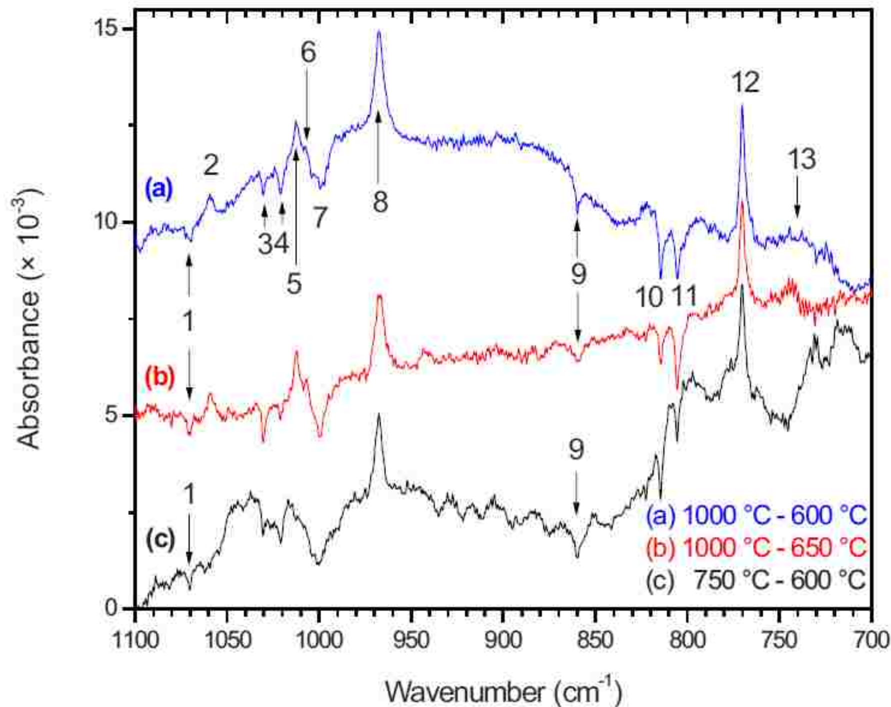

Figure 4.5 Difference spectra for nitrogen and oxygen containing defects in silicon, measured in a boron-doped CZ silicon sample with a N concentration between ~10^{14} and 1.4×10^{15} cm^{-3} and an O concentrations of about 7×10^{17} cm^{-3}.[4.11]

Number	Defect	Peak position (cm^{-1})
1	NO_2 (N–O–3)	1070
2	O_{2i} (O_i dimer)	1060
3	NNO	1031
4	NNO_2	1021
5	O_{2i} (O_i dimer)	1012
6	O_{3i} (O_i trimer)	1007
7	NNO	1000
8	NN	967
9	NO_2 (N–O–3)	860
10	NNO_2	815
11	NNO	805
12	NN	770
13	?	739

Table 4.1 Assignments of nitrogen and oxygen containing defects shown in Figure 4.5[4.11]

Electrically active nitrogen-oxygen complexes have also been studied in CZ silicon that contains nitrogen and oxygen impurities. Suezawa et al. observed the electronic transition of the nitrogen-oxygen complexes in the far IR (shown in Figure 4.6).[4.12] Group I lines are associated with 1s to $2p_0$ transitions and group II lines are associated with 1s to $2p_{\pm}$ transitions.

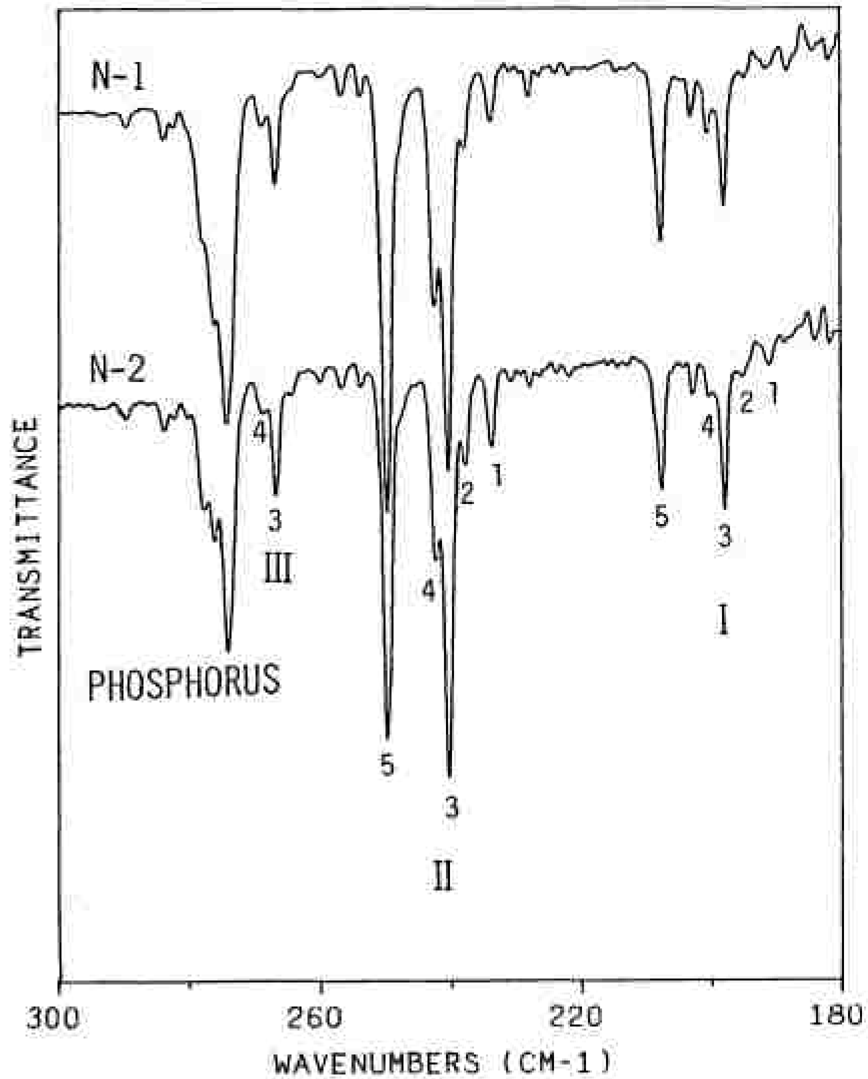

Figure 4.6 Absorption spectra showing electronic transitions of N-O_n complexes in Si[4.12]

Alt et al. have further investigated the far IR absorption spectra of the nitrogen-oxygen shallow donors.[4.11] As is shown in Figure 4.7, different groups of shallow donors were again detected. A heat treatment at 1000 ℃ caused the nitrogen-oxygen shallow donor centers to be annealed away. A subsequent annealing treatment at 650 ℃ regenerated these IR lines.

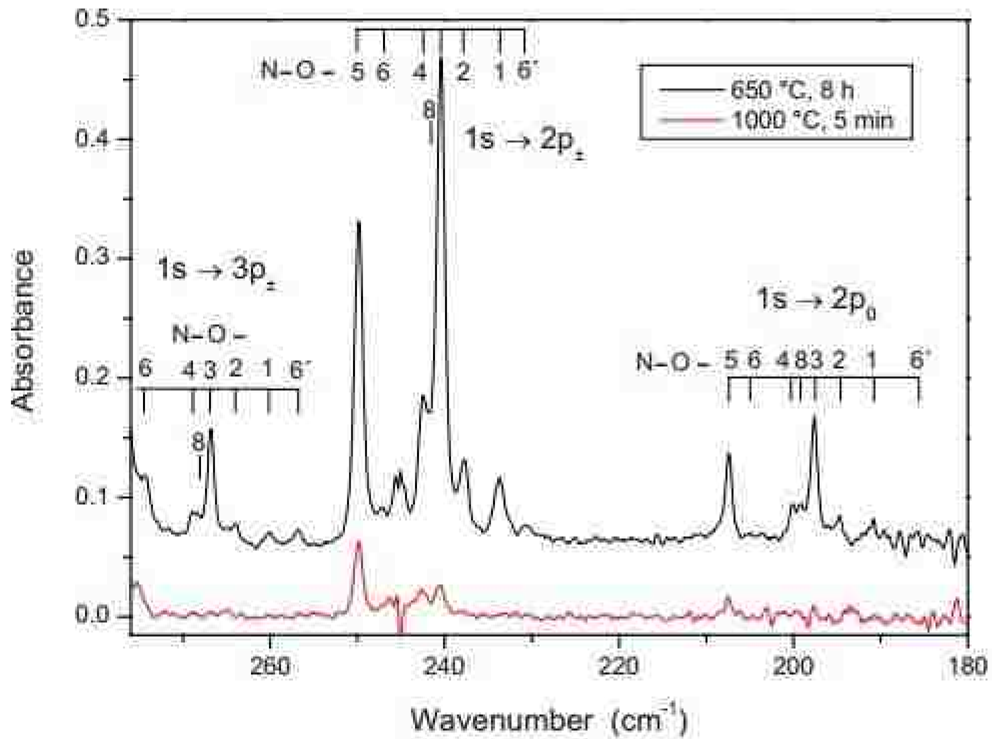

Figure 4.7 Nitrogen-oxygen shallow donor centers seen in far IR absorption spectra of CZ silicon that contains N impurities[4.11]. The spectrum shown in black is for a sample annealed at 650 °C. The spectrum shown in red is for a sample annealed at 1000 °C.

The spectrum for an individual shallow donor center would show hydrogenic transitions $1s \rightarrow 2p_0$, $1s \rightarrow 2p_\pm$, etc. The spectra shown in Figures 4.6 and 4.7 are complicated because there are several different N-O centers with different configurations and slightly different 1s ground state energies. The transitions for as many as 8 different centers have been reported. Group I lines are associated with the $1s \rightarrow 2p_0$ transition, group II lines are associated with the $1s \rightarrow 2p_\pm$ transition, and group III lines are associated with the $1s \rightarrow 3p_\pm$ transition. Table 4.2

shows the frequencies for the $1s \rightarrow 2p_{\pm}$ transitions of the family of shallow N-O donors.

STD	NO-1	NO-2	NO-3	NO-4	NO-5	NO-6	NO-6'	NO-8
$1s \rightarrow 2p_{\pm}$ freq. (cm^{-1})	**233.8**	**237.8**	**240.4**	**242.5**	**249.8**	**247.0**	**230.6**	**241.5**

Table 4.2 The frequencies of the $1s \rightarrow 2p_{\pm}$ transitions of the family of N-O shallow thermal donors (STDs) in Si.[4.13]

4.3 Mid IR spectra of nitrogen centers in multi-crystalline silicon

We measured IR absorption spectra for six multi-crystalline silicon samples provided by MEMC Electronic Materials in the mid-IR range from 400 cm^{-1} to 1200 cm^{-1} to probe N-related defects and to determine the concentrations of carbon and oxygen. We measured the absorption coefficient spectra (room temperature) shown in Figures 4.8(a) to 4.8(f). The strong absorption lines due to carbon at 605 cm^{-1} and oxygen at 1104 cm^{-1} are seen for samples that are 2 mm thick. The two weak N-N lines at 766 and 963 cm^{-1} are seen for samples that were 5 mm thick and are shown in the insets.

The absorption coefficients for the light elements C, O, and N have been calibrated so that the concentrations of substitutional C, interstitial O, and the N-N pair can be determined from the peak absorption coefficients of their IR lines. The concentration of carbon is 1×10^{17} cm^{-2} times the absorption coefficient at 605 cm^{-1}.[4.14] The concentration of interstitial oxygen is 3.15×10^{17} cm^{-2} times the absorption coefficient at 1104 cm^{-1}.[4.15] The concentration of the N-N pair is 1.83 $\times 10^{17}$ cm^{-2} times the absorption coefficient at 963 cm^{-1}.[4.7]

As an example, the multi-crystalline silicon sample LDK B2, whose spectra are shown in Figure 4.8(b), has a carbon concentration of 6×10^{17} cm^{-3}, an oxygen concentration of 3.2×10^{17} cm^{-3}, and a nitrogen-pair concentration of 4.2×10^{15} cm^{-3}.

Table 4.3 shows data for the concentrations of the light elements for all 6 samples from MEMC. Concentrations of C and O measured by FTIR at MEMC are given in units parts per million atomic (ppma). Results for C and O determined from the spectra measured at Lehigh shown in Figure 4.8(a)-(f) are given in units atoms/cm^3. The units conversion is 2 ppma = 1×10^{17} cm^{-3}. Results for O measured at Lehigh and at MEMC are in reasonable agreement. The discrepancies for the concentrations of C measured at Lehigh and MEMC are substantial, i.e., these results can differ by a factor of 2. We point out that it is difficult to accurately measure the strengths of the strong absorption lines due to C in samples 2 mm thick.

The concentration of N provided by MEMC in Table 4.3 was determined by secondary ion mass spectrometry (SIMS) and reflects the total nitrogen concentration in the sample. The concentration of N determined at Lehigh by FTIR reflects the concentration of N-N pair centers that give rise to the IR line at 963 cm^{-1} so the nitrogen concentration measured by IR should be less than the N concentration measured by SIMS, consistent with the results shown in Table 4.3.

Samples listed in Table 4.3 from the same brick of mc-Si have labels with the same prefix, LDK, for example. The suffix T2 indicates that a sample is from the top of a brick; the suffix B2 indicates that a sample is from the bottom of a brick.

The concentrations of O and C follow trends that are well known in mc-Si ingots that are solidified from the bottom up. The oxygen concentration is highest at the bottom of an ingot, whereas the carbon concentration is highest at the top of an ingot.

Sample	[C] – a (at•cm^{-3}) Lehigh	[C] – b (ppma) MEMC	[O] – a (at•cm^{-3}) Lehigh	[O] – b (ppma) MEMC	[N] – a (at•cm^{-3}) Lehigh	[N] – b (at•cm^{-3}) MEMC
LDK T2	8.2×10^{17}	8.6	1.0×10^{17}	0.6	3.3×10^{15}	2×10^{16}
LDK B2	6.0×10^{17}	4.3	3.2×10^{17}	4.2	4.2×10^{15}	7×10^{15}
A8 T3	4.6×10^{17}	5.6	1.2×10^{17}	3.1	2.0×10^{15}	4.7×10^{15}
A8 B3	1.2×10^{17}	1.6	4.7×10^{17}	7.4	0.5×10^{15}	2.7×10^{15}
E8 T3	2.3×10^{17}	2.5	1.3×10^{17}	0.5	3.7×10^{15}	7.9×10^{15}
E8 B3	0.3×10^{17}	0.5	0.6×10^{17}	0.8	3.5×10^{15}	5.7×10^{15}

Table 4.3 Concentrations of C, O and N from FTIR measurements at Lehigh and from the MEMC Company

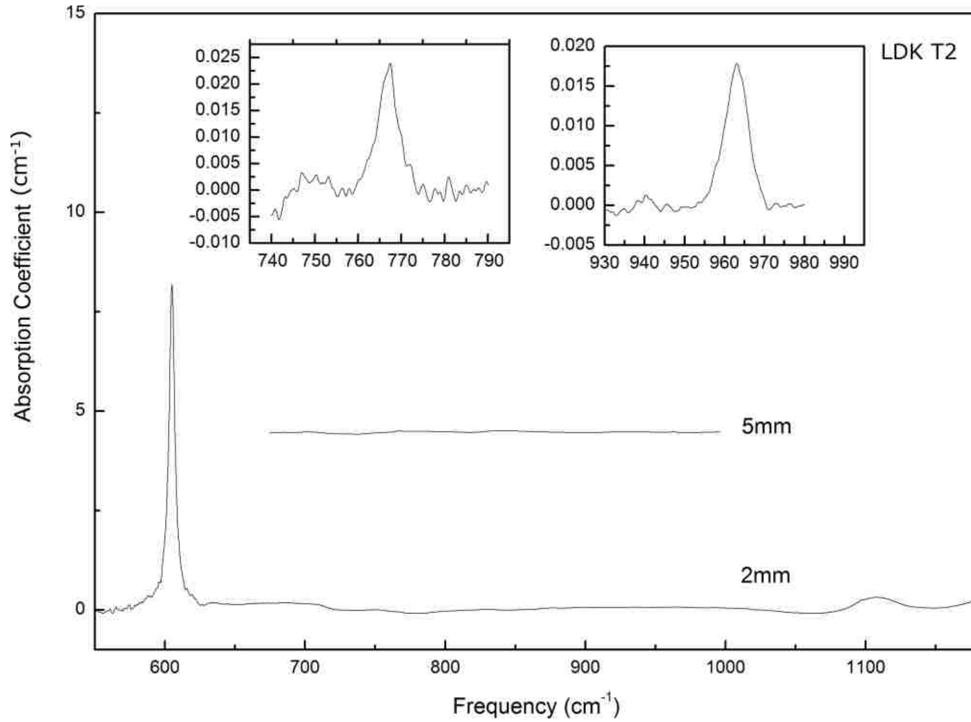

Figure 4.8(a) Room temperature IR spectra from sample LDK T2 with thicknesses of 2mm and 5mm. Spectra of the N-N pair lines are shown in the insert.

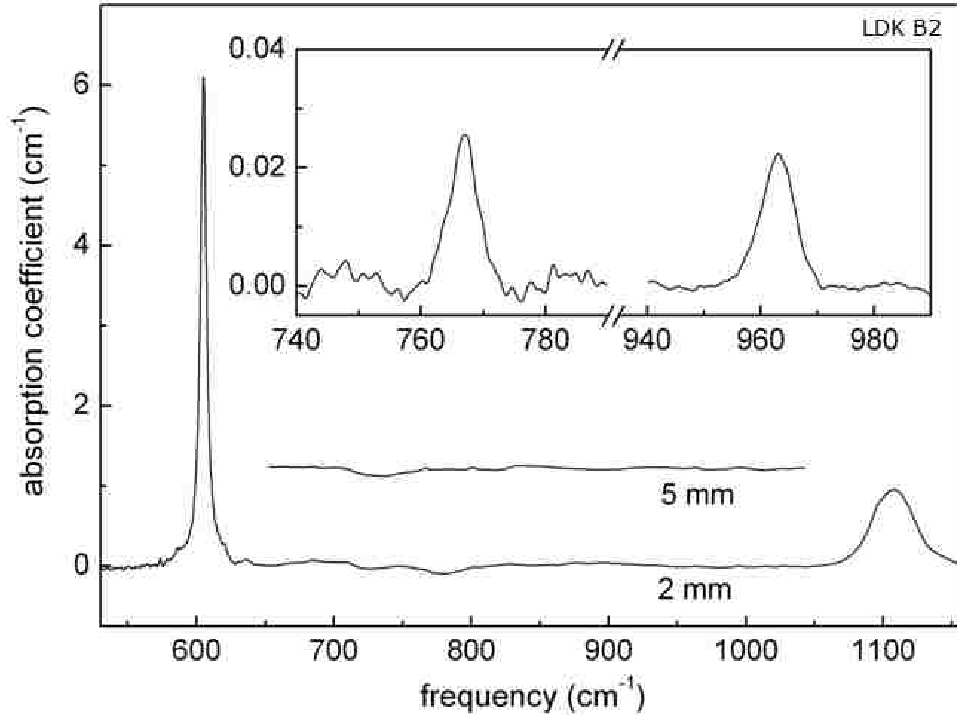

Figure 4.8(b) Room temperature IR spectra from sample LDK B2 with thicknesses of 2mm and 5mm. Spectra of the N-N pair lines are shown in the insert.

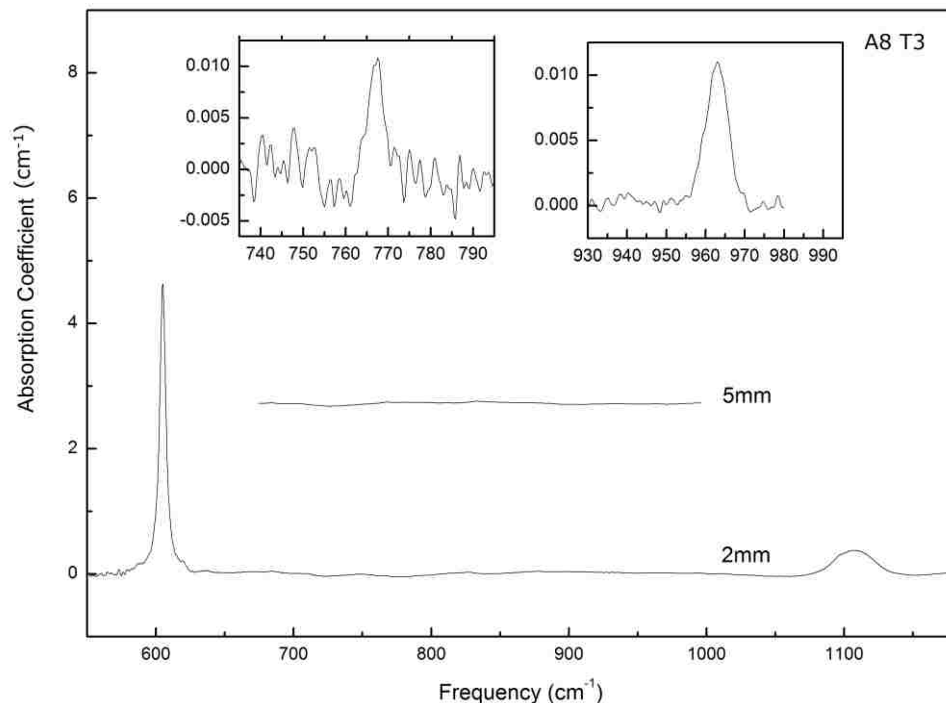

Figure 4.8(c) Room temperature IR spectra from sample A8 T3 with thicknesses of 2mm and 5mm. Spectra of the N-N pair lines are shown in the insert.

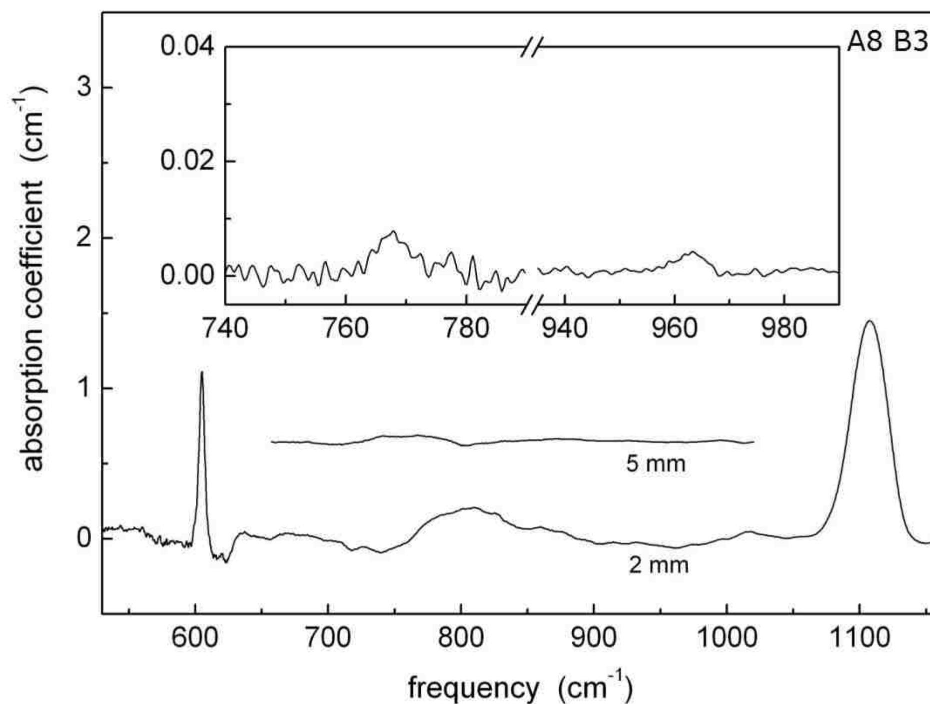

Figure 4.8(d) Room temperature IR spectra from sample A8 B3 with thicknesses of 2mm and 5mm. Spectra of the N-N pair lines are shown in the insert.

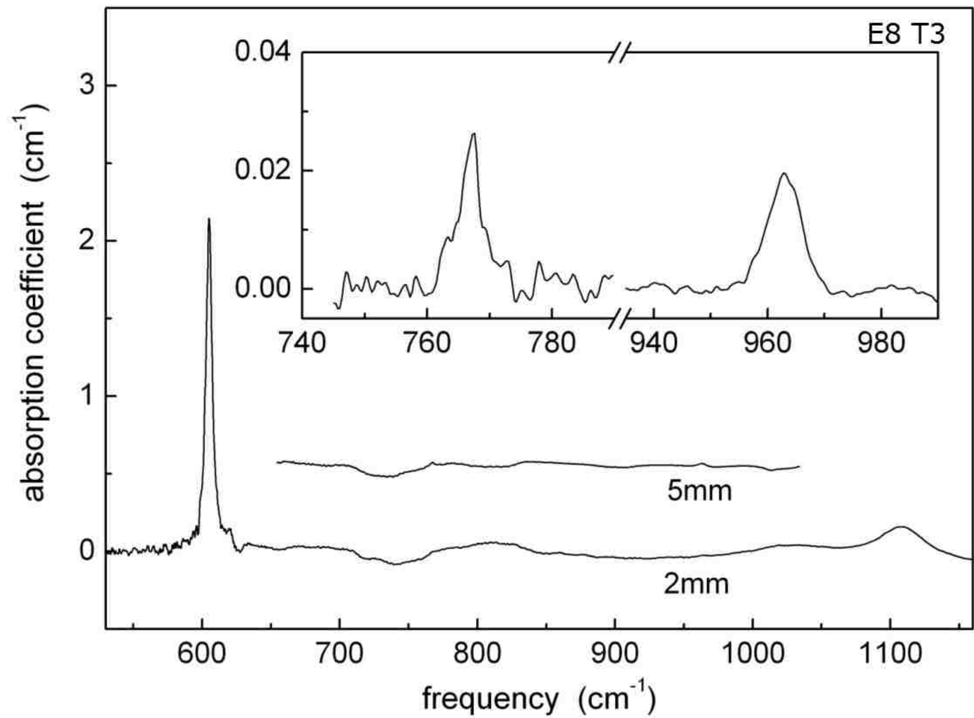

Figure 4.8(e) Room temperature IR spectra from sample E8 T3 with thicknesses of 2mm and 5mm. Spectra of the N-N pair lines are shown in the insert.

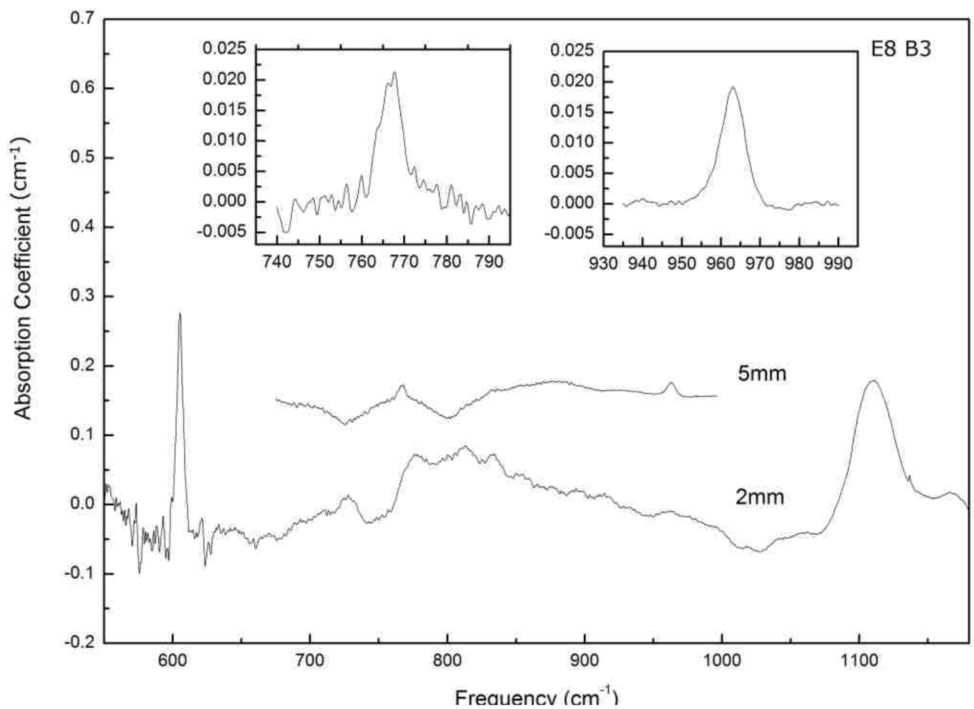

Figure 4.8(f) Room temperature IR spectra from sample E8 B3 with thicknesses of 2mm and 5mm. Spectra of the N-N pair lines are shown in the insert.

The vibrational line for the N-N defect at 963 cm^{-1} at room temperature narrows and increases in height when the temperature is lowered. Figure 4.9 compares spectra for sample LDK B2, annealed at 1000 ℃ for 30 min, that were measured at room temperature and at 77K. The N-N line shifts to 967 cm^{-1} and its peak height is found to be increased by a factor of 1.56. From the calibration of the 963 cm^{-1} line (room temperature) determined by Itoh *et al.*, our results find the calibration of the 967 cm^{-1} line (77K) to be:

$$[N] = 1.2\times10^{17}\ cm^{-2}\ \alpha_{967}\ (77K).$$

From the noise in the baseline of our IR data measured at 77K, we estimate that the detection limit for N measured with the N-N line at 967 cm^{-1} is 2×10^{14} cm^{-3} for a multi-crystalline sample with thickness 5 mm.

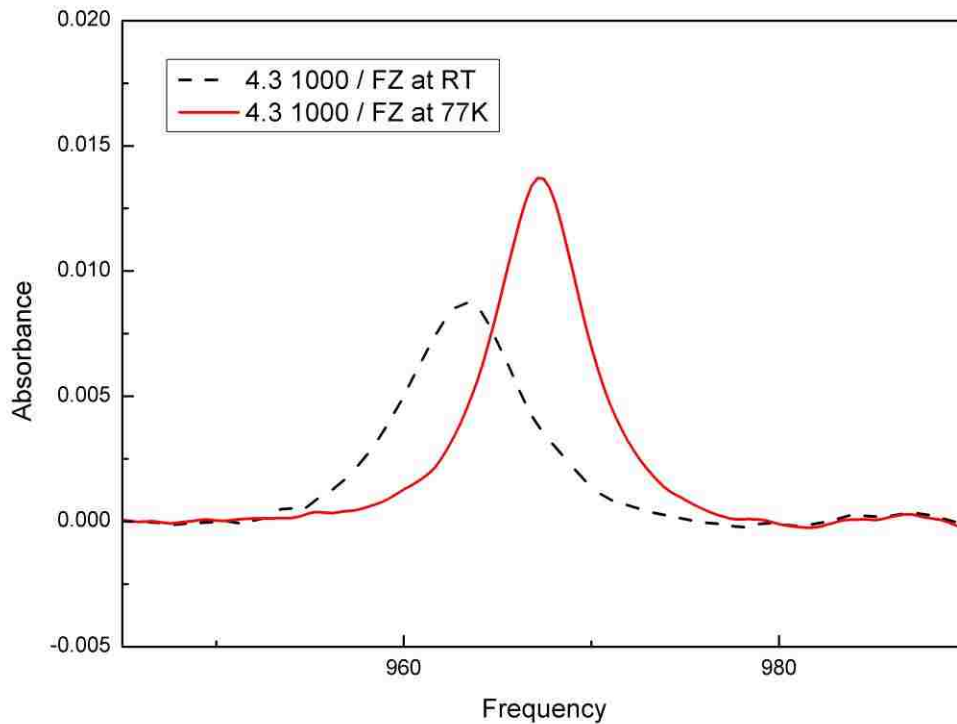

Figure 4.9 Absorbance spectra for sample LDK B2, annealed at 1000 °C, measured at both room temperature and 77 K.

We have measured IR spectra at 77K for the six mc-Si samples with different impurity content that had been provided by MEMC. Spectra for the 967 cm^{-1} line are shown in Figure 4.10 for as-solidified samples and for pieces of the same samples annealed at 1000 ℃. An absorbance spectrum calculated from these spectra reveals the differences between as-solidified and annealed samples. The concentrations of N-N centers determined from each of these spectra along with the differences produced by annealing are listed in Table 4.4.

Trends in our data can be seen.

(1) Annealing an as-solidified sample at 1000 ℃ causes the N-N line to increase in intensity compared to an as-solidified sample for some samples, but not others.

(2) The % increase of the N-N line's intensity is greatest for samples from the bottom of a mc-Si brick where the oxygen concentration is greatest. Samples LDKB2 and A8B3 with highest [O] show the greatest % change in the 967 cm^{-1} line intensity upon annealing at 1000 ℃. For samples with low oxygen concentrations, the change in the 967 cm^{-1} line's intensity upon annealing at 1000 ℃ is barely detectable.

These trends are consistent with the presence of NN-O_n complexes in samples in their as-solidified state, similar to the situation found for N in oxygen-rich, CZ-grown Si. These complexes are dissociated by an anneal at 1000 ℃, increasing the fraction of N in the form of isolated N-N centers that gives rise to the 967 cm^{-1} line.

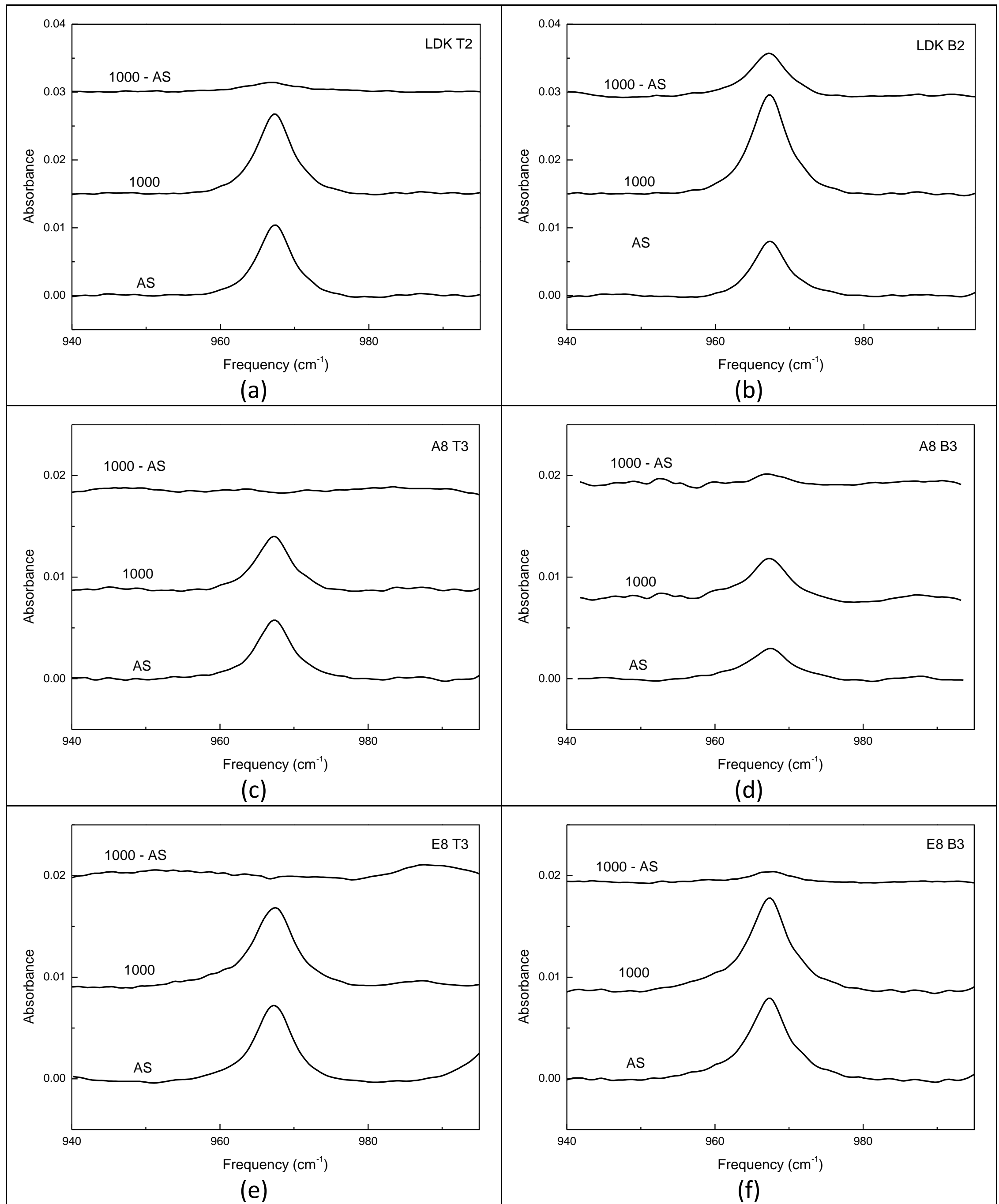

Figure 4.10 IR spectra (77K) for the line at 967 cm^{-1} due to N-N centers in Si. These results are for mc-Si samples provided by MEMC. Spectra are shown for samples in their as-solidified state, after an anneal at 1000°C, and for the difference of these results.

Table 4.4 Absorption coefficients and N concentrations for mc-Si samples obtained from MEMC determined from the IR data shown in Figure 4.10.

sample	α_{1000} (cm^{-1})	$[N]_{1000}$ (at•cm^{-3})	α_{AG} (cm^{-1})	$[N]_{AG}$ (at•cm^{-3})	$\Delta\alpha$ (cm^{-1})	$\Delta[N]$ (at•cm^{-3})
a. LDK T2	0.0536	6.3×10^{15}	0.0477	5.6×10^{15}	0.0046	0.5×10^{15}
b. LDK B2	0.0667	7.8×10^{15}	0.0377	4.4×10^{15}	0.0265	3.1×10^{15}
c. A8 T3	0.0240	2.8×10^{15}	0.0267	3.1×10^{15}	0	0
d. A8 B3	0.0177	2.1×10^{15}	0.0136	1.6×10^{15}	0.0038	0.4×10^{15}
e. E8 T3	0.0350	4.1×10^{15}	0.0333	3.9×10^{15}	0	0
f. E8 B3	0.0411	4.8×10^{15}	0.0363	4.2×10^{15}	0.0044	0.5×10^{15}

Figure 4.11 shows data for the absorption coefficient of the line associated with the N-N pair plotted vs the N concentration determined independently. The vertical scale on the right is for the absorption coefficient of the N-N pair line at 963 cm^{-1} measured at room temperature. The dashed line is the calibration line determined by Itoh *et al.* for the N-N pair center in FZ Si. The open circles are the data points reported by Itoh *et al.* for CZ Si (shown also in Figure 4.3), referenced to the vertical scale shown on the right.

The left vertical scale in Figure 4.11 is for the absorption coefficient of the N-N pair line at 967 cm^{-1} measured at 77K, scaled by a factor so that it corresponds also to the absorption coefficient scale shown on the right. That is, the left scale is related to the right scale by the factor 1/1.56 determined from the IR data in Figure 4.9. The open squares shown in Figure 4.11 are for the absorption coefficient at 967 cm^{-1} measured at 77K (Table 4.4) plotted vs the N concentration determined by SIMS for the mc-Si samples from MEMC in their as-solidified condition. (We have chosen to plot IR data measured at 77K because the N-N concentration can

be determined more accurately from the sharper N-N IR line at 967 cm^{-1} measured at 77K than from the corresponding line at 963 cm^{-1} measured at room temperature.) The absorption coefficient data for the N-N center from as-solidified multi-crystalline silicon are similar to those for CZ silicon. These results indicate that a portion of the nitrogen impurities is involved in structures other than the N-N pair. (There is one anomalous data point that suggests a very high N concentration for sample LDK T2. Multi-crystalline samples are inhomogeneous and can contain Si-N inclusions. The localized ion beam used for the SIMS measurement may have probed an N-rich spot on the sample to give this anomalous data point.)

We annealed the multi-crystalline Si samples at 1000 ℃ and measured the absorption coefficient at 967 cm^{-1} at 77K to obtain the data shown in Table 4.4. For several of these samples, the absorption coefficient at 967 cm^{-1} was increased by the annealing treatment. These data are shown by open triangles (in Figure 4.11). These results are consistent with the dissociation of NN-O_n centers to produce an increased concentration of the isolated N-N pair. We note that the samples that showed little change upon annealing at 1000 ℃ (the samples A8 T3, E8 T3, and E8 B3 with [N] = 4.7×10^{15}, 7.9×10^{15} and 5.7×10^{15} cm^{-3}, respectively) had a low concentration of oxygen.

Several of our data points in Figure 4.11 for samples annealed at 1000 ℃ fall close to the line measured by Itoh *et al.* for N in oxygen-free Si grown by the floating zone method. This result suggests that the N-N center is dominant in samples that have been annealed at 1000 ℃ in Figure 4.11. Furthermore, the nitrogen

concentration determined here by SIMS appears to be in reasonable agreement with the N concentration determined by Itoh *et al.* by neutron activation analysis.

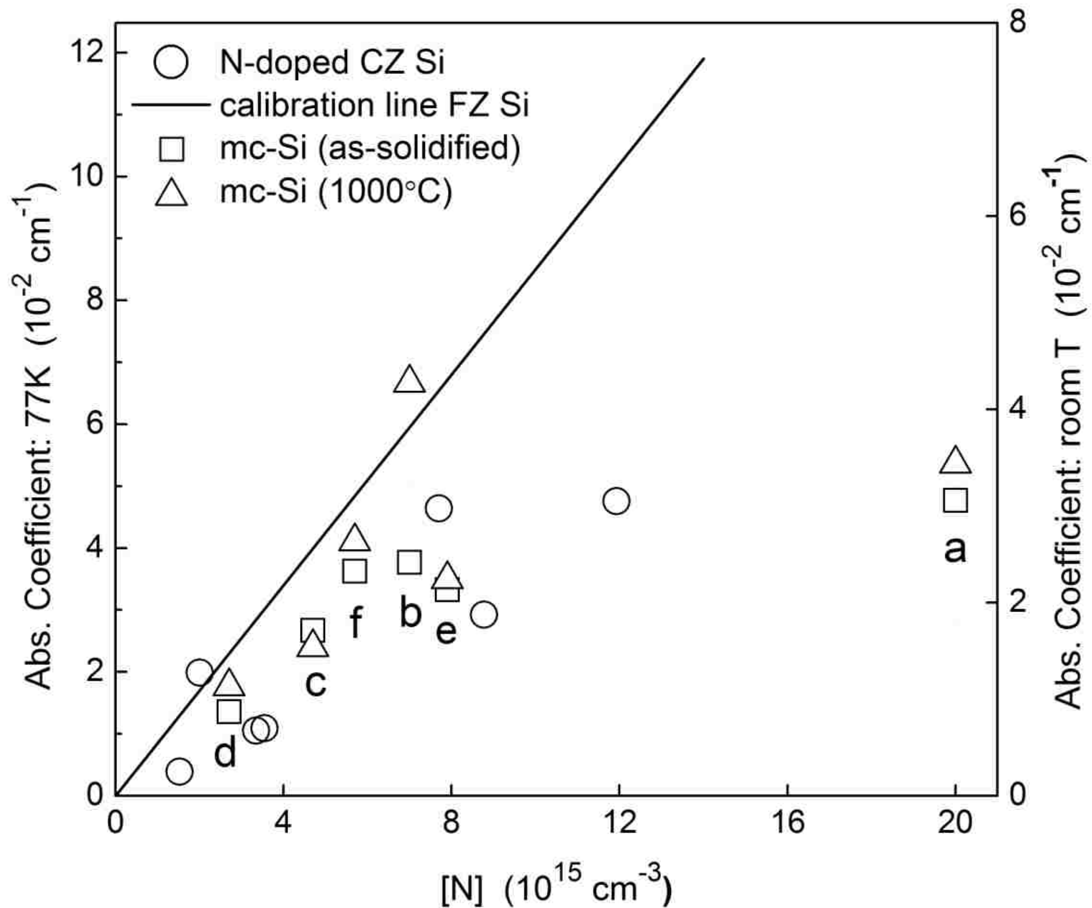

Figure 4.11 Calibration line for FZ silicon (solid line), data for CZ silicon taken from Itoh *et al.* (circles, right scale), and data for multi-crystalline silicon that combine absorption coefficients for the 967 cm^{-1} line measured at Lehigh (77K, left scale) with SIMS data for the N concentration provided by MEMC (squares). The absorption coefficient for the 967 cm^{-1} line is increased by an anneal at 1000 °C (triangles, left scale). Points for different samples are labeled with letters according to the labels in Figure 4.10.

IR spectra measured at 77K for mc-Si samples also reveal the NN-O_n centers that are present. Figure 4.12 shows spectra measured at 77K for the six mc-Si samples obtained from MEMC. We focus first on panel (b) for sample LDKB2 where the concentration of N-N defects complexed with oxygen is greatest.

These results establish that N-N centers are involved in complexes with O to form NN-O_n defects. The intensity of the 967 cm^{-1} line in sample LDK B2 annealed at 1000 ℃ shows that the concentration of N is 7.8×10^{15} cm^{-3} (Table 4.4). In the as-grown sample, approximately 60% of the N is in the form of N-N centers, meaning that 40% is complexed with oxygen.

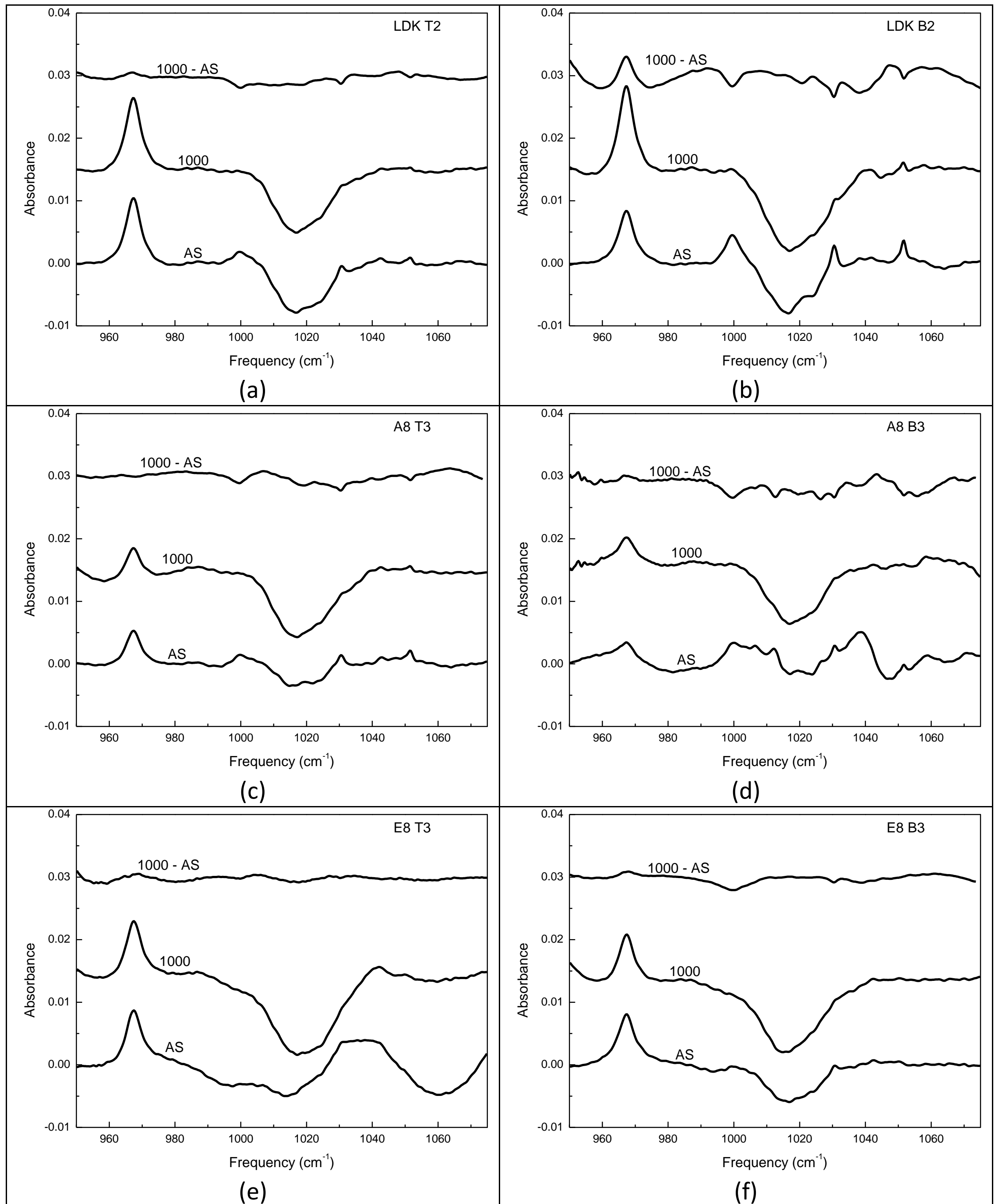

Figure 4.12 IR spectra (77K) due to NN-O_n centers in Si. These results are for mc-Si samples provided by MEMC. Spectra are shown for samples in their as-solidified state, after an anneal at 1000°C, and for the difference of these results.

A detailed difference spectrum for the sample LDK B2 annealed at 1000 ℃ minus the spectrum for the as-grown sample is shown in Figure 4.13 over a wide spectral range. Labels for the IR lines are given according to Table 4.1 to assign the N-related structures.

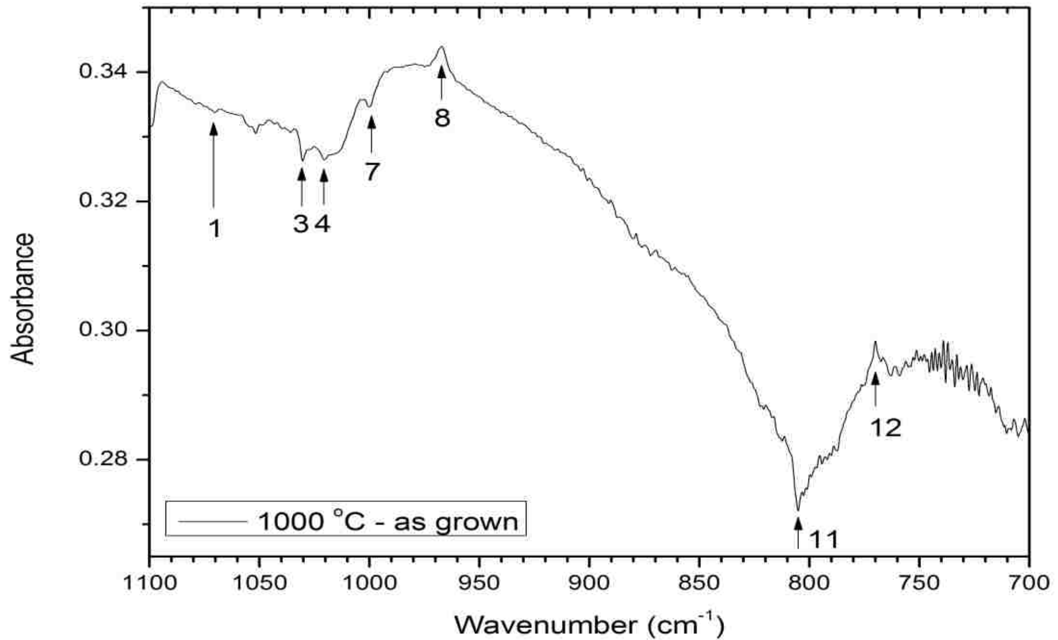

Figure 4.13 A difference spectrum for the multi-crystalline silicon sample LDK B2. Upward going lines are due to NN defects. Downward going lines are due to nitrogen-oxygen complexes removed by the anneal at 1000 °C. Assignments of lines are given in Table 4.1.

Figure 4.12, panel a, shows absorbance spectra for sample LDK T2 measured at 77 K. The intensity of the 967 cm^{-1} line in this sample annealed at 1000 ℃ shows that the concentration of N is 6.3×10^{15} cm^{-3}. In an as-grown sample, approximately 90% of the N is in the form of N-N centers and 10% is complexed with oxygen. Table 4.3 shows that the oxygen concentration for sample LDK B2 is 3.2×10^{17} cm^{-3} whereas for sample LDK T2 the oxygen concentration is [O] =

1.0×10^{17} cm^{-3}. The different oxygen concentrations in the samples are consistent with a greater concentration of NN-O_n centers in sample LDK B2.

Similarly, for sample A8 B3 with [O] = 4.7×10^{17} cm^{-3}, the results in Table 4.4 show that approximately 75% of the N in the sample is in the form of N-N centers and that 25% is involved in complexes with oxygen. For sample A8 T3, with its smaller oxygen content of [O] = 1.2×10^{17} cm^{-3}, near 100% of the N is in the form of N-N centers.

The oxygen concentration is small in both samples E8 B3 and E8 T3. In this case, Table 4.4 shows that approximately 90% or more of the N is in the form of N-N centers.

The N- and O-containing centers in the samples from MEMC, detected in difference spectra, 1000 ℃ – as solidified, are compared in Figure 4.14. Table 4.3 shows that sample LDK B2 contains relatively high N and high O. The spectrum in Figure 4.14 shows the NN-O center (1000 and 1031 cm^{-1}), and even NN-O_2 centers (1021 cm^{-1}). Sample A8 B3 contains the highest [O] of the set of samples and lower [N] than LDK B2. In this case NN-O and NN-O_2 centers are seen, but now centers containing only oxygen are also present [that is, the defects O_2 (1012 and 1060 cm^{-1}) and O_3 (1007 cm^{-1})]. Samples from the tops of bricks (LDK T2 and A8 T3) with their reduced oxygen content do not show the centers with O alone and modest concentrations of the NN-O defect. Finally, samples E8 T3 and E8 B3 both have substantial N concentrations but little O. Annealing treatments cause only small changes in the concentration of the N-N defect due to the formation of NN-O complexes.

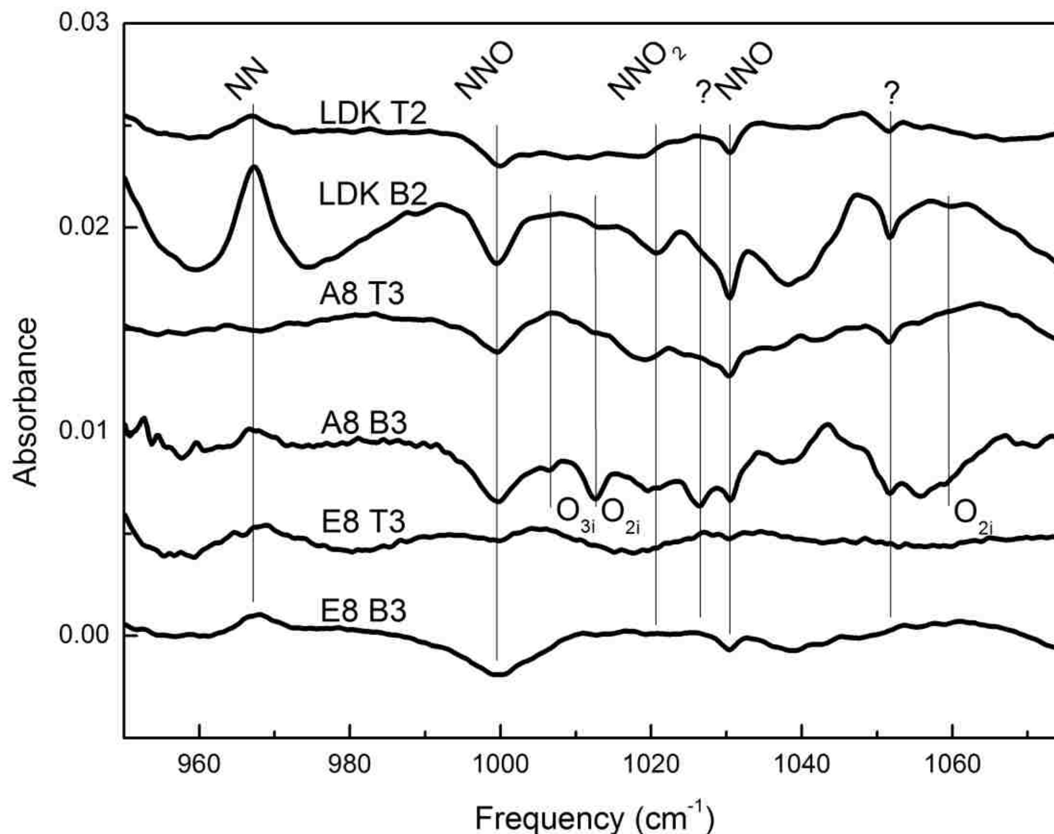

Figure 4.14 Difference spectra for mc-Si samples annealed at 1000°C and for samples from the same test slab in its as-solidified condition.

4.4 Far IR studies of nitrogen centers in multi-crystalline silicon

Vibrational spectroscopy finds that mc-Si samples containing nitrogen and oxygen with concentrations in the neighborhood of 4×10^{15} cm^{-3} and 4×10^{17} cm^{-3}, respectively, can contain up to a few times 10^{15} cm^{-3} NN-O_n complexes. These NN-O_n complexes are electrically inactive. What about the N-O_n complexes with a

single N atom that act as shallow thermal donors? While these defects do not show substantial vibrational absorption in our samples, that may be probed with high sensitivity by way of their electronic transitions.

We began our far IR experiments with studies of p-type Czochralski-grown Si with a nominal resistivity of 10 to 15 Ω-cm, a carbon concentration of [C] < 0.1 ppma, a nitrogen concentration of $[N] = 4\times10^{15}$ cm^{-3}, and an oxygen concentration of [O] = 12.5 ppma to demonstrate in our laboratory the strategies discussed in Sec. 2.2.2 to be used to probe electronic transitions in partially compensated Si samples.

It is well known that annealing CZ-Si near 450°C produces a family of “oxygen donors” with different binding energies. These defects contain different numbers of oxygen atoms and are helium-like double donors with IR lines that have been studied extensively.[4.16] A partially compensated Si test sample was made for our experiments by annealing a p-type, CZ-Si sample at 450 ℃ for 6 hours to produce oxygen donors.

Absorption spectra in the far IR are shown in Figure 4.15 for a CZ silicon sample annealed at 450 ℃. In the darkness (lower spectra), we observe the boron lines at 245, 278 and 320 cm^{-1}.[4.17] Lines that might arise from shallow donors are not seen in darkness. With supplementary, visible-light illumination from the side (upper spectra), the intensities of the boron lines are observed to be increased because holes have been produced that more fully populate the compensated shallow acceptor centers. Furthermore, the upper spectra in Figure 4.15 show the electronic transitions of shallow donors that have become populated by electrons that were also produced by side illumination. The absorption lines of the shallow

oxygen donors are labeled by their final states and assignments to specific donor centers of the oxygen donor family.

We can determine the concentration of neutral boron acceptors from the strength of the line due to B at 278 cm^{-1}. The calibration for B is that the concentration of B equals 1.5×10^{13} cm^{-1} times the integrated absorption coefficient for the line at 278 cm^{-1}. Results for the neutral B concentrations determined from Figure 4.15 are shown in Table 4.5.

The value $[B] = 1.2 \times 10^{15}$ cm^{-3} corresponds to a resistivity near 12 Ω-cm, a result that is consistent with the nominal resistivity of the sample.

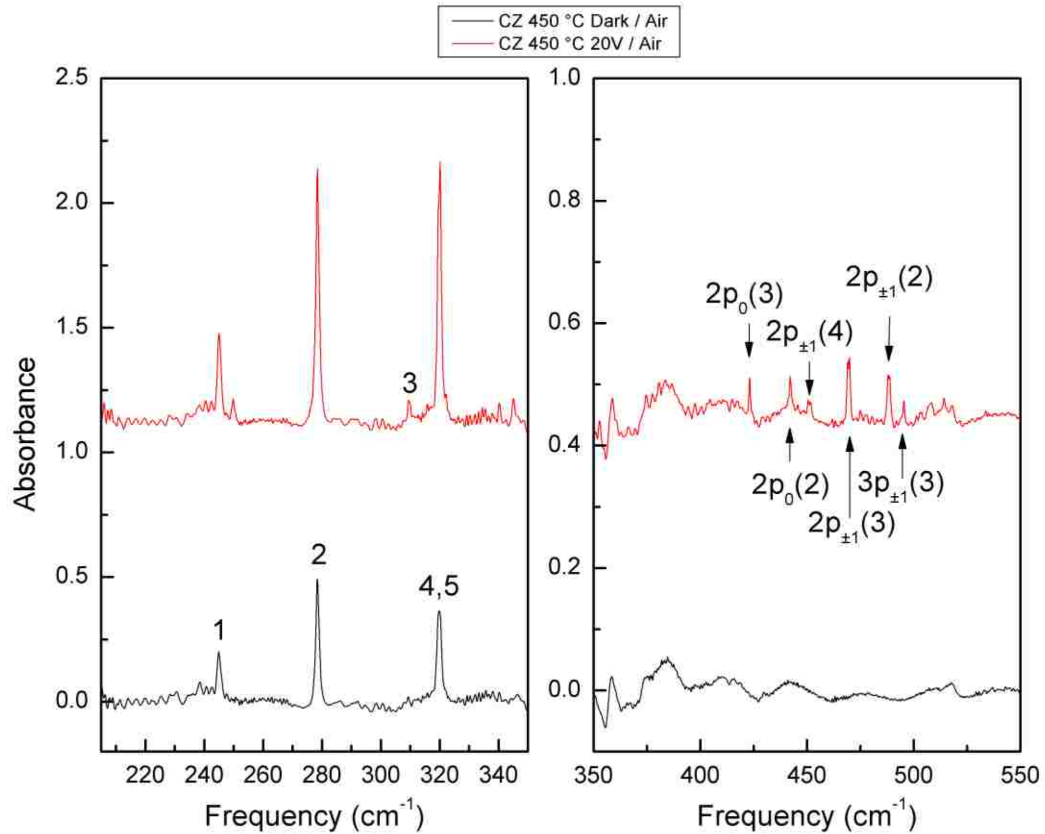

Figure 4.15 Absorption spectra (4.2K, resolution 0.5 cm^{-1}), measured with an empty sample holder for reference, for p-type CZ silicon annealed at 450°C for 6 hours. Label numbers on the left panel are boron lines.[4.18] Labels on the right panel are for thermal donor lines assigned previously.[4.19]

Defect	ω (cm^{-1})	α (cm^{-1})	IA (cm^{-2})	Concentration (at•cm^{-3})
B(dark)	278	23.286	37.784	5.7×10^{14}
B(120W)	278	46.861	79.505	1.2×10^{15}

Table 4.5 Data for the absorption coefficient of the B acceptor and the concentration of neutral B, determined from the data in Figure 4.15.

It also possible to produce the electrically active N-O centers of interest to us in our CZ-grown, Si test samples, in this case, by a long anneal at 600 ℃. IR spectra measured both in darkness and with side illumination are shown in Figure 4.16 for a Czochraski grown Si sample annealed at 600 ℃.

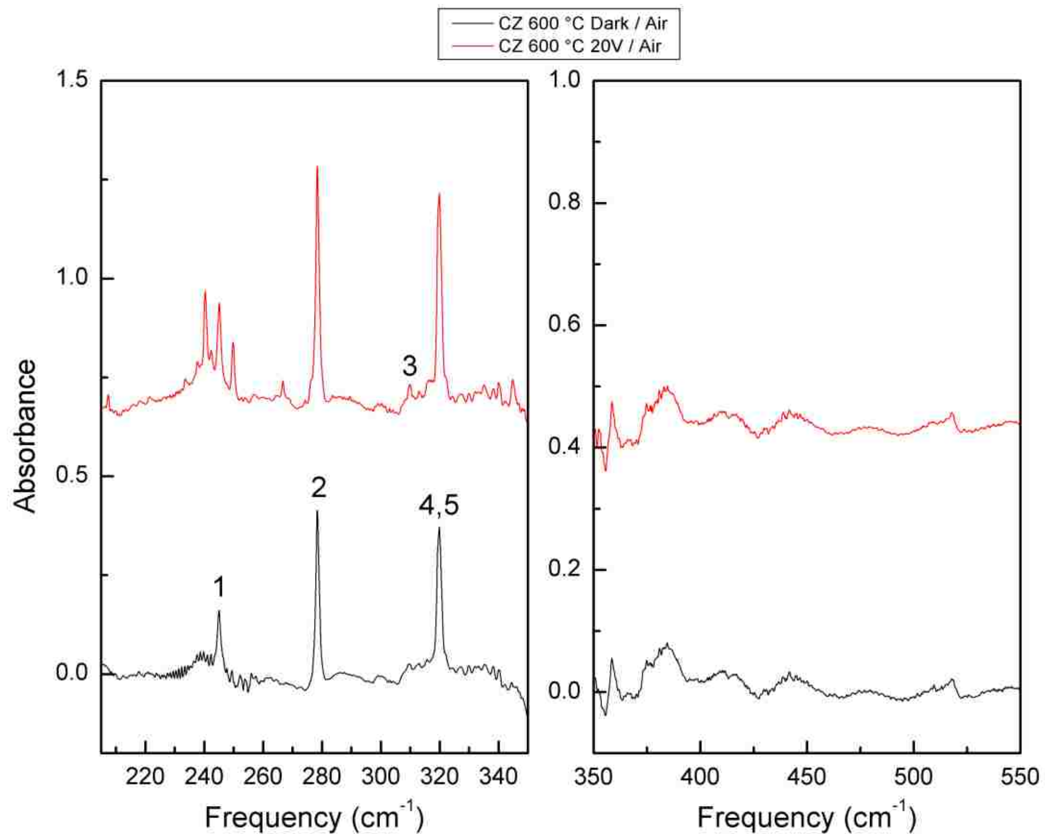

Figure 4.16 Absorbance spectra (4.2K, resolution 0.5 cm^{-1}) measured with an empty sample holder for reference, for p-type CZ silicon annealed at 600 °C for 15 hours. Label numbers on the left panel are boron lines[4.18].

Figure 4.17 shows an expansion of the spectrum presented in the upper left panel of Figure 4.16. The lines 1 and 2 assigned to the B acceptor are labeled in the figure. The N-O IR lines are labeled by their assignments given in Ref. 4.13 and in Table 4.2 here. The 1s → $2p_{\pm}$ lines of shallow donors 3 and 5 are the dominant N-O lines.

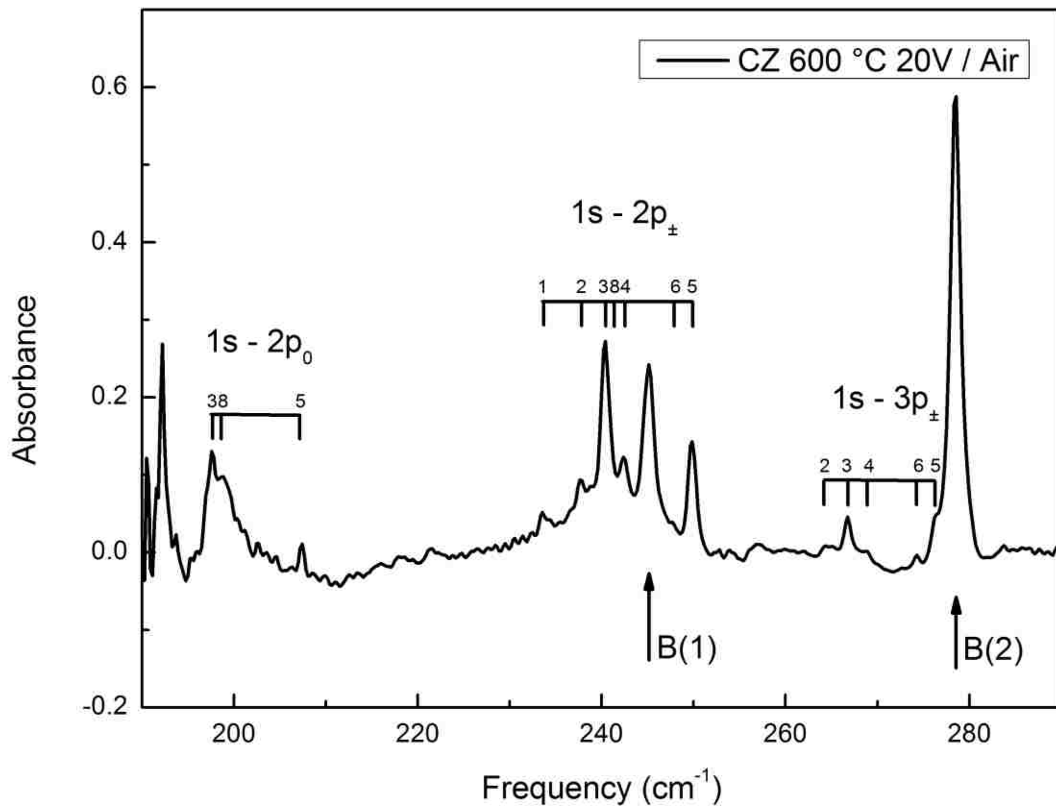

Figure 4.17 A spectrum for the same CZ Si sample as shown in Figure 4.16, in the N-O shallow donor FIR region. The labels are for N-O related lines.[4.13] Two boron lines are also labeled with number 1 and 2[4.18].

The concentrations of neutral B and of the N-O shallow donors can be estimated from the intensities of the IR lines shown in Figures 4.16 and 4.17. The B concentration is again obtained from the area of the 278 cm^{-1} line.

The calibration for the N-O lines is that the concentration of the N-O donor equals 5×10^{13} cm^{-2} times the peak absorption coefficient for its associated 1s to $2p_{\pm}$ line. The concentrations of B and the N-O centers shown in Figure 4.17 are listed in Table 4.6.

Defect	ω (cm^{-1})	α (cm^{-1})	IA (cm^{-2})	Concentration (at•cm^{-3})
B(dark)	278	19.844	31.129	4.7×10^{14}
B(120W)	278	27.625	44.584	6.7×10^{14}
NO(3)	240	8.330	8.593	4.2×10^{14}
NO(5)	250	5.994	6.852	3.0×10^{14}

Table 4.6 Data for the absorption coefficient of the B acceptor line at 278 cm^{-1} and N-O donor lines determined from Figures 4.16 and 4.17. The concentrations of neutral B and N-O donors estimated from these data are also shown.

Figure 4.18 shows spectra for the same CZ-grown Si material whose spectra are shown in Figures 4.15 and 4.16. In this case, the sample was annealed at 800 ℃ for 30 minutes. No N-O centers are seen following an 800 ℃ annealing treatment. Estimates for the B concentrations for Figure 4.18 are given in Table 4.7.

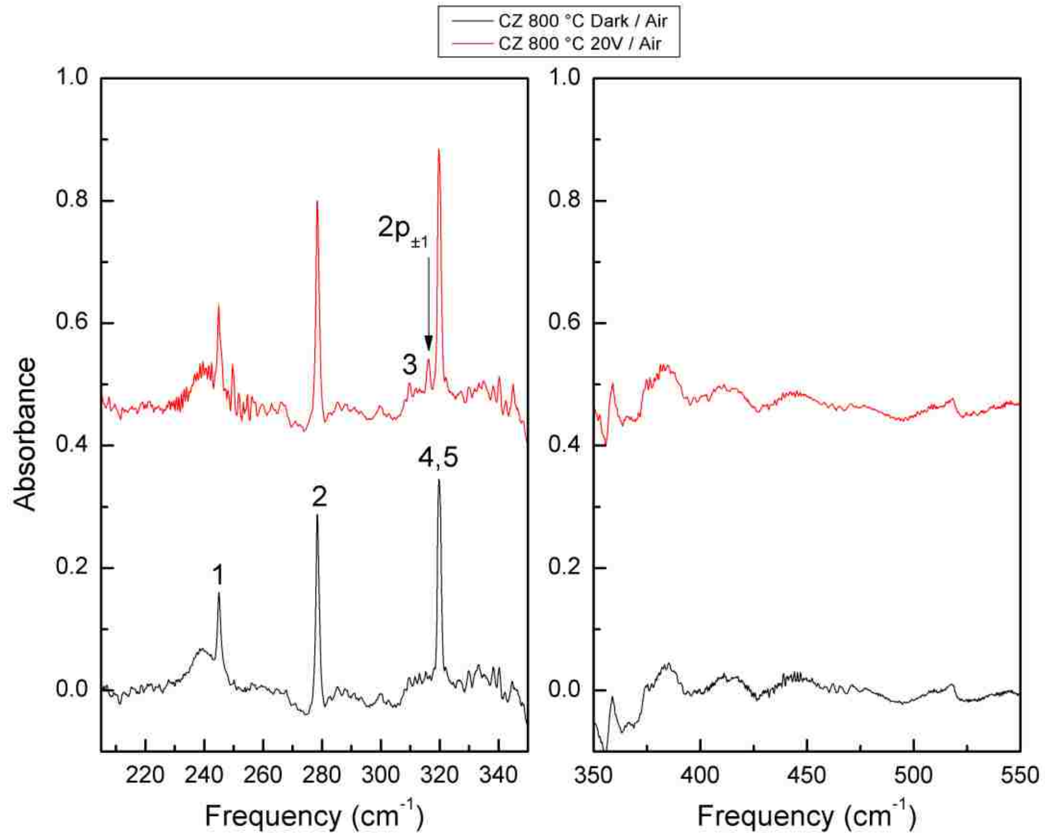

Figure 4.18 Absorbance spectra (4.2K, resolution 0.5 cm^{-1}) measured with an empty sample holder for reference, for p-type CZ silicon annealed at 800 °C. Label numbers on the left panel are boron lines[4.18]. A phosphorus line is also labeled[4.20].

Defect	ω (cm^{-1})	α (cm^{-1})	IA (cm^{-2})	Concentration (at•cm^{-3})
B(dark)	278	19.510	21.724	3.3×10^{14}
B(120W)	278	16.727	26.382	4.0×10^{14}

Table 4.7 Data for the absorption coefficient of the B acceptor line at 278 cm^{-1} shown in Figure 4.18 along with the concentration of neutral B determined from this data.

After confirming the detection of donor complexes formed in CZ silicon, the defects in multi-crystalline silicon sample LDK B2 were investigated. (This sample was chosen because it contained the largest concentration of electrically inactive N and O containing complexes of the samples that have been studied here.) The optical throughput of multi-crystalline silicon is smaller than for CZ silicon because of the imperfect structure of multi-crystalline silicon, leading to a reduced signal to noise ratio for our absorption measurements.

Only the N-O lines at 240 cm^{-1} and 250 cm^{-1} were detectable in our experiments. All absorbance spectra have a reference spectrum measured with no sample in the sample holder. The thin lines are for spectra measured when there was no supplementary light illuminating the sample, while the thicker lines (red in PDF) are for spectra measured with a 120 Watt light illuminating the sample. In Figures 4.19(a), (b) and (c), spectra for samples in the as grown, 800 ℃ annealed, and 600 ℃ annealed conditions are shown, respectively. (Because the transmission approaches zero at the boron peaks, the boron lines in the absorbance spectra are saturated. Although the changes of the spectra with and without supplementary light illumination are small, weak lines due to N-O complexes can be seen for the as-grown sample. After the sample was annealed at 800 ℃ for 30 minutes, the IR lines from the N-O complexes vanished. After the sample was annealed for 17 hours at 600 ℃, the N-O complexes reappeared. The 240 and 250 cm^{-1} lines produced by thermal annealing can be seen in Figures 4.19(d), (e), (f), which are expansions of Figures 4.19(a), (b), (c), respectively.

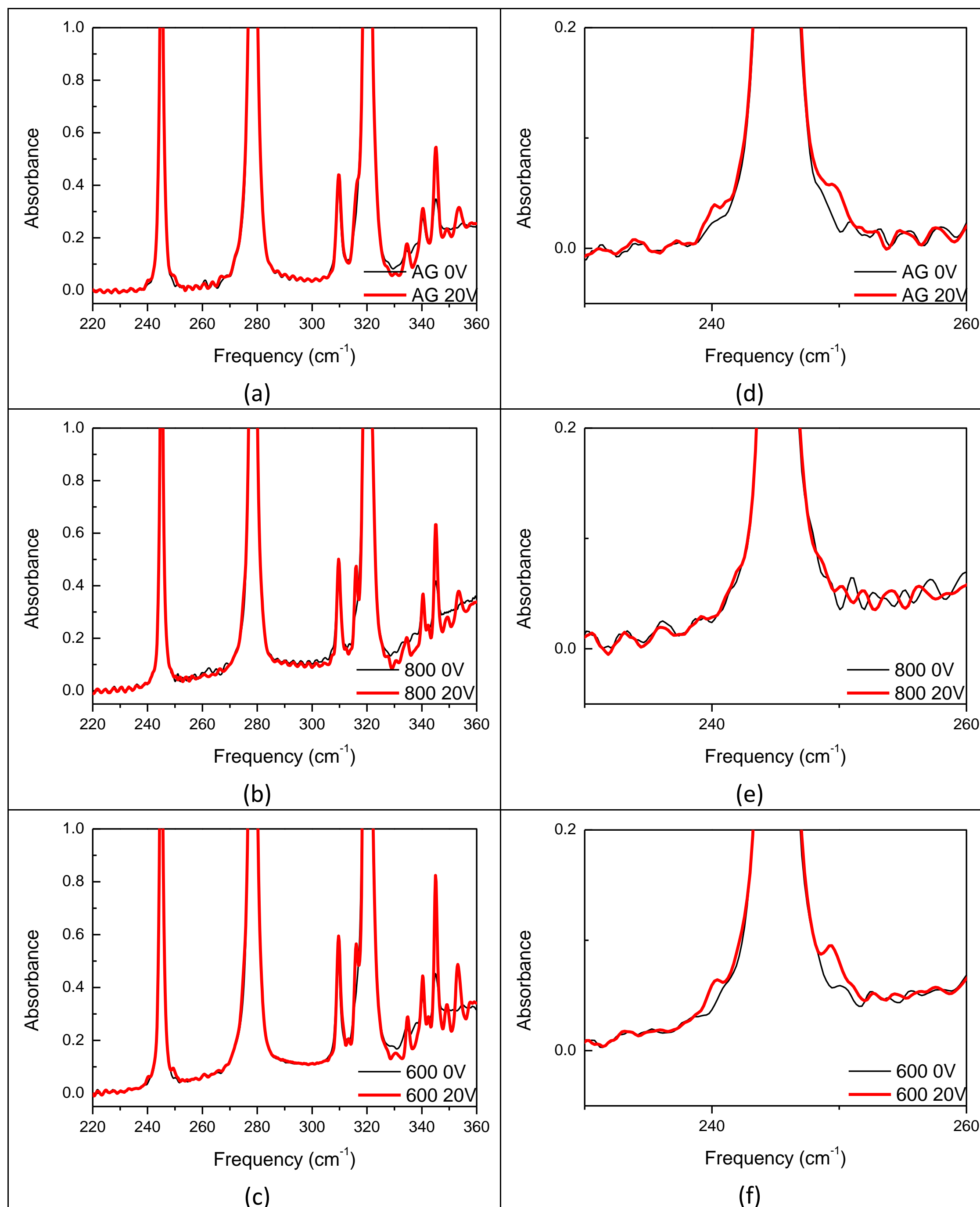

Figure 4.19 Far IR spectra measured for sample LDK B2 at 4.2K with a resolution of 0.5 cm^{-1}. Thin lines are for spectra taken without light illumination. Thicker lines (red in PDF) are taken with 120W light bulb illumination. (a), (b) and (c) are samples under as-grown, 800 °C annealed, and 600 °C annealed conditions respectively. (d), (e) and (f) are the same spectra in an expanded scale (5 X).

We have estimated the concentrations of donors NO(3) and NO(5) from the spectra shown in Figure 4.19. These results are presented in Table 4.8.

Defect	ω (cm^{-1})	α (cm^{-1})	Concentration (at•cm^{-3})
NO(3) - AG	240	0.700	3.5×10^{13}
NO(5) - AG	250	1.294	6.5×10^{13}
NO(3) - 800	240	-	-
NO(5) - 800	250	-	-
NO(3) - 600	240	0.821	4.1×10^{13}
NO(5) - 600	250	1.761	8.8×10^{13}

Table 4.8 Data for the peak absorption coefficient and shallow donor concentration for the donors NO(3) and NO(5) whose spectra are shown in Figure 4.19. These data are for sample LDK B2 in its as-solidified state, annealed at 800 °C and annealed at 600 °C.

The resistivity of our mc-Si samples is near 1 Ω-cm which corresponds to a boron concentration of [B] = 1.5×10^{16} cm^{-3}. The concentration of compensating N-O donors is near 1% of this value, that is, 1.3×10^{14} cm^{-3} from the data presented in Table 4.8.

We have performed similar experiments for sample A8 B3 which contained the highest concentration of O (4.7×10^{17} cm^{-3}) of our samples obtained from MEMC. In Figures 4.20(a) and (b), spectra for the sample A8 B3 in the as grown and 600 ℃ annealed conditions are shown, respectively. Lines due to N-O complexes may be only weakly seen in the as-grown sample. After the sample was annealed for 17 hours at 600 ℃, a greater concentration of N-O complexes appeared. The 240 and 250 cm^{-1} lines affected by thermal annealing can be seen in Figures 4.20(c), (d), which are expansions of Figures 4.20(a), (b), respectively.

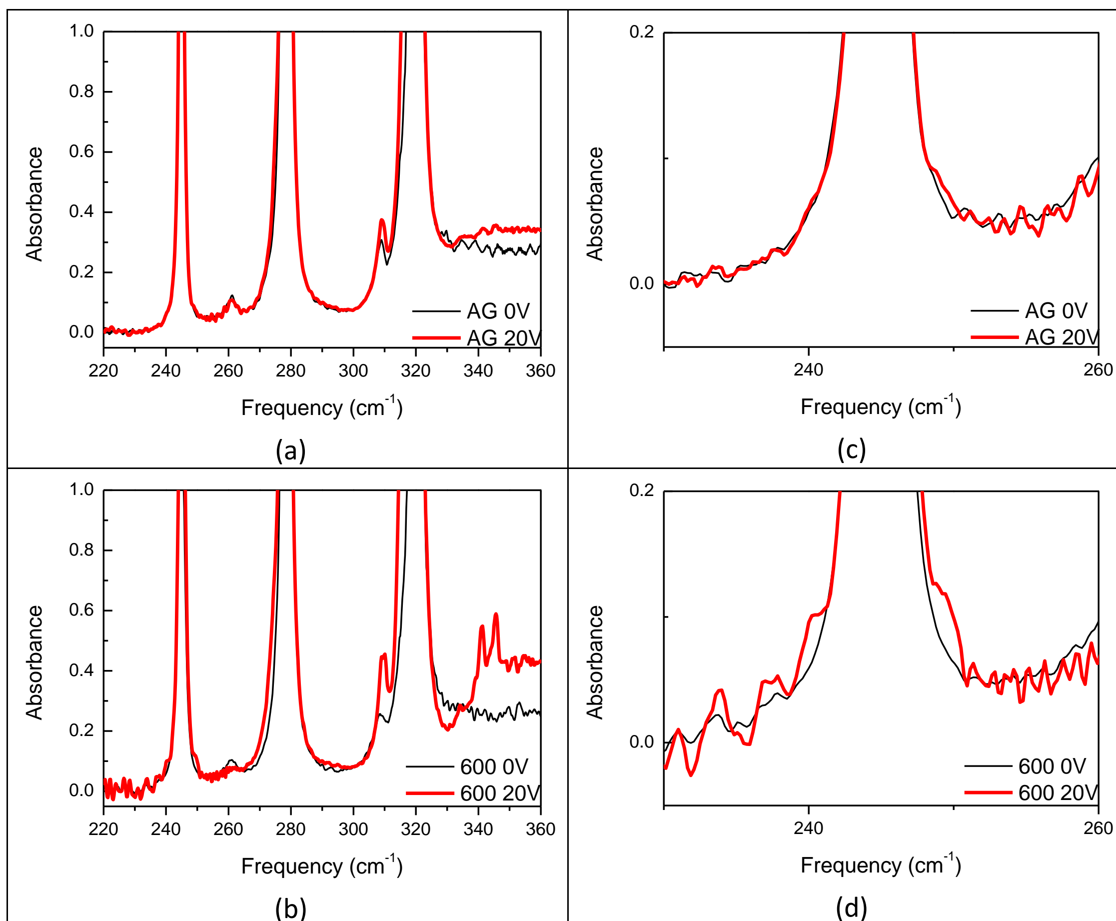

Figure 4.20 Far IR spectra measured for sample A8 B3 at 4.2K with a resolution of 0.5 cm^{-1}, thin lines are for spectra taken without light illumination. Thicker lines (red in PDF) are taken with 120W light bulb illumination. (a) and (b) are samples under as-grown and 600°C annealed conditions respectively. (c) and (d) are the same spectra in an expanded scale (5 X).

We have also estimated the concentrations of donors NO(3) and NO(5) from the spectra shown in Figure 4.20. These results are presented in Table 4.9.

Defect	ω (cm^{-1})	α (cm^{-1})	Concentration ($at\bullet cm^{-3}$)
NO(3) - AG	240	-	-
NO(5) - AG	250	0.542	2.7×10^{13}
NO(3) - 600	240	1.707	8.5×10^{13}
NO(5) - 600	250	2.029	10.1×10^{13}

Table 4.9 Data for the peak absorption coefficient and shallow donor concentration for the donors NO(3) and NO(5) whose spectra are shown in Figure 4.20. These data are for sample A8 B3 in its as-solidified state and annealed at 600°C.

The resistivity of our mc-Si samples is near 1 Ω-cm which corresponds to a boron concentration of [B] = 1.5×10^{16} cm^{-3}. The concentration of compensating N-O donors for sample A8 B3 is near 1% of this value, that is, 1.9×10^{14} cm^{-3} from the data presented in Table 4.9.

4.5 Conclusion: N-centers in mc-Si

In conclusion, defects containing N and O in multi-crystalline Si have been studied by IR spectroscopy. Multi-crystalline Si samples are found to contain N with concentrations in the range 2.7×10^{15} to 7.9×10^{15} cm^{-3}. The dominant N-containing point defect is the N-N, interstitial-pair center that is seen also in mono-crystalline Si grown by the floating zone or Czochralski methods. The unintentional concentration of N in mc-Si typically exceeds the concentration typically found in mono-crystalline Si materials by a factor near 4.

Nitrogen centers are also found to be complexed with oxygen impurities that are present in mc-Si. NN-O_n complexes are seen in our experiments, especially for samples at the bottom of a mc-Si brick, where the oxygen concentration is highest. In as-solidified mc-Si material, nearly 40% of the N can be found in the form of NN-O_n complexes in some samples. Presumably, these defects were formed during the time the mc-Si ingot cooled after it solidified.

We have also searched for N-O complexes with a single N atom that give rise to shallow donors with binding energies near 35 meV. The concentration of electrically active N-O centers was found to be $\approx 1.3\times10^{14}$ cm^{-3} in a p-type Si sample (LDK B2, resistivity near 1 Ω-cm, [B]=1.5×10^{16} cm^{-3}) rich in N (7.8×10^{15} cm^{-3}) and O (3.2×10^{17} cm^{-3}). Similar results were found for a second sample (A8 B3) that was richer in oxygen ([N-O] = 1.9×10^{14} cm^{-3}). These concentrations of N-O centers are lower than can be produced in Czochralski grown Si that contains N, presumably because of the lower concentration of O in mc-Si as compared to Cz-grown Si (>7x10^{17} cm^{-3}).

Our results show that electrically active N-O centers have little impact on the p-type doping of mc-Si because their concentration (near 2×10^{14} cm^{-3}) is small compared to the intentional B concentration (1.5×10^{16} cm^{-3}). However, even this small concentration of electrically-active shallow donors may have an effect on the minority carrier lifetime in Si.[4.21] These effects on lifetime are a subject of future investigation.

Our experimental results provide new insight into the behavior of N in multi-crystalline Si and its interactions with other defects in Si materials widely used for the fabrication of solar cells.

References

4.1 E. Dornberger, J. Virbulis, B. Hanna, R. Hoelzl, E. Daub, W. von Ammon, J. Crystal Growth, 229 (2001), p. 11.

4.2 W. Kaiser and C. D. Thurmond, J. Appl. Phys. 30, 427 (1959).

4.3 H. J. Stein, in Proceedings of the 13th International Conference on Defects in Semiconductors, Coronado, California, 1984, edited by L. C. Kimerling and J. M. Parsey, Jr. (The Metallurgical Society of AIME, Warrendale, PA, 1985), p. 839.

4.4 R. Jones, S. Öberg, B. Rasmussen, and B. Nielsen, Phys. Rev. Lett. 72, 1882 (1994).

4.5 J. P. Goss, I. Hahn, R. Jones, P. R. Briddon, and S. Öberg, Phys. Rev. B 67, 045206 (2003).

4.6 F. Sahtout Karoui and A. Karoui, J. Appl. Phys. 108, 033513 (2010).

4.7 Y. Itoh, T. Nazaki, T. Masui, and T. Abe, Appl. Phys. Lett. 47, 488 (1985).

4.8 P. Wagner, R. Öder, and W. Zulehner, Appl. Phys. A: Solids Surf. 46, 73 (1988).

4.9 A. Gali, J. Miro, P. Deak, C. P. Ewels, and R. Jones, J. Phys.: Condens. Matter 8, 7711 (1996).

4.10 M. W. Qi, S. S. Tan, B. Zhu, P. X. Cai, W. F. Gu, X. M. Xu, T. S. Shi, D. L. Que, and L. B. Li, J. Appl. Phys. 69, 3775 (1991).

4.11 H. Ch. Alt and H. E. Wagner, J. Appl. Phys. 106, 103511 (2009).

4.12 M. Suezawa, K. Sumino, H. Harada, and T. Abe, Jpn. J. Appl. Phys. 25, L859 (1986).

4.13 H. Ch. Alt, H. E. Wagner, W. v. Ammon, F. Bittersberger, A. Huber, and L. Koester, Physica B 401–402, 130 (2007).

4.14 G. Davies, Phys. Rep. 176, 83-188 (1989).

4.15 A. Baghdadi, W. M. Bullis, M. C. Croarkin, Y.-Z. Li, R. I. Scace, R. W. Series, P. Stallhofer, and M. Watanabe, J. Electrochem. Soc. 136, 2015–2024 (1989).

4.16 B. Pajot, *Optical Absorption of Impurities and Defects in Semiconducting Crystals*, Springer, 2010, p. 220.

4.17 M. Porrini, M. Pretto, R. Scala, A. Batunina, H. Alt, and R. Wolf, Appl. Phys. A 81, 1187 (2005).

4.18 B. Pajot, *Optical Absorption of Impurities and Defects in Semiconducting Crystals*, Springer, 2010, p. 287, Table 7.2.

4.19 B. Pajot, *Optical Absorption of Impurities and Defects in Semiconducting Crystals*, Springer, 2010, p. 223, Table 6.24.

4.20 B. Pajot, *Optical Absorption of Impurities and Defects in Semiconducting Crystals*, Springer, 2010, p. 175, Table 6.2.

4.21 J. Murphy, Oxford University, private communication.

VITA

Haoxiang Zhang was born to Chi Zhang and Mei Rong on May 9th, 1987 in Hubei, China. He graduated from Jingzhou Middle School in Jingzhou, Hubei, China, in 2002 and attended University of Science and Technology of China in Hefei, Anhui, China. He graduated with a bachelor of science in physics, in 2006. In August, 2007, Haoxiang began his graduate education at Lehigh University. He was a teaching assistant before he began work as a research assistant under Michael J. Stavola in June 2009. In 2010, he received his master's degree in electrical engineering from Lehigh University. Since June, 2009, Haoxiang has been conducting his dissertation studies, focusing on light element impurities in multi-crystalline silicon by vibrational spectroscopy.